A STUDY OF T = 2 STATES IN ^{12}B, ^{12}C, ^{20}F AND ^{28}Al

Thesis by

Patrick Henly Nettles, Jr.

In Partial Fulfillment of the Requirements

For the Degree of

Doctor of Philosophy

California Institute of Technology

Pasadena, California

1971

Submitted October 9, 1970

ACKNOWLEDGMENTS

It has been a distinct pleasure to work in the Kellogg Radiation Laboratory, and I am deeply indebted to all of the staff members for their interest and support in this work. I would especially like to thank Dr. C. A. Barnes, who has guided this program, for many fruitful suggestions and enlightening discussions.

Much of this work was done in collaboration with Dr. D. C. Hensley. Sincere thanks are extended to him for introducing me to these studies and for education in the laboratory. The assistance of Dr. D. B. Nichols and P. Dyer in the later part of the work at Caltech is appreciated.

The experiments at Oak Ridge were done in collaboration with Dr. C. D. Goodman. His assistance in arranging beam-time for these experiments and in planning and executing the measurements is gratefully acknowledged.

Finally, I would like to thank my wife, Cathy, for her patience and support through the many long days and late nights while this work was in progress.

ABSTRACT

The lowest T = 2 states have been identified and studied in the nuclei ^{12}C, ^{12}B, ^{20}F and ^{28}Al. The first two of these were produced in the reactions ^{14}C(p,t)^{12}C and ^{14}C(p,^{3}He)^{12}B, at 50.5 and 63.4 MeV incident proton energy respectively, at the Oak Ridge National Laboratory. The T = 2 states in ^{20}F and ^{28}Al were observed in (^{3}He,p) reactions at 12-MeV incident energy, with the Caltech Tandem accelerator.

The results for the four nuclei studied are summarized below:

(1) ^{12}C: the lowest T = 2 state was located at an excitation energy of 27595 ± 20 keV, and has a width less than 35 keV.

(2) ^{12}B: the lowest T = 2 state was found at an excitation energy of 12710 ± 20 keV. The width was determined to be less than 54 keV and the spin and parity were confirmed to be 0^{+}. A second ^{12}B state (or doublet) was observed at an excitation energy of 14860 ± 30 keV with a width (if the group corresponds to a single state) of 226 ± 30 keV.

(3) ^{20}F: the lowest T = 2 state was observed at an excitation of 6513 ± 5 keV; the spin and parity were confirmed to be 0^{+}. A second state, tentatively identified as T = 2 from the level spacing, was located at 8210 ± 6 keV.

(4) ^{28}Al: the lowest T = 2 state was identified at an excitation of 5997 ± 6 keV; the spin and parity were confirmed to be 0^{+}. A second state at an excitation energy of 7491 ± 11 keV is tentatively identified

as $T = 2$, with a corresponding (tentative) spin and parity assignment $J^{\pi} = 2^+$.

The results of the present work and the other known masses of $T = 2$ states and nuclei for $8 \leq A \leq 28$ are summarized, and mass-equation coefficients have been extracted for these multiplets. These coefficients were compared with those from $T = 1$ multiplets, and then used to predict the mass and stability of each of the un-observed members of the $T = 2$ multiplets.

TABLE OF CONTENTS

PART	TITLE	PAGE

viii

LIST OF TABLES

ix

I. GENERAL INTRODUCTION

From a variety of phenomena observed in various facets of nuclear physics and particle physics, it has been found that the strong (nuclear) forces are charge-independent to within about 2% (Henley 1969). This fact is manifested, among other ways, in the existence of isobaric analogue states, i.e., states which have the same structure in each isobar of a particular mass-number, except that the total nuclear charge is different from one member to another. The principal charge-dependent forces -- the Coulomb and spin-orbit interactions -- give rise to a mass splitting for these states, which is easily predicted from perturbation theory, at least in principle.

The studies to be described in the present work are part of a continuing program at Caltech, and a considerable effort at many other laboratories, to measure the mass splitting for these multiplets. The experimental techniques involved in this particular work are outlined in the following chapter. In Chapter III the previous work from the Caltech program is summarized and the goals of the program are discussed in more detail. Also, some elementary concepts used in this work are introduced. Chapter IV discusses two experiments performed at Oak Ridge, using protons from the Isochronous Cyclotron to excite two members of the lowest isospin quintet in mass 12. Chapters V and VI deal with ^{3}He-induced reactions studied at Caltech, which excited one member of each of the lowest quintet in A = 20 and 28, respectively. In Chapter VII

a survey of the available measurements for isospin quintets in light nuclei with A = 4n is compared with the mass formula predicted from first-order perturbation theory, and the masses and decay modes of the unobserved members of these multiplets are discussed.

II. EXPERIMENTAL METHOD

A. Introduction

The experiments discussed in the following chapters have a
number of experimental techniques in common. In all of these
experiments, charged-particle reaction products were identified
by combining energy, momentum/charge, and energy-loss measurements.
These were obtained by first momentum-analyzing the reaction pro-
ducts at a known laboratory angle in a magnetic spectrometer, then
allowing these particles to penetrate a foil of known thickness, and
finally measuring the resulting particle energy spectrum in a solid-
state detector (Figure 1). Generally, the reaction was observed in
transmission geometry, where the incident beam enters one side of
the target and the reaction product to be observed exits through
the opposite side, which required that the targets be reasonably
thin (i.e., the fractional energy loss for both beam and reaction
products should be small). Then from a knowledge of the target
thickness obtained from energy loss or resolution measurements and
a measurement of the magnetic field and focal-plane position, the
exiting particle energy before leaving the target could be deter-
mined precisely. By comparing the energy of a particle group of
interest to that of one or more groups from the same target and
beam with precisely known Q-value(s), the Q-value for the reaction
of interest was determined. Most of the details of this procedure
and the analysis of the probable errors incurred have been discussed

previously by Hensley (1969).

B. Target Preparation

To meet the requirements outlined above, the targets used in these experiments were prepared either as thin self-supporting foils of more or less uniform composition or as multilayer foils with one layer of target material and the remaining layer(s) for support. The supporting foils for most of the work were ~100 to 300 $\mu g/cm^2$ gold, evaporated by the standard techniques in vacuum. For most of the experiments, the target materials were (relatively expensive) isotopically-enriched substances, so the preparation procedures were required to be reasonably efficient, to avoid unnecessary waste.

For the experiments done at Caltech, foils were mounted on the customary 10-mil tantalum frames over a 5/16-inch-diameter hole. The targets used at Oak Ridge were mounted on a 15-mil tantalum frame adapted to fit the standard target holders in use there. These targets were mounted over a 1/2-inch diameter hole to allow for the larger beam area from the cyclotron.

(1) ^{26}Mg Targets. The ^{26}Mg targets were prepared by reducing MgO, enriched to 99% in ^{26}Mg, under vacuum, by heating a mixture of MgO and Ta powders in a carbon boat. To improve the efficiency of the evaporation, the boat was made in the form of a vertical cannon, after a design by Goosman (1970). Magnesium freed by the reduction process at the bottom of the cannon was then confined to a relatively small cone above the source. This ^{26}Mg vapor was condensed on a thin gold foil mounted on a target frame and suspended about 2 inches

above the cannon.

Carbon-backed Mg targets used in early experiments were prepared in a slightly different manner. In the procedure outlined above, it was found that the Mg vapor would not condense satisfactorily on a thin (20 - 100 $\mu g/cm^2$) mounted carbon foil. However, the vapor was easily collected on a carbon foil before it was removed from the glass slide. The foil was then cut into suitable squares, floated from the slide and successfully mounted. This process allowed the collection of a larger fraction of the released vapor; however, it was still a rather unsatisfactory technique since thin Mg layers deteriorate quickly by chemical reaction with water (including water vapor). The appearance of the targets was noticeably different near the edges after a few minutes in the floating dish. No detailed investigation of the quality of the targets was made, so the results are uncertain. The same technique was attempted with gold foils; in that case, pinholes in the gold foil allowed direct contact between the water and the Mg, with disastrous results.

In the evaporation process, it was found that the MgO apparently released a considerable amount of absorbed gases when initially heated, until the boat was bright red. Unless the temperature was increased very slowly, the powder in the cannon had a strong tendency to jump out. To avoid this annoyance, the design of the cannon was modified slightly. The top of the boat was extended above the electrode about 0.3 inch so that a horizontal copper cover-plate, which could be moved from outside the vacuum system, would cover and nearly touch the top of the boat. With this cover in place, the

powder could be heated rapidly without any appreciable loss of MgO.

(2) ^{18}O Targets. Solid oxygen targets were prepared by oxidizing thin nickel foils, by heating them in an oxygen atmosphere with a projection lamp. Since the commercial nickel foils were prepared with a thick copper backing for easier handling, the foils were generally first mounted on the frames with silver print or epoxy, after which the copper backing was etched away chemically with a mixture of ammonium hydroxide and trichloroacetic acid (Richards 1960). In this procedure, the thinner nickel foils became very tightly stretched on the frame, and they consequently showed a strong tendency to break or split as they were heated. To improve the yield of useable targets, a special foil holder was devised which shielded the target frames from the direct heat of the lamp, allowing only the central 1/4-inch diameter of the foil to be heated. With this simple device a considerable reduction was achieved in the number of foils lost during the oxidation process.

For the thinnest (500 Å) nickel foils, a further improvement in yield was desirable. Before mounting the foils, the copper backings were removed by floating the foil on the surface of a pool of the etching solution. The bare nickel foil was then lifted out of the etch on a glass slide and placed in a pool of distilled water. This wash step was repeated several times, after which the foil was lifted from the surface on a target frame. Foils prepared in this way were considerably looser on the frame, and were much easier to oxidize without breakage.

(3) ^{14}C Targets. The process for preparing ^{14}C targets was
developed jointly with Hensley (1969), from an idea of Douglas (1956).
An A.C. discharge was established in ^{14}C-enriched acetylene between
two electrodes separated by ~0.5 cm. The acetylene deposited as a
polymer on foils mounted on the electrode surfaces. The foils con-
sisted of 300 $\mu g/cm^2$ Au with a backing of 0.1-mil commercial rolled-
copper foil. After the polymerized-acetylene layer was deposited,
the foils were mounted on Ta frames and the copper was etched away
chemically. For the thicker targets used in the experiments
described in this thesis, an additional thin layer of gold was
evaporated over the carbon layer to provide better electrical con-
ductivity.

In the deposition of thick layers (of the order 0.5 mg/cm^2)
it was found that the discharge often produced sparks or hot spots
on the target surface. Subsequent examination of the surface in-
dicated that these sparks were associated with flaws such as pin-
holes in the deposited layer, which offered a path of lower
resistance for the discharge. To retard the aggravation of flaws
by this hot-spot phenomenon, a current-limiting resistor was
introduced between the tesla coil and electrode, of the order of
100 KΩ. With this modification, there was a noticeable reduction
in hot spots, and it was possible to prepare reasonably uniform
targets of the required thickness.

C. Determination of Target Thickness

For solid targets, the thickness can be determined from yield

comparisons, energy-loss measurements, or resolution measurements as illustrated below.

(1) Magnesium targets. The thicknesses of the magnesium targets used for this work were measured by observing elastically scattered ^{3}He from the gold (or carbon) backing, both directly and through the Mg layer, in the spectrometer at 90° in the lab (Figure 2). The inverse process (scattering from the Mg) was used to measure the thickness of the backing (Figure 3). An additional measurement of the thickness was obtained from the energy-width of the elastically scattered particle group when the target thickness was greater than the instrumental resolution.

(2) NiO Targets. The thickness of the Ni^{18}O targets was determined from the nominal Ni-foil thickness and a comparison of the yields from the (^{3}He,α) reaction on the Ni^{18}O target and on pure ^{18}O, in a gas cell. Additional thickness information was extracted from the width of elastic scattering groups from ^{58}Ni and ^{18}O.

(3) ^{14}C targets. The ^{14}C target material was enclosed between two layers of gold, one of which was considerably thicker than the other. The thickness of the polymer layer (assumed to be entirely carbon, for energy-loss calculations) was measured by observing the elastic scattering of 12-MeV ^{3}He from the gold layers, in the magnetic spectrometer at 90° in the lab (Figure 4). The target thickness was extracted from the energy difference of the two peaks corresponding to the two gold layers. The thickness of

the thicker gold layer was determined from the width of the directly-
observed elastic scattering peak. This thickness was scaled by the
ratio of yields to give the thickness of the thinner gold layer.

D. Magnetic Analysis

The separation of charged particles by magnetic analysis is
an established technique for nuclear spectroscopy, in use in many
laboratories. It offers the advantages of excellent particle
identification (especially when combined with an energy measurement
at the focal plane), and lower count rates (by selecting for obser-
vation only the small portion of the particle spectrum of interest).
These are gained at the expense of solid angle and field of view in
the particle momentum spectrum; the technique is best applied to
precise measurement of a particle spectrum over a reasonably narrow
and well-defined range of energy.

In all the experiments under consideration in this work,
charged-particle reaction products were observed in either the
61-cm-radius, double-focusing magnetic spectrometer at Caltech, or
the broad-range magnetic spectrograph at the Oak Ridge cyclotron
laboratory.

The Caltech spectrometer has been discussed in detail by
Groce (1963), McNally (1966), and Moss (1968), and some details of
importance for the present work were considered by Hensley (1969).
The expression used to determine particle energy from the measured
NMR frequency is presented in Appendix A for this instrument.

The broad-range spectrograph at Oak Ridge is patterned in

principle after a design by Borggreen et al (1963), which differs
from that of the Caltech double-focusing spectrometer in several
ways. The usable focal plane is 2 meters long, spanning a large
range in momentum (for the experiments discussed here, this design
feature was not utilized). Since it is a uniform-field magnet, the
spectrograph has focusing properties in only one dimension, aside
from the small effect of the fringing field at the edge of the
magnet. The instrument is oriented horizontally so that the
focusing occurs along the direction of the kinematic angle for a
reaction. By selecting the position of the moveable focal plane
correctly for a particular reaction, the focusing can be made to
cancel (approximately) the peak broadening associated with the
kinematic energy shift across the aperture, $\frac{\partial E}{\partial \theta} \Delta \theta$ allowing
measurements to be made with experimental resolution considerably
better than the kinematic shift over the aperture. The orientation
of the focal plane for this instrument is thus a critical parameter,
since improper positioning introduces excessive broadening for the
observed particle groups. Since the reactions studied with this
instrument involved light nuclei which give large angle-dependent
kinematic broadening, the focal-plane position was reset after each
change in angle. With the focal plane adjusted in this way, the
resolution (calculated by a computer code at Oak Ridge) was domi-
nated by the effect of the last quadrupole focusing magnet before
the scattering chamber, for the (p,t) reaction, and by the target
thickness, for the $(p, {}^3\text{He})$ study.

The orientation of the focal plane enters the calculation of

particle energy from the measured position along the focal plane. This calculation is discussed in detail in Appendix A.

Since there is essentially no focusing in the other angular dimension for this instrument, the effective solid angle for an observation depends on the position along the focal plane and on the height of the detector. This relationship is given by (Ball 1968)

$$\Delta\Omega = \left\{ \sum_{n=0}^{3} C_n R^n \right\} h \, \Delta\Theta$$

where $\Delta\Omega$ is the solid angle in msr, R the average orbit radius in inches (Appendix A), h the detector height in inches, and $\Delta\Theta$ the total angular opening of the spectrometer entrance slits along the kinematic angle, in degrees. The coefficients C_n are:

n	C_n
0	0.88611
1	-3.6023×10^{-2}
2	5.653×10^{-4}
3	-3.116×10^{-6}

E. Particle Detection and Position Measurements

To determine the energy of a particle group observed in a magnetic analyzer precisely, it is necessary to measure the location of the group on the focal plane precisely. For the experiments with the Caltech spectrometer, this was achieved through the use of a 16-counter array spanning the focal plane or a position-sensitive

solid-state detector (~5 cm long). The measurements at Oak Ridge were made with two position-sensitive detectors on the focal plane.

The design and operation of the 16-counter array has been discussed by McNally (1966) and Moss (1968). Hensley (1969) has discussed the details of peak profiles and yield measurements with this system, which apply to the present work.

The operation and calibration of position-sensitive particle detectors is discussed in some detail in Appendix B. The associated electronic circuits used for these detectors are shown schematically in Figure 6 (Caltech) and Figure 7 (Oak Ridge). These systems are also discussed in Appendix B.

III.   INTRODUCTION TO T = 2 STATES

The study of $T = 2$ states in $T_z = 0$ or $T_z = 1$ light nuclei is a natural extension of the earlier studies of $T = 3/2$ states in $T_z = \pm 1/2$ nuclei in this laboratory (Lynch 1965, Dietrich 1965, Adelberger 1967, Hensley 1969 and McDonald 1969). In most cases the $T = 3/2$ or $T = 2$ states were populated as final states in an isospin-allowed reaction, $(^3He,n)$ (Adelberger 1969a, 1970) or $(^3He,p)$ (Hensley 1968 and the present work), on $T = \frac{1}{2}$ or $T = 1$ targets. Because of the general interest in the $T = 2$ states in mass 12 and the difficulty in obtaining a highly enriched ^{10}Be target for $(^3He,p)$ and $(^3He,n)$ studies, the (p,t) and $(p,^3He)$ reactions on ^{14}C described in this thesis were included in the program.

The principal goals of the program have been (1) identification of the $T = 2$ levels and (2) precise measurement of the reaction Q-values to extract accurate excitation energies for these levels. The strong interest in measuring the excitations accurately is motivated by the continuing need for a more reliable mass formula, to predict masses of nuclei far from the line of stability for astrophysical as well as nuclear purposes. The masses of such nuclei are closely related to those of the analogue excited states and the latter are frequently more easily produced in the laboratory. Thus the program was established to produce precision measurements by which any proposed mass formula or relationship could be tested in detail.

The identification of an energy level as an analogue state is necessarily an indirect process. The features which have been useful

in identifying these states are their predicted spins and parities, excitation energies, widths and their transition strengths in various reactions.

The reactions (^{3}He,p), (p,t), and (p,^{3}He) are assumed to proceed by the direct transfer of a T = 1, $J^\pi = 0^+$ di-nucleon, to populate the levels of interest. The selection rules for these reactions are discussed in Appendix C. The T = 2 states studied in this work were all members of multiplets with even-even parent nuclei; the spin and parity are therefore expected to be 0^+, from nuclear systematics. To populate such a level in one of the above reactions on a (T = 1) 0^+ target, the L-value for the transferred particles must be zero, uniquely. This generally gives the characteristic forward-angle peaking for the differential cross section, if the state is populated by a direct reaction.

Since the reactions in which the T = 2 states were excited are allowed by isospin selection rules, it is expected that the measured cross sections should be larger than for similar processes that are forbidden by these rules. Thus a T = 2 state should be absent or only very weakly excited by an (α,d) reaction on a T = 1 target, while it should be strongly excited by a (^{3}He,p) reaction on the same target. Such comparisons are one-way devices however, since the effects of structure and reaction mechanism are still to be accounted for. Thus the strong excitation of a suspected T = 2 level as the final state of an isospin-forbidden reaction is good evidence that it is not T = 2, while the absence of the level in an isospin-allowed reaction is of little significance (without

additional information or assumptions about the structure). Specific
examples of the effects of structure on transition strength have been
discussed by Adelberger (1967) in the case of (^{3}He,n) versus (p,n)
reactions, and Hensley (1969) in the case of (^{3}He,α) versus (^{3}He,p)
reactions. In the A = 4n nuclei, the T = 2 states are described as
two-particle, two-hole states. These should be excited easily by
the isospin-allowed two-nucleon transfer reactions under consideration.

The excitation energy for a T = 2 state can be predicted
approximately, if the mass of the parent nucleus is known, by assuming
the mass splitting of a multiplet to be mainly the result of the
neutron-proton mass difference and the repulsive Coulomb interaction
between the protons. It is assumed in addition that the repulsive
interaction gives rise to a mass splitting of the form KZ(Z - 1) where
K is constant across a multiplet. The constant K can be evaluated
approximately from the ground-state mass difference for the T_z = +1
and T_z = -1 members of the multiplet. This gives the following
results for the excitation energies $E_x(T, T_z)$ in nuclei of mass
number A:

$$E_x(2,1) = [m(2,2) - m(1,1)] + \frac{A-4}{2(A-1)} [m(1,-1) - m(1,1)] - \frac{3}{A-1} \Delta m_{np}$$

$$(III-1)$$

and

$$E_x(2,0) = [m(2,2) - m(0,0)] + \frac{A-3}{A-1} [m(1,-1) - m(1,1)] - \frac{4}{A-1} \Delta m_{np}$$

$$(III-2)$$

where $m(T,T_z)$ is the mass excess of the mass-A nuclide with isospin T and z-projection T_z $(T_z = \frac{N-Z}{2} = \frac{A}{2} - Z)$, and Δm_{np} is the neutron-hydrogen mass difference. From the difference of these two equations, we can write a useful relationship:

$$E_x(2,1) = E_x(2,0) - [m(1,1)-m(0,0)] - \frac{A-2}{2(A-1)}[m(1,-1)-m(1,1)] + \frac{\Delta m_{np}}{A-1}$$

$$(III-3)$$

Although they are naive in concept, these formulas have been quite useful in selecting the region of excitation energy to be examined in a search for T = 2 states in nuclides for which the parent $(T_z = +2)$ mass has been measured. In most cases studied in this laboratory, these predictions have been accurate within (roughly) 100 keV.

A more general prediction is contained in the familiar quadratic mass law for isobaric multiplets (Wigner 1957, Weinberg and Treiman 1958, Wilkinson 1964a, b, c):

$$m(T,T_z) = a(A,T) + b(A,T)T_z + c(A,T)T_z^2 \qquad (III-4)$$

This formula can be derived under the assumptions (1) that the T-nonconserving interactions are sufficiently weak that first-order perturbation theory is adequate for calculating the energy shifts and (2) that these interactions are (at most) quadratic in isospin-space (i.e., of tensorial rank 2 or less). The principal T-non-conserving interaction is, of course, the Coulomb force, for which these assumptions are justified. Some additional discussion of this

is included in Appendix D. The formulas presented above were derived
from a special case of this formula. From the assumptions outlined
(that the Coulomb corrections can be expressed as $Z(Z - 1)K - Z \Delta m_{np}$
the coefficients b and c were evaluated approximately in terms of
mass differences

$$b = \frac{1}{2} [m(1,-1) - m(1,1)]$$

and

$$c = \frac{1}{2(A-1)}[m(1,-1) - m(1,1) + \frac{\Delta m_{np}}{A-1}] \quad .$$

(III-5)

By combining a Coulomb energy sum rule with the nuclidic mass
relationship of Garvey and Kelson (Garvey 1966, Kelson 1966, Garvey
1969), and considering the special case of $T = 2$ states in $T = 0$
nuclei, Jänecke (1967,1969) has predicted a relationship between
excitation energies $E_x(A,T,T_z)$

$$E_x(A,2,0) = E_x(A - 1, 3/2, \pm 1/2) + E_x(A + 1, 3/2, \pm 1/2)$$

(III-6)

This rule is expected to be less accurate than the mass
relationship since excitation energies should be more sensitive to
details of nuclear structure than Coulomb-energy differences.
Adelberger (1970) has tested this prediction for $A = 4n$ nuclei from
$A = 12$ to 32, and found discrepancies ranging from 30 keV to 339 keV.

From the excitation energies predicted by the schemes out-
lined above, for $A = 4n(n > 1)$, $T = 0$ or 1 nuclei, it is expected
that the $T = 2$ levels are bound (or only slightly unbound, as in
the case of ^{12}C and ^{12}B) with respect to isospin-conserving heavy-

particle decay. In many of these nuclei (^{20}F and ^{28}Al are exceptions)
there are energetically allowed isospin-nonconserving particle decays.
In these cases, the small width of the T = 2 levels, reflecting the
isospin inhibition in the energetically allowed decay channels, is
as additional characteristic to be used for identification. In the
case of ^{12}C (and ^{16}O) Adelberger (1970) has noted that the energeti-
cally allowed and isospin-allowed decay by diproton emission is
severly inhibited by a small penetration factor, so that the width
should remain small compared with the widths of neighboring (T < 2)
states.

IV.   THE LOWEST T = 2 STATE IN ^{12}C AND ^{12}B

A.   Introduction

In a review article, Cerny (1968) presented excitation energies for the lowest T = 2 states in ^{12}C, observed in the ^{14}C(p,t) reaction, and ^{12}B, observed in the ^{14}C(p,^{3}He) reaction. The uncertainties quoted for these excitation energies (100 keV and 70 keV, respectively) were considerably larger than the limits desired for the present program. In addition, the data from these experiments have not been published, although the measurements were made several years ago. For these reasons, a decision was made in this laboratory to repeat these measurements (with ^{14}C targets prepared previously for other experiments) using a magnetic spectrograph to aid in particle identification and to improve the energy resolution.

The excitation energy of the lowest T = 2 state in ^{12}C can be predicted from relation III-6, proposed by Jänecke, or from relation III-2 using either the upper limit for the ^{12}Be mass (from β-decay endpoint energy estimates) (Poskanzer 1965) or the ^{12}Be mass predicted by the Garvey-Kelson mass formula (Garvey 1966). The results of these predictions are summarized in Table 2, along with the corresponding prediction for the T = 2 level in ^{12}B, from III-3, and the pertinent references. For convenience, the experimental results reported by Cerny are also included in this table.

The Q-values for the reactions in question are probably the most negative of any reaction yet studied in nuclear physics

($Q \sim -31$ MeV). Thus the bombarding energy required to initiate the reactions is for beyond the maximum available from the Caltech tandem accelerator, and the measurements had to be made at another laboratory which offered a higher-energy proton beam and a spectrograph. In addition, photographic plates could not distinguish the particles of interest well enough from other particles that were expected to be present, so the spectrograph should be equipped with adequate detectors, at the focal plane.

A first attempt at these measurements was made by Barnes in collaboration with workers at the University of Minnesota (Olsen 1968), using the proton linear accelerator. For this work the bombarding energy was 40 MeV, and an array of 32, 1000-μ, surface-barrier detectors was employed for particle detection at the focal plane of the spectrograph. No groups were seen in the regions of interest in either the triton or ^{3}He spectrum at 30° in the lab, but the results were inconclusive because of serious problems in particle identification.

In return for assistance from the Caltech group in the production of a set of ^{14}C targets for another experiment of interest to physicists at Oak Ridge, machine time on the Oak Ridge Isochronous cyclotron was made available for a second attempt to find the T = 2 states of interest, with the new and thicker targets. These measurements were also made at 40-MeV incident proton energy. Particles from the reaction were observed at the focal plane of the broad-range spectrograph by two solid-state position-sensitive detectors, 5 cm in length. This run was plagued by a number of problems, some

associated with the experimenters' unfamiliarity with the laboratory, and some attributed to instrumentation difficulties. Though a considerable amount of time was lost, the (p,t) reaction was studied at 30°, over a wide range of excitation energies centered at the value predicted for the T = 2 state in ^{12}C. Again, no groups were seen above the continuum yield and background. However, some particle-identification problems persisted, so that the conclusions still remained uncertain. From observations of lower excited states during this run, it was obvious that particle identification was considerably improved at higher triton energy. Thus another run was scheduled at Oak Ridge, to be made at 50 MeV bombarding energy. Again, the (p,t) reaction was studied in detail, and finally a narrow ($\Gamma \leq 50$ keV) group was located. Again a survey was made over several MeV in excitation energy. The data from this run will be discussed in detail in Section B of this chapter.

A third run was scheduled at Oak Ridge to examine the (p,^{3}He) reaction. In sharp contrast with the two previous occasions, this run was quite straightforward, partly as a result of the experience gained from the previous work, and also because the particle identification was considerably improved for ^{3}He particles. The bombarding energy was chosen to be 63 MeV, to improve the yield of the reaction, and the particles were again observed by position-sensitive detectors at the spectrograph focal plane. Two reasonably narrow groups corresponding to states in ^{12}B were observed in the region of excitation from 10 to 15 MeV. These measurements are discussed in Section C of this chapter.

The final section of this chapter is concerned with the prediction of the mass of ^{12}Be from the results of these experiments.

B. The Reaction ^{14}C(p,t)^{12}C

1. Experiment

For the final measurements of the reaction ^{14}C(p,t)^{12}C, the beam energy determined from the 153° analyzing magnet was 50.535 MeV. The two position-sensitive detectors were placed approximately midway along the focal plane of the Oak Ridge broad-range spectrograph. Both detectors were covered with foils consisting of 3-mil aluminum plus 1-mil mylar.

The first observations were made to establish the identification of the tritons in the energy spectra from the detectors. To this end, particles produced by bombarding an aluminum foil were observed at a magnetic field set for ~17 MeV tritons (near the energy calculated for tritons from the ^{14}C(p,t)^{12}C reaction corresponding to the predicted excitation of the T = 2 state). At this field setting, nuclear reactions on aluminum produce deuterons, tritons and alphas at the detectors, but no ^{3}He^{++} (from Q-value considerations). The tritons and alphas were stopped in the detector while the deuterons penetrated through the active region. Thus the highest-energy events forming a narrow line in the energy spectrum were identified as alpha particles. The tritons were then located as a sharp line at an energy $\frac{E(\alpha)}{3}$. To confirm this identification, the ^{14}C target was inserted, and alpha-particle groups were observed from the ^{14}C(p,α)^{11}B reaction

corresponding to the ground and low-excited state of ^{11}B.

A typical energy spectrum from the detectors is shown in Figure 8. The gains were adjusted so that the alpha line was off-scale, for the triton measurements. The triton group falls at ~channel 30. The broader group at ~ channel 14 is identified as deuterons. The smooth background is produced by a high-energy tail associated with the elastic proton groups (which have nearly the same rigidity as the tritons of interest), and, in part, by neutrons. (The latter contribution was confirmed by a short run with the spectrograph field turned off). The elastic protons apparently produce the high-energy background by scattering from nuclei within the detector along the active region; the protons thus deposit a considerably greater energy in the detector than the mean energy-loss for the protons passing through the detector.

The two-dimensional data array corresponding to this energy spectrum is shown in Figure 9. The diagonal cutoff on the right side is associated with the edge of the detector (see Appendix B). The triton line is again evident at (energy) channel 30. The high-energy tail from the elastic protons is seen as a broad smear on the left side of the array. Because of the logarithmic display scheme used, the deuteron group is lost in the background in this figure.

The triton spectrum was surveyed at 30° in the lab, over a range of energy corresponding to excitations in ^{12}C from 24.3 MeV to 29.4 MeV. The results of this survey are shown in a composite spectrum (Figure 10). Only one narrow group identified as tritons was observed above the continuum yield. The second group in the composite spectrum, to the left of the triton group, is associated

with the elastic protons discussed above. To confirm the identi-
fication of the one triton group with a level in ^{12}C, the ^{14}C target
was replaced by a natural carbon target of similar thickness and
construction, and the tritons produced by bombarding this target
were observed in the region where the group had been seen (insert
in Figure 10). The ^{14}C target was then reinserted and the group of
interest was observed at 25° and 20° in the lab. A typical triton
spectrum is shown in Figure 11, for a run at 25° spanning the
observed triton group. It was not seen in runs at 15° and 10°.

In changing from one angle to another, the focal plane was
not adjusted for changes in the kinematic broadening of the group.
A calculation of this effect showed that the group should be quite
broad at 10°, with the focal plane adjusted as it was for 30°. The
focal plane was reset for the 10° kinematics, and a survey of the
triton spectrum was again made (Figure 12). No narrow groups
(other than that associated with the elastic protons) could be
clearly discerned above the continuum at this angle.

Because of the limited accelerator time remaining, no
further investigation of the angular distribution was possible.
The magnet was moved to 20° and the focal plane was suitably ad-
justed. The narrow group was quickly located. A careful position
and field measurement was then made, with the kinematic-angle
defining slits at the spectrograph entrance reduced to improve the
resolution. Several alpha-particle groups from the ^{14}C$(p,\alpha)^{11}$B
reaction, corresponding to the ground and first-three-excited
states of ^{11}B, were observed for position and Q-value calibrations.

An alpha-particle spectrum produced by bombarding the aluminum target was also observed at approximately the same fields, to establish clearly the edges of the detector. Some typical alpha spectra are shown in Figure 13.

The ^{14}C target used for these measurements was brought back to Caltech where the thickness and composition were measured (see Section II-C, and Figures 5 and 6). The thickness data are summarized in Table 3.

2. Excitation Energy

For an accurate determination of the excitation energy of the observed ^{12}C state, the position of the group (and hence its energy) must be precisely extracted from the data. The relationship between pulse height, in the recorded position spectra, and position along the focal plane was constructed from a comparison of the calculated positions and observed spectra for the alpha-particle groups corresponding to states of ^{11}B. In particular, the ground-state alpha group was carefully observed at three points along the detector spanning the region where the triton group of interest had been observed. The positions of the alpha groups were calculated from the beam energy measured by the field at the 153° analyzing magnet, the measured target thickness, the spectrograph field, and the known masses and excitations (Mattauch 1965, Ajzenberg-Selove 1968). A best-fit polynomial (in the least-squares sense) was constructed for calculating positions (Figure 14). The excitation energy for the level in ^{12}C was then calculated from the position

determined from this calibration, the spectrograph field, the beam

energy, target thickness and nuclear masses.

The results of this calculation are summarized in Table 4,

for the ^{12}C level and the observed alpha particle groups. The data

in this table include all the observations of the triton group in

the number-2 detector, chosen for the Q-value measurement. (The

number-1 detector was not calibrated carefully, so no final results

have been taken from the data observed by this detector.) During

the 30° scan, the deuteron group from the $^{14}C(p,d)^{13}C$ reaction

corresponding to the lowest T = 3/2 state in $^{13}C(E_x = 15.112$ MeV)

was observed. The calculated excitation for this level is included

in Table 4 for completeness. However, this observation was not used

as an additional calibration because:

(1) a small change was made in the electronic circuitry

after the 30° scan, but before all the observations listed in Table 4,

which could have affected the position calibration, and

(2) the deuterons observed fell at ~ channel 15 in the

energy spectrum, while the alphas and tritons were generally ob-

served near channel 40. Thus the zero point correction for the

position spectrum is very important in comparing these spectra, and

the measurement of position zero was somewhat in doubt.

Energy loss in the target was calculated from the stopping

power formula given by Barkas (1964), with shell corrections. The

reaction angle was not adjusted to an effective value depending on

the kinematic-angle aperture (see Hensley 1969), since the focusing

properties of the Oak Ridge spectrograph should compensate for this

effect in first order, and the effect is small in any case.

The final value for the excitation energy was determined by averaging the results in Table 4, with the observation made at 20° with reduced kinematic-angle aperture having twice the weight of the remaining observations.

Because of the procedure used for calibration which located the triton peak in relation (principally) to the ground-state alpha group, the uncertainty in the excitation energy is rather sensitive to (and dominated by) the uncertainty in the beam energy. Since the alpha-particle and triton groups were observed at the same position and the uncertainty in the position of the tritons is equal to that in the position of the alphas, the dependence of the excitation on the beam energy can be written

$$\frac{dE_x}{dE_1} = \left(\frac{\partial E_x}{\partial E_1}\right)_t + \left(\frac{\partial E_x}{\partial E_3}\right)_t \left(\frac{\partial E_3}{\partial R}\right)_t \left(\frac{\partial R}{\partial E_3}\right)_\alpha \left(\frac{\partial E_3}{\partial E_1}\right)_\alpha$$

For a uniform-field spectrograph,

$$\frac{\partial E_3}{\partial R} = \frac{2E_3}{R}$$

so the above relation becomes

$$\frac{dE_x}{dE_1} = \left(\frac{\partial E_x}{\partial E_1}\right)_t + \left(\frac{\partial E_x}{\partial E_3}\right)_t \frac{(E_3)_t}{(E_3)_\alpha}$$

Inserting the numerical values for the kinematic factors at 20° gives the result

From a comparison of calculated and observed focal-plane
positions of states with precisely know Q-values in numerous nuclei,
observed in elastic scattering or reactions such as (p,d) by photo-
graphic emulsions at the focal-plane, the precision of the beam energy
has been found to be approximately 30 keV or less. Then the resulting
excitation energy and uncertainty for this level is

$$E_x = 27.595 \pm 0.020 \text{ MeV}.$$

3. Angular Distribution

The partial angular distribution measured for the 27.59-MeV
state is shown in Figure 15. The horizontal bars indicate the spectro-
graph aperture (in the center-of-mass system), while the vertical bars
indicate the uncertainty resulting from counting statistics and back-
ground subtraction. An additional uncertainty of 20% is assigned to
the absolute normalization. The points indicated at 14° and 19° are
upper limits estimated from the data in the region where the level
was expected, although no group could be discerned above background
at either of these angles. The target thickness used in extracting
the cross section was obtained from the measurements in Table 3,
corrected for hydrogen content in the target, assuming the polymer
to be $(CH)_n$.

Though the observed distribution is far from complete, it
does not appear to be consistent with the usual L = 0 pattern
expected for the lowest T = 2 state, since the forward-angle peaking
was not observed. However, a DWBA calculation of the L = 0 distri-

bution, using the potentials suggested by Cosper (1967) for $^{12}C(p,t)^{10}C$ (Appendix C), predicts an angular distribution which is qualitatively similar to the observed distribution (Figure 15); while the detailed shape of the predicted distribution is sensitive to the radial dependence of the absorptive potential, no strong forward-angle peaking is predicted at this bombarding energy.

Since the distribution measurements are incomplete and the experimental uncertainties were rather large, no firm L-value assignment can be made from these data. Because of the inconclusive nature of these measurements and the unorthodox shape predicted for the angular distribution at this bombarding energy, further study of this reaction is of considerable interest, both to extend the measurements at this energy and to measure the distribution at higher energy, where the L = 0 shape is predicted to be peaked at forward angles.

4. Width

From the observed width of the triton group and the calculated resolution at the focal plane of the spectrograph, an upper limit can be placed on the width of the 27.59 MeV state. The resolution was calculated by adding quadratically the contributions from energy losses in the target, residual kinematic broadening, and broadening produced by the last beam-focusing quadrupole lens before the target chamber. The last two contributions were calculated by a computer code (available at Oak Ridge) from the reaction kinematics, spectrograph aperture, focal plane orientation and quadrupole current. For observations of the ground-state alpha-particle group and the 27.59-

MeV state of ^{12}C at 20°, the various contributions to the resolution
and the observed widths (in particle energy) are summarized in Table 5.

The calculated resolution is dominated by the contribution
associated with the beam focusing (quadrupole). From a comparison
of the calculated resolutions and observed widths, it is apparent
that this term was overestimated in the initial calculation. The
quadrupole term was re-estimated by fitting the observed width of
the ^{11}B(g.s.) alpha group, using the target and focal plane terms
listed. The new value extracted for the quadrupole term was scaled
by the ratio of the previous values for this term for the two groups,
and this value was used to compute the revised total resolution
listed in the table. This entry is consistent (at least) with the
observed widths, though not reliable enough to extract a meaningful
value for the width of the ^{12}C level of interest. An upper limit
for the width can be established by dropping the quadrupole term
from the resolution and calculating a minimum resolution from the
target and focal-plane terms. The results for the two observations
listed are

$$\Gamma < 35 \text{ keV}$$

It is likely that this is a conservative estimate and that
the actual width is considerably less than this limit.

5. Conclusions

In this study of the reaction ^{14}C(p,t)^{12}C at 50.55 MeV
bombarding energy, only one narrow triton group corresponding to a

state in ^{12}C was observed in the region of excitation energy near that predicted for the lowest T = 2 state. Because of its narrow width (for such high excitation energy), and the excellent agreement between the predicted and measured excitation energies, this level is identified as the lowest T = 2 state. Because of the ambiguity resulting from the incomplete measurement of the angular distribution, further study of this state by the same reaction is of considerable interest, to verify the spin and parity of the state.

An intensive effort has been made by Black and collaborators at the Australian National University to locate this level as a resonance in an isospin-forbidden compound-nuclear reaction. Results for studies of ^{10}B + d and ^{11}B + p have indicated no resonances in the region of interest (Black 1970). With the aid of the results of the present ^{14}C(p,t)^{12}C measurement, a study was undertaken by the Australian group of the capture reaction ^{9}Be(^{3}He,$\gamma\gamma$)^{12}C, over a narrow range of excitation. The γ-decay is assumed to cascade through the lowest T = 1 state at 15.1 MeV. Preliminary results of this search indicate a weak, narrow resonance corresponding to a ^{12}C excitation of 27.585 ± .005 MeV, in good agreement with the present experiment. The width of the resonance observed is of the order of 5 keV or less.

C. The Reaction ^{14}C(p,^{3}He)^{12}B

1. Experiment

For the ^{14}C(p,^{3}He)^{12}B study, a ^{14}C target similar to the one used in the ^{14}C(p,t)^{12}C measurements was employed. These two targets

were prepared simultaneously; the polymer layers are expected to have equal thickness, within ~30%, and the gold layers were expected to be of the same thickness within ~10%. For this run, the beam energy was 63.4 MeV. The detectors were again placed midway along the focal plane. For the initial work, a 1-mil mylar foil was placed in front of the detectors.

To establish the particle identification, the energy scale in each detector was calibrated by observing the two alpha-particle groups from a ThC' source positioned directly in front of the detectors. The $^3\text{He}^{++}$ ions were then identified from combined energy and rigidity measurements. A particle group identified as alphas were evident at $\frac{3}{4} \text{E}(^3\text{He})$ confirming the particle identification. A typical spectrum of energy deposited in the detector is shown in Figure 16.

The ^3He spectrum was surveyed over a continuous region corresponding to ^{12}B excitations from 5 to 17 MeV, at 20° in the lab. A prominent, narrow group was observed near the predicted excitation for the ^{12}B (T = 2) state, as shown in the composite 20° spectrum (Figure 17). Another group observed at somewhat higher excitation was not as strongly populated, and in subsequent runs there was inconclusive evidence of a closely spaced doublet of levels. To confirm the correspondence of the observed groups with levels in ^{12}B, the ^{14}C was replaced by a ^{12}C target prepared in the same way, and the ^3He spectrum produced by bombarding this target was observed at the appropriate field settings (insert in Figure 17).

The ^{14}C target was then reinserted and a study of the angular

distributions was begun. A typical ^{3}He spectrum showing the ^{12}B
state at 12.7 MeV excitation from a single run at 8° is shown in
Figure 18. At first an attempt was made to study the angular dis-
tributions for both of the observed groups simultaneously by observing
one group in each detector. This was not feasible, however, since the
detectors could not be placed sufficiently close together to provide
unambiguous results for both groups, because of the mounting hardware
used. The two groups were then observed in separate runs at 6°, 10°,
and 15°, but the measurements on the weaker group (or doublet) at
higher excitation had to be discontinued to save time. The lower
level was then observed at 8°, 12.5°, 17.5°, 25°, 30°, 35°, and 41°
to provide a more complete angular distribution. For these measure-
ments, the focal plane was readjusted to the proper position for each
angle.

With the spectrograph positioned at 8° in the lab and a 5-mil
Al foil added in front of each detector (to provide better particle
identification at higher particle energies), careful position and
field measurements were made for the 12.7-MeV state, for a Q-value
determination. Then the ^{3}He group corresponding to the ground state
of ^{12}B was observed for a Q-value calibration.

Finally, the 5-mil Al foils were replaced by ladder masks of
10-mil Al. Alpha particles from a ThC' alpha source were observed
through these masks, to provide zero determinations (see Appendix B)
and position-dispersion measurements. The dimensions of the masks
were measured later by a travelling microscope.

2. Excitation Energy

The excitation energies for the two levels observed in the
region of interest were calculated from the exiting particle energy
measured by the spectrograph, the beam energy determined by the
beam-analyzing magnet, the target thickness measured for the match-
ing ^{14}C target (Table 3), and nuclear mass tables (Mattauch 1965).
For the spectrograph energy measurements, a position calibration
curve was constructed, for one of the detectors, from the ThC'
alpha-particle spectra observed through the ladder mask (Figure 19).
The effective center of the detector was adjusted to give zero ex-
citation energy for the ^{12}B-ground-state group observed at 8°. The
center determined in this way agreed within 0.5 mm with the nominal
center of the detector. The second detector was not calibrated
precisely for Q-value calculations, since most of the measurements
were made with the first detector, including all the observations
of the calibration groups (principally the ^{12}B ground-state group).

The results of these calculations are presented in Table 6
for observations of the 12.7-MeV state at seven angles, and for
one observation of the 14.9-MeV state. In addition, excitations
calculated for the ^{12}B ground and first-excited states and for the
first excited state of ^{14}N (observed at 8°) are included.

For the determination of the final value for the excitation
energies, the values in Table 6 were averaged, with the results for
6° and 8° having twice the weight of those from the other angles
because of the higher resolution used for these measurements, and

the higher yield. The uncertainty in the result was calculated by
adding quadratically the contributions from the uncertainty in
beam energy (see Section IV-B-2)

$$\Delta E_x = 0.284 \; \Delta E_1$$

and that from the uncertainty in exiting particle energy resulting
from uncertainty in position, estimated from the scatter in Table 6.
The final result for the excitation energy for the 12.7-MeV level is

$$E = 12.710 \pm 0.020 \; MeV$$

and for the 14.9-MeV level is

$$E = 14.860 \pm 0.030 \; MeV.$$

3. Angular Distribution

The angular distribution measured for the 12.7-MeV state
and the partial distribution measured for the 14.9-MeV state are
shown in Figure 20. The horizontal bars indicate the spectrograph
aperture (in the center-of-mass) and the vertical bars indicate the
uncertainty resulting from counting statistics and background sub-
traction. An additional uncertainty of 20% is assigned to the
absolute normalization. The target thickness used to extract these
cross sections was taken from the results in Table 3, corrected for
hydrogen content, assuming the polymer to be $(CH)_n$.

The smooth curve shown for the angular distribution of the
12.7-MeV state is the calculated L = 0 distribution from the code

JULIE. The details of the potentials used and the method of cal-
culation are summarized in Appendix C. The experimental distri-
bution is clearly in good agreement with the predictions for L = 0.

The partial distribution for the 14.9-MeV group is insuffi-
cent to make an unambiguous assignment of L-value.

4. Width

From the widths of the observed ^{3}He groups and the calculated
resolution at the focal plane of the spectrograph, estimates for
the widths of the two observed levels have been made. For several
observations at 8° with a kinematic aperture of 2° and at 10° with
a 4° aperture, the contributions to the resolution for the ground
state and two excited states of interest, and the observed widths,
are summarized in Table 7.

For these measurements, the calculated resolution is dominated
by the energy loss in the target. The estimated energy-loss strag-
gling in the target is small compared with the remaining terms, and
has been neglected. The observed width of the ground-state group
is somewhat larger than the calculated resolution. This may result
in part from the position resolution of the detector itself, since
the group is quite narrow in distance along the focal plane (~1.9 mm
FWHM). By assuming that the difference in observed and calculated
width for the ground-state group arises from this source (only),
an additional term can be extracted for the resolution function,
corresponding to a detector position resolution of 1.5 mm (FWHM).
The corrected resolution for the 12.7-MeV state determined in this

way is listed in the last column of Table 7. Using this calculated resolution, the width extracted for the 12.7-MeV state is

$$\Gamma(12.71) = 27.5 \pm 18 \text{ keV}$$

where a 15 keV uncertainty has been assigned to the corrected resolution. An upper limit for this width, obtained from the uncorrected resolution listed in Table 7, is

$$\Gamma(12.71) \leq 54 \text{ KeV}$$

Since the width of the 14.9-MeV group is considerably larger than the calculated resolution, it can be extracted with more confidence, if it is assumed to be a single state. Using the calculated resolution, the width is found to be

$$\Gamma(14.86) = (226 \pm 30) \text{ keV} .$$

A lower limit for this width can be found by assuming that the width of the 12.71 MeV state measures the resolution, and by adjusting this width for the small difference in energy loss for the two groups. The result of this calculation gives

$$\Gamma(14.86) \geq 221 \text{ keV} .$$

5. Conclusions

In this study of the $^{14}C(p, ^{3}He)^{12}B$ reaction at 63.44 MeV bombarding energy, two reasonably narrow groups corresponding to states of ^{12}B were observed in the region of excitation energy

between 10 and 15 MeV. Because of the agreement between the pre-
dicted and measured excitation energy, the small width, and the
L = 0 angular distribution for the 12.71-MeV state, this level is
identified as the lowest T = 2 state in ^{12}B. There is insufficient
evidence for an isospin assignment for the 14.86-MeV state; the
width is somewhat larger than would normally be expected for a
T = 2 state unless the observed group is, in fact, a doublet of
levels. [This level is unbound by only ~300 keV to the isospin-
allowed channel ^{10}B + d*(T = 1)].

D. Prediction of the Mass of ^{12}Be

Since the report of the discovery of the particle-stable
isotope ^{12}Be (Poskanzer 1965), no measurement has been made to
accurately determine the mass of this nuclide. An estimate for the
mass can be determined from the estimated beta-decay endpoint energy,
in the reference above. Cerny (1968) has quoted an upper limit for
this mass, presumably based on the estimated upper limit for the
beta-decay endpoint energy. A prediction by means of the Garvey-
Kelson mass formula (Garvey 1966) is lower than this upper limit
by 3.3 MeV. It is of interest to use the measured excitation energies
of the lowest T = 2 states in ^{12}C and ^{12}B to predict the mass of ^{12}Be,
for a comparison with these values.

From the quadratic nature of the mass law, it is readily
apparent that a prediction of the mass of ^{12}Be cannot be made dir-
ectly from the excitations of the two T = 2 states alone, since
there are three constants to be determined. Two schemes can be

proposed to provide an additional number to use for determining the constants:

(1) Assume the T-dependence of the coefficient of T_z can be neglected, and determine this coefficient from the mass difference $\Delta(1)$ of the $T = 1$ ground-state masses $(^{12}B - {}^{12}N)$.

(2) Use the Garvey-Kelson Formula for predicting the $(T = 2)$ mass difference $\Delta(2) = (^{12}Be - {}^{12}O)$, from which the coefficient of T_z can be determined directly.

There are indeed a number of mass relations attributed to Garvey and Kelson (e.g., see Garvey 1969). In the latter procedure outlined above, two such relations can be used, based on $T = 1$ or $T = 1/2$ nuclei, respectively:

$$\Delta(2) = (^{12}Be - {}^{12}O) = (^{10}Be - {}^{10}C) + (^{14}C - {}^{14}O)$$

and

$$\Delta(2) = (^{12}Be - {}^{12}O) = (^{9}Be - {}^{9}B) + (^{11}B - {}^{11}C) + (^{13}C - {}^{13}N) + (^{15}N - {}^{15}O)$$

where the nuclide symbols represent the ground-state mass of the nuclide indicated.

From the point of view of (1) above, the difference $\Delta(2)$ could be written

$$\Delta(2) = 2\Delta(1) = 2(^{12}B - {}^{12}N).$$

The G-K relations given above are thus seen as the use of a T_z-coefficient for $T = 2$ nuclei, obtained by averaging the T_z coefficient for $T = 1$ or $T = \frac{1}{2}$ nuclei over mass number in the region

of interest. In a review article on Coulomb-energy systematics, Jänecke (1969) has concluded that the vector Coulomb energy (i.e., the coefficient of T_z) to be essentially independent of T, for $T = 1/2$, $T = 1$, and $T = 3/2$ data over a wide range of nuclei, and to depend approximately linearly on A within a given subshell. Then to the extent that the T-independence of the vector Coulomb energy is also valid for $T = 2$ nuclei, either of the schemes proposed should provide an accurate estimate for the mass of ^{12}Be.

For either scheme, the resulting mass prediction becomes

$$^{12}\text{Be} = {}^{12}\text{C} + 4({}^{12}\text{B} - {}^{12}\text{C}) - \frac{\triangle(T)}{T}$$

where the nuclidic symbols now represent the $T = 2$ excesses of the nuclide indicated. The quantities $\frac{\triangle(T)}{T}$ and the resulting mass predictions for ^{12}Be are summarized in Table 8, along with the mass estimate and the upper limit established from the beta-decay end-point energy and the G-K prediction.

V. T = 2 STATES IN ^{20}F

A. Introduction

The identification of the lowest T = 2 states in ^{20}F and ^{20}Ne was first reported by Cerny (1964) from studies of the reactions ^{22}Ne(p,t)^{20}Ne and ^{22}Ne(p,^{3}He)^{20}F. These measurements have been repeated to provide more precise Q-value determinations (Hardy 1969). The precision of the excitation energy for the lowest T = 2 state in ^{20}F, from these more recent measurements, is 35 keV.

The T = 2 analogue state in ^{20}Ne has been located with a precision of 6 keV by Adelberger (1967a,b) in a study of the reaction ^{18}O(^{3}He,n)^{20}Ne. The results of these measurements have been confirmed and improved on by the observation of this state as an isospin-forbidden compound-nuclear resonance (Block 1967, Kuan 1967). The precision of these combined measurements of the excitation energy of the lowest T = 2 state in ^{20}Ne is 2.8 keV.

The excitation energy for the lowest T = 2 state in ^{20}F can be predicted either from the known mass of ^{20}O or from the excitation of the analogue state in ^{20}Ne, according to the relations given in Chapter III. These predictions are summarized in Table 9, together with the results of the ^{20}F measurements discussed above.

The present study of the reaction ^{18}O(^{3}He,p)^{20}F was undertaken shortly after the work by Adelberger (discussed above) on the ^{20}Ne analogue state, to provide a value for the ^{20}F(T = 2) excitation energy of comparable precision. The details of these measurements are discussed in the following section. Section C deals with the

determination of the excitation energies for the two states of interest. The angular distributions for the proton groups corresponding to these states are discussed in Section D. The last section summarizes the results and conclusions from this study.

B. Experiment

All the measurements of the reaction $^{18}O(^{3}He,p)^{20}F$ under consideration in this chapter were made at an incident energy of 12 MeV. The first data obtained for this study were collected simultaneously with deuteron and alpha spectra, by the use of the sixteen-detector array at the focal plane of the Caltech spectrograph. The results for the study of $^{18}O(^{3}He,\alpha)^{17}O$ have been reported separately (Hensley 1969); since this study was of considerable current interest, the measurements of the proton spectra were not optimized at that time. In particular, singly-charged ^{3}He ions were not adequately separated from the protons (which were passing through the detectors), so that a considerable background was superimposed on the proton spectra. Measurements were made both with self-supporting $Ni^{18}O$ targets and with a gas-cell filled with ^{18}O gas. The gas-cell target had a considerably smaller fraction of impurities (particularly ^{12}C and ^{16}O) than the $Ni^{18}O$ foils, but the experimental resolution was also considerably poorer. Because the proton spectra contained many groups in the region of interest, the gas-cell measurements were not adequate to allow separation and identification of the groups arising from ^{18}O, ^{16}O and ^{12}C.

The final data were taken with a freshly made $Ni^{18}O$ target

(to keep the ^{12}C and ^{16}O contamination as small as possible), and
a thick foil was placed over the detector array so that only protons
were observed. Although the loss of energy calibration groups from
the deuteron and alpha spectrum was regrettable, the improvement in
background more than justified this procedure. Proton spectra were
collected at 10° and 20° with this arrangement. The 10° spectrum
is shown in Figure 21, along with a similar gas-cell spectrum and
contaminant spectra (^{16}O and ^{12}C). A prominent group is apparent
at the expected position of the lowest T = 2 state in the spectrum,
corresponding to a state at 6.51-MeV excitation in ^{20}F. At ~1.7-MeV
higher excitation a weaker group was located. This group was seen
more clearly in the 20° spectrum (Figure 22). With a thin $Ni^{18}O$
target, to provide good resolution of the groups near the 6.51-MeV
state, the angular distributions was measured in the position-sensitive
detector. A typical position spectrum is shown in Figure 23. Because
of the difficulty in separating the 8.12-MeV state from an adjacent
proton group, only incomplete distribution measurements were made
for this group of protons.

C. Excitation Energy

The excitation energies of the two states of interest were
extracted from the proton spectra measured at 10° and 20° in the
sixteen-counter array. The ^{18}F ground-state group from $^{16}O(^{3}He,p)^{18}F$
(from ^{16}O impurities in the $Ni^{18}O$ target) was chosen for calibration,
since it falls near the 6.51-MeV ^{20}F group in the proton spectrum.
Since the groups of interest are all protons of comparable energies,

the Q-value measurements are relatively insensitive to errors in the spectrometer calibration, or to an incorrect (but consistent) assumption about the shape of the peaks in determining the central frequency. If the distributions of ^{16}O and ^{18}O in the target are similar, the energy losses are comparable for the ^{18}F calibration group and the 6.51-MeV ^{20}F group, and consequently the excitation energy extracted from these data is insensitive to the target thickness. The distributions of the oxygen isotopes in this kind of target has been studied in some detail by Hensley (1969), in his study of the $^{18}O(^{3}He,\alpha)^{17}O$ reaction. He found no evidence that the ^{16}O distribution is unsymmetric, with respect to the center of the target, and no disagreement between calibration groups based on ^{16}O and ^{18}O in the target. The ^{18}O distribution is expected to be symmetric from the procedure used to produce the targets. Thus for the present analysis the distributions of ^{16}O and ^{18}O in the target were assumed to be symmetric, and the same nickel and oxygen thicknesses were used for calculating energy losses for all the proton groups under consideration. Since deuteron and alpha spectra were not collected simultaneously with the proton spectra, no additional calibrations could be obtained from these particles. The proton groups from the reaction $^{12}C(He,p)^{14}N$ were not used for calibration purposes, because of the uncertainty in the location of the ^{12}C impurity within or on the targets.

The excitation energies extracted from the data are presented in Table 10, for the two observations of each of the two ^{20}F groups of interest and the ^{18}F calibration group. The tabulated uncertainty

is only that contribution from the estimated uncertainty in locating the centroid of each group. Additional contributions to the uncertainty of the final results arise from:

(1) the uncertainty in the $^{16}O(He,p)^{18}F$ Q-value

(2) the uncertainty in the calibration constant of the spectrometer

(3) the uncertainty in target thickness.

These contributions are listed for the two ^{20}F states of interest in the table below.

Contributions to the Uncertainties of ^{20}F Excitation Energies

(all entries in keV)

E_x	Q-value	Spectrometer	Target	Frequency	Total
6513	1	.4	.2	1.6	2.8
8210	1	.6	.3	2.4	3.4

To allow for possible small differences in the ^{16}O and ^{18}O distributions in the target, an additional (arbitrarily chosen) contribution of 2 keV was folded in to obtain the total uncertainty given in the table.

The final results for the Q-value measurements are shown in the table below. Since the ground-state mass excess of ^{20}F has been assigned an uncertainty of 4.7 keV (Mattauch 1965), the reaction Q-values as well as the excitation energies are presented. The uncertainties given for the excitation energies include the ground-

state mass uncertainty.

Q-values and Excitation Energies for T = 2 States in ^{20}F

State	Q-value (keV)	Excitation (keV)
Lowest T = 2	+258.5 ± 2.8	6513.3 ± 5.5
First-excited T = 2	-1338.5 ± 3.4	8210.3 ± 5.8

D. Angular Distribution

The angular distribution measured for the 6.51-MeV state is shown in Figure 24. The experimental errors shown are the result of counting statistics and a 5% uncertainty in the beam charge integration. An additional uncertainty of 30% is assigned to the absolute scale to include the target-thickness uncertainty for the thin Ni^{18}O target used for these measurements. The experimental points at 50° and 60° are estimated upper limits; the group was not identified above background at these angles.

The smooth curve shown in this figure is an L = 0 DWBA calculation for this reaction. The optical potentials used for this calculation are discussed in Appendix C. The excellent agreement between the measured and calculated distributions allows an unambiguous assignment of L = 0 for this transition.

A complete angular distribution was not obtained for the 8.21 MeV state because of the difficulty in separating this group from nearby groups. From the observations at 10° and 20°, this

group appeared to be the only one present, consistent with L = 2, near the predicted excitation of the first-excited T = 2 state.

E.   Conclusions

The T = 2 assignment for the 6.51-MeV level is confirmed by the L = 0 angular distribution and the good agreement of the measured excitation energy with that predicted for the lowest T = 2 state. The excitation energy determined in this experiment is in agreement with the results from the ^{22}Ne(p, ^{3}He)^{20}F measurements of Hardy (1969).

A T = 2 assignment for the 8.21-MeV state is tentative, based only on the difference in excitation energy from that of the 6.51-MeV state, and the consistency with an L = 2 assignment from the observations at 10° and 20°. More complete data are required for an L-value assignment. The measured excitation energy is roughly consistent with the early results presented by Cerny (1964) but falls slightly outside the probable error quoted for that measurement.

VI. T = 2 STATES IN ^{28}Al

A. Introduction

In a tabulation of the known T = 2 states in A = 4n, T = 0 or 1 nuclei, Cerny (1968) listed excitations for all such nuclei for $12 \leq A \leq 40$ with the exception of ^{28}Al and ^{28}Si. In a letter published later that year, McGrath (1968) presented data for the reaction ^{30}Si(p,t)^{28}Si from which the lowest T = 2 state in ^{28}Si was identified. Along with the excitation energy extracted for that state, a result is quoted for the excitation of the lowest T = 2 state in ^{28}Al from a study of ^{30}Si(p,^{3}He)^{28}Al. The data and final results from this work were presented in a more recent publication by the Berkeley group (Hardy 1970).

An independent study of the ^{28}Al T = 2 state, in the reaction ^{26}Mg(^{3}He,p)^{28}Al, has been reported by Clark (1970). In this work, the T = 2 state was identified from the predicted excitation energy and angular distribution, and from a comparison of the average yields for various levels in the reactions ^{26}Mg(^{3}He,p)^{28}Al and ^{27}Al(d,p)^{28}Al. The usefulness of such a comparison was considered briefly in Chapter III; although the isospin conservation should inhibit the T = 2 state in the (d,p) reaction, the effects of nuclear structure should be considered carefully, since the two reactions being com-pared are rather dissimilar. At best, the comparison can provide only a negative confirmation (a level strongly populated in (d,p) is not likely to be T = 2) or consistency check, as in the present case. An additional difficulty arises in this particular case from

the high density of T = 1 levels in the region near the T = 2 state in ^{28}Al; very precise measurements are required to confirm that the same levels are indeed being considered in the two reactions. In the study in question, no discussion of the precision is given; the excitation energy was taken from a compilation of levels of ^{28}Al (Endt 1967).

Table 11 summarizes the predicted excitation of the lowest T = 2 state in ^{28}Al and the results of the previous measurements of this excitation from the experiments discussed above.

The study of the reaction ^{26}Mg(^{3}He,p)^{28}Al was begun at Caltech before the publications described above had appeared, and the work was continued to complement the work already completed here and in other laboratories. Since the Caltech program has concentrated on precise Q-value measurements, and the precision of the work by Clark is uncertain, there is no serious duplication of effort. In addition to the study of the lowest T = 2 state, special attention has been given to the excitation energy region near that predicted for the first-excited T = 2 state ($E_x \approx 7.5$ MeV). The next section describes the details of the experimental measurements. Section C deals with the determination of the excitation energies for the states observed. The angular distributions of the proton groups are discussed in Section D. The results and conclusions from this study are summarized in the final section.

B. Experiment

All measurements of the reaction ^{26}Mg(^{3}He,p)^{28}Al were made at

12-MeV incident energy. Because of special difficulties in pro-
ducing thin transmission targets of ^{26}Mg from ^{26}MgO (see Section II-B)
the initial measurements were made on a target with $100\,\mu g/cm^2$
carbon backing. From a comparison of Q-values, it is evident that
the predicted ^{28}Al (lowest T = 2) group should be nearly coincident
in energy with the proton group corresponding to the first-excited
state of ^{14}N (^{14}N$_1$), from the ^{12}C(^{3}He,p)^{14}N reaction. In these
first measurements, the ^{14}N groups were much stronger than those
from ^{28}Al; however, a definite shoulder was observed on the high-
energy side of the ^{14}N$_1$ group indicating the presence of an un-
resolved group. Subsequently, ^{16}Mg targets were successfully
produced on thin gold backings, and new data were collected. A
comparison of proton spectra is shown in Figure 25, for the gold-
backed ^{26}Mg targets, and targets of the principal contaminants
expected in the ^{26}Mg target (^{12}C, ^{16}O and ^{24}Mg). These spectra are
plotted from observations made at 10°. A strong proton group is
observed in the spectrum from the ^{26}Mg target close to the predicted
excitation of the lowest T = 2 state. A comparison of the ^{14}N
ground-state group in this spectrum with that in the spectrum from
a carbon target confirms that the group of interest was not pro-
duced by ^{12}C impurities in the target.

The sixteen-detector array was used for precise Q-value
measurements; proton, deuteron, and alpha-particle spectra from ^{3}He-
induced reactions were collected at several angles. Considerable
care was taken to separate the protons from singly-charged ^{3}He
particles, in these measurements. The target thickness was measured

by the elastic-scattering techniques described in Chapter II.

The angular distributions of several proton groups near the lowest T = 2 state were obtained during the above measurements. For the final angular distribution measurements for the lowest T = 2 state, a complete distribution was measured using the position-sensitive detector at the spectrograph focal plane. A typical position spectrum is shown in Figure 28.

The array data were studied carefully in an attempt to locate the first-excited T = 2 state. At forward angles, the region of interest contained proton groups from the first several excited state of ^{18}F. From a comparison of the proton spectra from ^{16}O and ^{26}Mg in Figure 26, it is evident that the oxygen content of the ^{26}Mg target is reasonably small, as shown by the ^{20}F ground-state group. By a careful consideration of relative yields in these two spectra, the proton group at 33.35 MHz has been identified as a state in ^{28}Al. A detailed spectrum from this energy region is shown in Figure 27, for 20°, where the composite group is partially resolved into a doublet. The ^{28}Al identification is substantiated from kinematic tracking at 20°, 30° and 40°.

C. Excitation Energy

The primary Q-value calibration was taken from the deuteron group corresponding to the lowest T = 3/2 state in ^{27}Al at (6.815 ± .002) MeV (Endt 1967). Additional calibration checks were obtained from the ^{25}Mg-ground-state alpha group and the tritons feeding the 1.059-MeV state of ^{26}Al (Endt 1967). The rigidity of

the deuterons was quite similar to that of the (^{28}Al) proton group
of interest; the alphas and tritons had higher rigidity, similar
to that of the ground-state protons. Both the deuteron group and
the alpha group were strongly populated at forward angles; the
triton group was considerably weaker. The ground-state proton
group was also weak and could not be resolved from the first-excited
state (E_x = 31 keV). Although the ^{28}Al T = 2 proton group was very
close to the ^{18}F ground-state group (from ^{16}O contamination in the
target) and the ^{14}N first-excited state (from ^{12}C in the target),
these groups were not used for calibration because of the uncertainty
in the location of the carbon and oxygen in the target, relative to
the magnesium. For the Q-value calculations the ground-state masses
were taken from recent tabulations (Mattauch 1965).

Excitation energies calculated from the data are presented
in Table 12, for several observations of the 6.00-MeV state and
the members of the 7.5-MeV doublet. The excitations calculated
for the calibration groups discussed above are also included in
this table. The uncertainties listed in the table are the contri-
butions to the total uncertainty associated with the determination
of the central frequency for the group under consideration. Addi-
tional contributions to the probable error of the Q-value arise from
uncertainties in the target thickness, spectrometer calibration and
calibration Q-values. These contributions and the resulting assigned
probable error of the Q-values are listed in the table below.

Contributions to the Uncertainties of Measured Q-Values

(all entries in keV)

State	Frequency	Q-value	Spectrometer	Target	Total
Lowest $T = 2$	2.5	2.7	1.5	1	4.1
7.5-MeV doublet	10	2.7	1.5	1	10.5

The reaction Q-values and excitation energies determined for the three ^{28}Al states of interest are presented in the table below. The uncertainty of the excitation energy in each case was determined by combining the uncertainty for the corresponding Q-value with the uncertainties of the ground-state masses of ^{26}Mg and ^{28}Al (1.8 keV and 3.7 keV, respectively).

Q-values and Excitation Energies for States in ^{28}Al

Q-value (keV)	Excitation (keV)
2287.0 ± 4.1	5996.6 ± 5.8
835 ± 11	7448 ± 11
792 ± 11	7491 ± 11

D. Angular Distribution

The angular distribution for the 6.00-MeV state is shown in Figure 28 (from the measurements made with the position-sensitive detector). The experimental uncertainties are the result of counting

statistics and background subtractions. An additional uncertainty of 10% is assigned to the absolute normalization, arising from uncertainties in target thickness and beam integration.

The smooth curve shown is an L = 0 DWBA calculation for this reaction. The optical potentials used for this calculation are discussed in Appendix B. The good agreement between the calculated and measured distributions allows an unambiguous assignment of L = 0 for this transition.

The doublet observed at ~7.5 MeV excitation was studied carefully in the array spectra, in an attempt to extract angular distributions for the separate members. The distributions extracted for these two groups are shown in Figure 29. As a result of the difficulties in separating the two weakly populated groups in the region where the background is somewhat uncertain, the errors are rather large. The points indicated at 32° and 42° for the 7.45-MeV state are upper limits only; the group was not clearly resolved from contaminant peaks at these angles.

Calculated distributions for L = 1 and 2 are shown with the measured distributions. The distribution of the 7.49-MeV state is in reasonable agreement with the L = 2 distribution; that of the 7.45-MeV state is more likely to be L = 1, though no firm assignment can be made.

E. Conclusions

From the L = 0 angular distribution and the agreement of the measured excitation energy with that predicted for the lowest T = 2 state, the 6.00-MeV state is identified as the lowest T = 2

state in ^{28}Al. From this T = 2 assignment, the spin and parity for this level are inferred to be 0^+. From an examination of the doublet near 7.5-MeV excitation, the member at higher excitation is tentatively identified as the first-excited T = 2 state, on the basis of the L = 2 angular distribution and the agreement of the measured excitation (relative to the 6.00-MeV state) with the known level spacing of ^{28}Mg. A corresponding tentative assignment of spin and parity 2^+ is therefore made for this state.

Although the measured excitation energy of the 6.00-MeV state is in reasonable agreement with that of a state identified in the ^{27}Al(d,p)^{28}Al reaction (5989 ± 10 keV) (Endt 1967), there is insufficient evidence for assuming these to be the same state. In particular, if such an identification is made, it is of considerable interest -- not that the level is somewhat inhibited in the ^{27}Al(d,p)^{28}Al reaction, as Clark (1970) has pointed out -- but rather that it is so strongly excited in an isospin-forbidden reaction. This would imply an unusually large admixture of T = 1 strength in the state. While it seems likely that two different states at nearly the same excitation have been observed in the two reactions, it would be worthwhile to attempt to confirm this hypothesis by additional high-resolution studies of the two reactions.

VII. T = 2 MULTIPLETS AND THE QUADRATIC MASS EQUATION

A. Introduction

In recent studies of $T = 3/2$ multiplets, the quadratic mass law has been tested by a comparison of measured masses for the members of completed quartets to the predictions of the mass formula. Although six multiplets have been completed, for A = 7, 9, 13, 17, 21, and 37 (Jänecke 1969), only one (A = 9) has precision mass measurements for all four members. In this case, as well as the other five listed, the deviations of the measurements from the predictions of the quadratic mass formula are relatively small and appear to be consistent with the contributions expected from higher-order perturbation terms (Nettles 1969).

The $T = 2$, $A = 4n$ multiplets discussed in this report cannot be used at present to test the quadratic nature of the mass law, since mass measurements have been made for only three members of each multiplet (except A = 8 and 12, where only the masses for two members have been measured). However, if the quadratic law is assumed to be exact, the three coefficients for this formula are determined by the three measured masses for each multiplet.

In his review article, Jänecke (1969) has investigated the (A,T) dependence of Coulomb energies $E_C^{(1)}$ and $E_C^{(2)}$ (determined from the coefficients of the mass equation by the relations given in Appendix D) for $T = 1$ and $T = 3/2$ multiplets. It is of some interest, then, to compare the results obtained from $T = 2$ multiplets with those

previous results.

In the following sections, the quadratic form of the mass formula is assumed to be exact. In Section B, the Coulomb energies and the isoscalar term determined for $T = 2$ multiplets in $A = 8$, 12, 16, 20, 24, and 28 are discussed. Section C deals with some of the predicted properties of the unobserved members of these multiplets.

B. Mass-Equation Systematics for $T = 2$ Multiplets

The measured masses for $A = 4n$, $T = 2$ multiplets are summarized in Table 14, with references. The simple formulas used for calculating the coefficients a, b, and c for the mass law

$$m(A,T,T) = a(A,T) + b(A,T)T_z + c(A,T)T_z^2$$

are given in Appendix D, along with the definition of Coulomb energy terms.

Table 15 summarizes the coefficients a, b, and c determined for the $A = 4n$ multiplets. For $A = 8$ and 12, the assumption outlined in Chapter IV that b is independent of T has been used to extract the c coefficient. The Coulomb energies $E_C^{(1)}$ and $E_C^{(2)}$ are also tabulated.

In Figure 30, the vector Coulomb energies $E_C^{(1)}$ for $T = 2$ multiplets are compared with those extracted from $T = 1$ multiplets. The experimental uncertainties are less than 20 keV in all cases. No $T = 2$ data are given for the p-shell multiplets ($A = 8$ and 12) since masses for only two members of the multiplets are known.

A definite break in the curve is seen at $A = 16$, corresponding

to the closing of the p-shell. The $T = 1$ data at $A = 16$ are in question, since there is an inversion of the analogue levels in ^{16}O, resulting from substantial Thomas-Ehrman shifts, since the $T = 1$ states are unbound in ^{16}O and ^{16}F. It is nevertheless interesting to note that the value of $E_C^{(1)}$ for mass-16 is much closer to the extrapolated s-d shell results than to that of the p shell, for both the $T = 1$ and $T = 2$ multiplets. If the Coulomb energy is approximated by that for a charged sphere of radius $r_0 A^{1/3}$, then the vector term $E_c^{(1)}$ should be proportional to $(A-1)/A^{1/3}$. From the data, it appears that the A-dependence is more nearly linear within a subshell, as already noted by Jänecke. The vector term appears to be nearly independent of T for the $T = 1$ and $T = 2$ multiplets in the s-d shell, which supports the validity of the procedure used in Chapter IV for the ^{12}Be mass prediction.

The data for $E_c^{(2)}$ for $T = 1$ and $T = 2$ multiplets are compared in Figure 31. The experimental uncertainties are less than 10 keV for all cases except the $T = 2$, $A = 8$ and $A = 12$ data, where an uncertainty of 30 keV is assigned to take account of the procedure used to extract these numbers. There is an additional uncertainty of 10 keV for the $A = 8$ value from experiment. As noted by Jänecke, the $T = 1$ data are divided into two classes, for $A = 4n$ and $A = 4n + 2$ respectively. With the exception of $A = 12$, there is rough agreement of the $T = 1$ and $T = 2$ values for $A = 4n$ nuclei. The effects observed for the $T = 1$ multiplets at $A = 16$ and 28 may be the result either of shell closure or of large energy shifts resulting from threshold effects or isospin mixing. From the charged-sphere approximation,

the A-dependence of the tensor term is predicted to be $A^{-1/3}$. From

the available data, there is insufficient evidence to test this

prediction decisively; the data (for T = 2 multiplets, except A = 12)

are consistent with an $E_c^{(2)}$ that is nearly independent of A.

In Figure 32, the isoscalar coefficients, a, obtained from the

T = 2 data are compared with those for the lowest T = 1 multiplets

and the T = 0 ground-states for A = 4n nuclei. These values, which

are dominated by the binding energy arising from the strong nuclear

interactions, show definite evidence for the shell closure at mass

16, in the T = 0 and T = 1 values, but no comparable effect for the

T = 2 data.

C. Predictions for Unobserved Proton-Rich
Members of T = 2 Multiplets

The relationship predicted from the quadratic mass law for

the masses of T_z = -1 or -2 members of a T = 2 multiplet, in terms

of the T_z = 0, 1, and 2 masses, is given in Appendix D. Using

this relation, the masses of the unobserved T_z = -2 nuclei ^{12}O,

^{16}Ne, ^{20}Mg, ^{24}Si, and ^{28}S were calculated from the data in Table 14.

These masses are compared with the p and 2p thresholds in Table 16.

From this comparison, it is evident that the nuclei ^{20}Mg, ^{24}Si and

^{28}S are expected to be stable with respect to heavy-particle decays

while ^{12}O and ^{16}Ne should be unbound. The masses and excitation

predicted for the T = 2 analogue in the corresponding T_z = -1 nuclei

are summarized in Table 17 and compared with the isospin-allowed

decay channels, p + (A - 1, T = 3/2), and 2p + (A - 2, T = 1). The

levels in ^{20}Na, ^{24}Al and ^{28}p are thus expected to be bound relative to isospin-allowed decays, while those in ^{12}N and ^{16}F are unbound to isospin-allowed channels.

D. Conclusions

The data for T = 2 multiplets in A = 4n nuclei are not yet complete enough to test the accuracy of the quadratic mass formula for isobaric multiplets. However, these data do provide values for the mass formula coefficients, under the assumption that the formula is exact.

The comparison of values of $E_c^{(1)}$ (related to the coefficient of T_z) for T = 1 and T = 2 multiplets supports the assumption often made that this term is practically independent of T. The dependence on mass number is very nearly linear within a subshell, with a distinct break at the shell closure. The tensor Coulomb energy term $E_c^{(2)}$ (related to the coefficient of T_z^2) shows no distinctive dependence on A or T, though the values for T = 1 and T = 2 are somewhat different. It is likely, since this term is most sensitive to the omission of higher-order terms in the mass formula and to energy shifts resulting from isospin mixing or threshold effects in the members of a multiplet, that systematic effects for $E_c^{(2)}$ cannot be firmly established until additional members of these multiplets are observed, to establish in each case whether the deviations from the quadratic formula are small. The isoscalar coefficient a, which is dominated by the nuclear binding energy terms, reflects the energy required to promote particles from the lowest allowed configuration

(T = 0) to the first configuration in which the particles can be coupled to T = 2. This term is very nearly linear in A in the s-d shell multiplets; the relatively large variations at A = 8 and 12 are not understood.

From the assumed quadratic mass formula, the masses for the proton-rich members of the A = 4n multiplets for A = 12 through 28 have been predicted and their stability to heavy-particle decay estimated. It is of considerable interest in the extension of these studies to attempt to measure the masses for these nuclides, and to observe the analogue states in the T_z = -1 nuclei.

VIII. CONCLUSION

The two-nucleon-transfer reaction (^{3}He,p), (p,^{3}He) and (p,t) on $T = 1$ target nuclei have been utilized quite successfully to excite $T = 2$ states in $T = 0$ or 1, $A = 4n$ nuclei. Of these three reactions, considerable experience has been developed in this laboratory only with the (^{3}He,p) reaction, at Van de Graaff energies. This reaction has become less selective in populating $T > |T_z|$ states as the studies have extended beyond the p-shell. In particular, the relative strength for populating excited $T = 2$ states is considerably weaker at $A = 20$ or 28 than for (say) $A = 16$ (Hensley 1968). This results in part from the fact that the $T > |T_z|$ states of interest have occurred at successively lower excitation energy as the studies have been extended up in mass number, so that the adjacent $T_<$ states have been   relatively simpler in structure and hence have competed more strongly in the reactions observed.

The use of magnetic analysis techniques has been extremely successful and rewarding, in these studies, for clarifying particle-identification and facilitating precision Q-value measurements. The observations of reactions (^{3}He,d), (^{3}He,α) and (^{3}He,p) simultaneously have been useful for providing Q-value calibrations for the observations of interest, as well as additional data on states with $T > |T_z|$ in other nuclei.

The measurement of masses for several members of a given multiplet has made possible the prediction of the masses of the remaining proton-rich members and the available decay modes for these

nuclides. In the continuation of these studies, it will be of great
interest to explore new reactions which might produce the stable $T = 2$,
proton-rich nuclides and allow a mass measurement. In addition, it
is of great interest to obtain a measurement of the ^{12}Be mass and
that of the $T = 2$ state in ^{8}Li, to complete these studies in the p-
shell. The latter measurements should be possible in the near future
by means of two-nucleon transfer reactions on the high-quality ^{10}Be
targets now in preparation at Brookhaven and Los Alamos. Other more
esoteric reactions have been proposed, such as $(^7\text{Li}, 2p)$ or $(^7\text{Li}, 2n)$
but these offer considerable experimental problems and are not so
likely to be favored by nuclear structure considerations.

The extension of the study of $T = 2$ states can also be
attempted in the $A = 4n + 2$ nuclei, by using charge-exchange reactions
such as (p,n), $(^3\text{He},t)$, $(t,^3\text{He})$, $(^7\text{Li},^7\text{Be})$, $(^7\text{Li},t)$, etc. The $T = 2$
states are less likely to be bound in these cases (since the parent
nuclei are odd-odd). These studies are expected to be more difficult,
too, because of the uncertainty in reaction mechanisms for reactions
such as those outlined above, and as a result of the uncertainty in
predicting spins for the parent nuclei.

The uncertainty in interpreting the angular distribution for
the observed lowest $T = 2$ state in ^{12}C requires that this state be
studied further. In the systematics discussed in the previous chapter,
there were noticeable deviations for $A = 12$ which may be associated
with this difficulty. It will be very interesting to compare the
present results with those from $^{10}\text{Be}(^3\text{He},n)^{12}$C studies, if the latter
reaction becomes feasible.

Finally, the extension of these studies to the measurement of isospin-forbidden decay channels, such as the recent studies of Adelberger and McDonald in $T = 3/2$ multiplets (e.g., Adelberger 1969b), and McGrath (1969) in $T = 3/2$ and $T = 2$ multiplets, will allow a better understanding of the structure of these states and may provide more detailed evidence of the nature of the isospin-dependent forces in the nucleus.

APPENDIX A

PARTICLE-ENERGY DETERMINATION FROM SPECTROGRAPH DATA

A key step in the procedure outlined in Chapter II for extracting precise reaction Q-values from the Oak Ridge and Caltech spectrograph data is the calculation of the particle energy from the measured position of the group at the focal plane. Since the two instruments used in the present work have quite different design and instrumentation, as well as diverse histories, the calculations will be discussed separately for the two devices.

A. The Broad-Range Spectrograph at Oak Ridge

The kinematic energy of a particle with charge Ze and mass M, bent in an arc of radius R by a uniform transverse magnetic field B, is

$$E = M\left(\sqrt{1 - \left(\frac{Z\,B\,R}{K\,M}\right)^2} - 1\right)$$

where K is a constant determined by the units used. For B in kilogauss, R in inches, and M and E in MeV,

$$K = 1.3132417$$

Since the focal plane can be both tilted and translated to adjust the focusing properties for different reactions, the orbit radius R is a complicated function of the observed position X_d on the focal plane. The average radius R is calculated from the effective position X_e of a group (determined by a straight-line

projection of the observed position onto a nominal focal plane

position, as discussed below) by means of the relation (Ball 1968)

$$R = \sum_{n=0}^{3} C_n X_e^{\,n}$$

For X in cm and R in inches, the coefficients C_n are:

n	C
0	27.52
1	1.9227×10^{-1}
2	-0.50623×10^{-6}
3	$+0.76329 \times 10^{-9}$

The geometry of the projection to determine X_e from X_d is

illustrated in Figure 5. The orientation of the focal plane is

controlled by two screw shafts, one of which is rigidly mounted

to a reference surface. The orientation is measured by the di-

mensions D_1 and D_2. Using the notation of Figure 7, the effective

position X_e is related to the observed position X_d by

$$X_e = X_d \cos \Theta + \Delta_1 + \Delta_2$$

where

$$\Delta_1 = L(1 - \cos \Theta),$$

$$\Delta_2 = \frac{(D_1 - D_0) - [X_d \cos \Theta + L(1 - \cos \Theta) - L_2] \tan \Theta}{\tan \Psi}$$

and

$$\Theta = \tan^{-1} \frac{D_1 - D_2}{L_1}$$

The dimensions used for the calculations were :

$$L_1 = 52.058 \text{ inches}$$

$$L_2 = 0.87 \text{ inches}$$

$$L = 86.92 \text{ inches}$$

$$D_0 = 3.074 \text{ inches}$$

$$\Psi = 37.5°$$

B.   The Caltech Spectrograph

The data for precise Q-value measurements observed in the Caltech 61-cm-radius, double focusing spectrograph were measured by the sixteen-counter array at the focal plane. The calibration of this system and the data handling have been discussed in detail by McNally (1965) and Moss (1967). In brief, the counter positions and the dispersion characteristics of the instrument were combined with the measured field (NMR frequency) to determine an effective field f for each detector. Then the data were plotted as counts versus effective field. The kinetic energy of a particle of mass M (units of the proton mass) and charge Ze is determined from the effective field f by the relation

$$E = M\left(\sqrt{1 - K\left(\frac{fZ}{M}\right)^2} - 1 \right)$$

The calibration factor K is slightly field dependent (McNally 1965). The value of K was calculated from the relation

$$K = K_0(1 + \Delta)$$

where Δ was determined by a smooth interpolation (using Lagrangian coefficients for first and second differences) in Table 1. The constant K_0 is defined to be the value of K for the 8.795 MeV ThC" α-particle group. Usually the correct K for a particular data set was inferred from a best fit (in the chi-square sense) to several calibration groups. The nominal value of K_0 (corresponding to the observation of the α-source group at $f = 27702$ kH$_z$) is

$$K_0 = 1.1383484 \times 10^{-5} \ (\text{keV/kH}_z)^2 \ .$$

APPENDIX B

POSITION-SENSITIVE DETECTORS

The construction and principles of operation of a solid-state position-sensitive detector are described in several articles (for example, Bock 1966, Kalbitzer 1967, Doehring 1968, Melzer 1968, and Kalbitzer 1970) and will not be reviewed here in detail. The detectors used for the experiments discussed here were 4 or 5 cm in length, 1 cm in width, and about 400 microns in (active) thickness. The detector provides two signals of opposite polarity. The integrated charge of the first signal is proportional to the energy E deposited in the detector, while that of the second signal is proportional to $(\frac{X}{L})E$ where L is the detector length and X is the distance lengthwise along the detector at which the event was detected. To extract the position information properly, the second signal should be divided by the first. Such arrangements have been used successfully (Bock 1966) but require some care, as well as moderately sophisticated instrumentation.

If the energy E is essentially constant across the detector $[(\frac{\Delta E}{E})^2 \ll (\frac{\Delta P}{P})^2$ where ΔP is the desired position resolution], and the group of interest produces a distinct line with little or no background in the energy spectrum, then the position spectrum can be monitored directly with a simple gating arrangement, such as the one shown schematically in Figure 6 for the measurements at Caltech. This system could be modified to store spectra for several particle

groups, though the operation grows increasingly complex with the addition of more channels. It is especially awkward if the experiments involve frequent and substantial changes in particle energy.

A more versatile approach was chosen for the work at Oak Ridge (Figure 7). The events were recorded in a two-dimensional array according to the two signals from the detector. In such an array (Figure 13) the upper edge of the PSD appears as a line ($X = L$). These arrays [(dimensioned 50 x 200 for E x (PxE)] were dumped to an on-line computer where the spectra were summed over fixed limits in the energy spectrum, to monitor the position spectrum during the run. The data were then stored on magnetic tape for further analysis offline. To obtain final spectra, the particle group was located in the energy spectrum (Figure 12). To "divide out" the energy dependence, the position spectra corresponding to the several energy channels spanning the peak and adjacent background were compressed to equal lengths (100 channels) and summed. A smooth background was subtracted in each position channel, when necessary. This process (or any equivalent procedure) is sensitive to the zero levels for both energy and position. The energy zero was checked by observing two particle groups of known energy (e.g., alpha particles and tritons) in the detector at the same time. The position zero could then be obtained from the intersection of the edge line with the energy zero. These measurements were confirmed in the (p,t) experiment by pulser measurements, and in the (p,^{3}He) by observing the two α lines from a ThC' alpha source through a ladder mask, and extrapolating to the common zero point.

In actual operation, the position signal, when corrected
for energy dependence, is not precisely proportional to distance
along the detector, but rather is a smooth function of position
with small quadratic and cubic dependence on X. This departure
from linearity affects not only the centroid of peaks observed
in the detector, but also the relative yield from channel to chan-
nel, since equal increments of pulse height (i.e., channels) at
different locations along the detector span slightly different
increments of position. This effect does not alter the inte-
grated yields, provided the background is subtracted properly,
but does produce some distortion in a spectrum that should be flat.
This shape can be removed by multiplying the counts in each channel
by $(\frac{dX}{d \text{ channel}})^{-1}$, which can be calculated from the position versus
pulse-height calibration. This procedure was used to construct the
composite spectra presented in the present work (Figures 10, 12, 17),
but the single-run spectra (such as Figure 11) were left uncorrected.

APPENDIX C

ANALYSIS OF ANGULAR DISTRIBUTIONS FOR
TWO-NUCLEON-TRANSFER REACTIONS

The mechanism of the two-nucleon-transfer reactions under consideration in this work was assumed to be the direct transfer of an s-state di-nucleon for the cases of interest. Several aspects of this assumption have been discussed by Glendenning (1961), Newns (1960), and Adelberger (1967a). The theory of direct reactions has been discussed rather completely by a number of authors (e.g., Tobocman 1961, Bassel 1962, and Satchler 1964), and will not be reviewed here. The $(p, {}^3He)$ and $({}^3He, p)$ reactions transfer a (n-p) di-nucleon in either a singlet or triplet spin state; the (p,t) transfers a di-neutron in a singlet state. The selection rules for these reactions are different for the two spin states. Since the target nuclei for all the reactions in the present work were $J^\pi = 0^+$, $T = T_z = 1$ nuclei, these rules can be written:

$$
\begin{array}{ll}
\underline{\vec{S} = 0} & \underline{\vec{S} = 1} \\
T_f = 0, 1, 2 & T_f = 1 \\
\vec{J}_f = \vec{L} & \vec{J}_f = L + 1 \\
\pi_f = (-1)^L & \pi_f = (-1)^L
\end{array}
$$

where $\vec{S}$ is the spin of the transferred di-nucleon, $\vec{L}$ is the angular momentum of the di-nucleon around the core nucleus, and T_f, J_f, π_f are the isospin, spin, and parity, respectively, of the residual nucleus. Obviously the (p,t) reaction is the only one of these

three reactions which can populate T = 0 states, since only this
reaction feeds T_z = 0 nuclei, for the target nuclei employed in
the present study.

The shape of the angular distribution is determined prin-
cipally by the angular momentum transfer L. If L is determined
from the measured distribution, the selection rules can be used to
interpret this information in terms of the spin and parity of the
residual nucleus.

For the determination of the angular momentum transfer, an-
gular distributions for several values of L were calculated for
each reaction, from the (zero-range) Distorted-Wave Born-Approxi-
mation (DWBA) theory of direct reactions, by the computer code
JULIE (Bassel 1966). These calculated distributions were subse-
quently compared with the experimental results. For this calcu-
lation, the transition amplitude is determined from wave functions
that are eigenfunctions of the optical plus Coulomb potentials in
the entrance and exit channels, i.e., wave functions which asymp-
totically describe the elastic scattering process for the channel
of interest. The general form of the optical potentials used for
the calculations is

$$U(r) = -V \, f(x) - i(W - W' \, \frac{d}{dx}, [f(x')] + (\frac{h}{m_\pi c})^2 \, V_{so} \, \frac{1}{x} \, \frac{d}{dx} \, [f(x)] \, \vec{1} \cdot \vec{\sigma}$$

$$x = \frac{r - r_0 A^{1/3}}{a} \, , \quad f(x) = (1 + e^x)^{-1}$$

In practice, since elastic scattering has not been studied
for a number of the channels under consideration, the procedure has

been to select potentials determined for similar channels, and similar energies, to those of interest. Table 13 summarizes the parameters used for analysis in this work and the sources of these parameters. In general, these potentials were chosen as the simplest and/or most readily available potentials which produced satisfactory fits to the data. The potentials for the $^{14}C(p, {}^{3}He)^{12}B$ distribution were taken from a study by Cosper (1967) of the reaction $^{12}C(p,t)^{10}C$ at a number of energies up to 50 MeV. The potentials for the $^{14}C(p,t)^{12}C$ and $^{14}C(p, {}^{3}He)^{12}B$ distributions were initially taken directly from a study by Cosper (1967) of the reaction $^{12}C(p,t)^{10}C$ at a number of incident proton energies up to 50 MeV. These data were fitted with an optical potential similar in form to the potential given above with $W = 0$ (i.e., a surface-absorption potential only). The parameters obtained from that study were presented as smoothly varying functions of incident energy and excitation energy in the residual nucleus. It was found in the present work that the fit to the $(p, {}^{3}He)$ distribution was substantially improved by assuming a volume-absorbing potential $(W' = 0$, above). The calculated (p,t) distribution was altered slightly by a similar change in radial dependence of the absorptive potential, but in either case, the strong forward-angle peaking usually obtained for $L = 0$ transitions was not predicted. For the $^{18}O(He,p)^{20}F$ distribution, the potentials chosen were those used by Hensley to fit $({}^{3}He,p)$ distributions for reactions on ^{11}B, ^{15}N and ^{19}F. These potentials did not produce satisfactory fits for the $^{26}Mg \, ({}^{3}He,p)^{28}Al$ distribution, so the potentials used by Clark (1970) in a similar study of this reaction

at 10 MeV incident energy, were chosen instead. No attempt was made to adjust the parameters for an optimum fit to the reactions studied, beyond the selection procedure outlined above.

The bound-state wave function for the di-nucleon relative to the core was calculated as an eigenstate of the potential

$$U(r) = U_c - V_0(1 + e^x)^{-1}$$

$$x = (r - R)/a, \; R = r_{on} A_c^{1/3}$$

$$U_c = \begin{cases} \dfrac{Z_x Z_c}{2R_c} \left(3 - \dfrac{r^2}{R_c^2}\right) \; r < R_c \\ \dfrac{Z_x Z_c}{r} \end{cases}$$

$$R_c = r_{oc} A_c^{1/3}$$

where Z_x is the charge of the di-nucleon, Z_c is the charge of the core and A_c is the mass of the core. The well depth V_0 was adjusted to produce the correct binding energy for the di-nucleon. The radius and diffuseness parameters used for all the calculations in this work were

$$r_{on} = 1.5 \; f,$$

$$r_{oc} = 1.3 \; f,$$

$$a = 0.6 \; f.$$

APPENDIX D

THE QUADRATIC MASS FORMULA; COULOMB ENERGIES;
AND MASS PREDICTIONS

Jänecke (1969) has discussed in some detail the derivation
of the quadratic mass formula for isobaric multiplets

$$m(A,T,T) = a(A,T) + b(A,T)T_z + c(A,T)T_z^2$$

By assuming the isospin-nonconserving interaction to be of the form

$$H_c = K \sum_{i < i} (\tfrac{1}{2} - t_z^{\ i})(\tfrac{1}{2} - t_z^{\ i}) = H_c^{(0)} + H_c^{(1)} + H_c^{(2)}$$

where the sum extends over all pairs in the nucleus. The coefficients
a, b, and c can be expressed in the form (using Jänecke's notation)

$$a = 1/2(m_n + m_H)A + < H_0 > + E_c^{(0)} - T(T + 1) E_c^{(2)}$$

$$b = (m_n - m_H) - E_c^{(1)}$$

$$c = 3E_c^{(2)}$$

The terms $E_c^{(i)}$ are related to the reduced matrix elements (from the
Wigner-Eckhart theorem) as follows:

$$E_c^{(0)} = \ <\ T\ \|\ H_c^{(0)}\ \|\ T >$$

$$E_c^{(1)} = \frac{-1}{\sqrt{T(T+1)}}\ <\ T\ \|\ H_c^{(1)}\ \|\ T >$$

$$E_c^{(2)} = \frac{1}{\sqrt{T(T+1)(2T-1)(2T+3)}}\ <\ T\ \|\ H_c^{(2)}\ \|\ T >$$

The addition of charge-dependent forces arising from other sources than the Coulomb energy of tensorial rank less than 3 will not change the form of the equation outlined above. The Coulomb force is assumed to be the major isospin-nonconserving interaction in nuclei, and the terms $E_c^{(i)}$ are generally referred to as Coulomb energies.

If the masses of three members of a $T = 2$ multiplet have been measured, the coefficients a, b, and c can be determined immediately from the relation

$$\begin{bmatrix} a \\ b \\ c \end{bmatrix} = \begin{bmatrix} 1 & 0 & 0 \\ -\frac{3}{2} & 2 & -\frac{1}{2} \\ \frac{1}{2} & -1 & \frac{1}{2} \end{bmatrix} \begin{bmatrix} m(0) \\ m(1) \\ m(2) \end{bmatrix}$$

where $m(T_z)$ is the $T = 2$ mass for the member with projection T_z. The Coulomb energies $E_c^{(i)}$ can then be determined from the relations given above. Also the masses of the $T_z = -1, -2$ members can be calculated from the relations (obtained immediately from above)

$$\begin{bmatrix} m(-1) \\ m(-2) \end{bmatrix} = \begin{bmatrix} 3 & -3 & 1 \\ 6 & -8 & 3 \end{bmatrix} \begin{bmatrix} m(0) \\ m(1) \\ m(2) \end{bmatrix}$$

REFERENCES

Adams, J. M., A. Adams and J. M. Calbert 1968, J. Phys. A Series 2, $\underline{1}$, 549.

Adelberger, E. G. 1967a, Ph. D. Thesis, Caltech (unpublished).

Adelberger, E. and A. B. McDonald 1967b, Physics Letters $\underline{24B}$, 270.

Adelberger, E. G., A. B. McDonald and C. A. Barnes 1969a, Nuc. Phys. $\underline{A124}$, 49.

Adelberger, E. G., C. L. Cocke, C. N. Davids and A. B. McDonald 1969b, Phys. Rev. Letters $\underline{22}$, 352.

Adelberger, E. G., A. V. Nero and A. B. McDonald 1970, Nuc. Phys. $\underline{A143}$, 97.

Armini, A. J., J. W. Sunier and J. R. Richardson 1968, Phys. Rev. $\underline{165}$, 1194.

Ajzenberg-Selove, F. and T. Lauritsen 1968, Nuc. Phys. $\underline{A114}$, 1.

Ajzenberg-Selove, F. 1970, Nuc. Phys., to be published.

Ball, J. B. and R. L. Auble 1968, private communication (ORIC computer code, Magdoc IV).

Barkas, W. H. and M. J. Berger 1964, in Studies in Penetration of Charged Particles in Matter, NAS-NRC Publication 1133, page 103.

Bassel, R. H., R. M. Drisko and G. R. Satchler 1962, Oak Ridge National Laboratory Report ORNL-3240 (unpublished).

Bassel, R. H., R. M. Drisko and G. R. Satchler 1966, Preliminary Report on the Code JULIE (Supplement to Oak Ridge National Laboratory Report ORNL-3240) (unpublished).

Batusov, Yu. A., S. A. Bunyatov, B. M. Sidorov and V. A. Yarba 1967,
Joint Inst. Nucl. Res. (Dubna), Report P1-3372.

Black, J. L., W. J. Caelli, D. L. Livesey and R. B. Watson 1969,
Phys. Letters 30B, 100.

Black, J. L. 1970, Private Communication.

Bloch, R., R. E. Pixley and P. Truöl 1967, Phys. Letters 25B, 215.

Boch, R., H. H. Duhm, W. Melzer, F. Puklhofer and B. Stadler 1966,
Nucl. Instr. and Meth. 41, 190.

Borggreen, J., B. Elbeck and L. P. Nielson 1963, Nucl. Instr. and
Meth. 24, 1.

Cerny, J., and R. H. Pehl 1964, Phys. Letters 12, 234.

Cerny, J. 1968, Ann. Rev. Nucl. Sci. 18, 27.

Cerny, J., S. W. Cosper, G. W. Butler, R. H. Pehl, F. S. Goulding,
D. A. Landis and C. Detraz 1966, Phys. Rev. Letters 16,
469.

Clark, G. J., P. B. Treacy and S. N. Tucker 1970, Nucl. Phys. A143,
109.

Cosper, S. W., H. Brunnader, J. Cerny and L. McGrath 1967,
Phys. Letters 25B, 324.

Dietrich, F. S. 1965, Nuc. Phys. 69, 49.

Doehring, A., S. Kalbitzer and W. Melzer 1968, Nucl. Instr. and
Meth. 59, 40.

Douglas, R. A., B. R. Gasten and A. Mukerji 1956, Can. J. Phys. 34,
1097.

Endt, P. M. and C. van der Leun 1967, Nuc. Phys. A105, 1.

Freeman, J. M., J. G. Jenkin and G. Murray 1966, Physl Letters 22, 177.

Garvey, G. T. and I. Kelson 1966, Phys. Rev. Letters 16, 197.

Garvey, G. T., W. J. Gerace, R. L. Jaffe, I. Talmi and I. Kelson 1969, Rev. Mod. Phys. 41, S1.

Glendenning, N. K. 1961, Nuc. Phys. 29, 109.

Goosman, D. R. and R. W. Kavanagh 1970, Phys. Rev. C1, 1939.

Groce, D. E. 1963, Ph. D. Thesis, Caltech (unpublished).

Hardy, J. C., H. Brunnader and J. Cerny 1969, Phys. Rev. 183, 854.

Hardy, J. C., H. Brunnader and J. Cerny 1970, Phys. Rev. C1, 561.

Henley, E. M. 1969, in Isospin in Nuclear Physics, edited by D. H. Wilkinson, North Holland Publishing Company, Amsterdam, page 15.

Hensley, D. C., P. H. Nettles and C. A. Barnes 1968, Phys. Letters 26B, 435.

Hensley, D. C. 1969, Ph. D. Thesis, Caltech (unpublished).

Hensley, D. C. and P. H. Nettles 1970, Private Communication.

Jänecke, J. 1969, in Isospin in Nuclear Physics, edited by D. H. Wilkinson, North Holland Publishing Company, Amsterdam, page 297.

Kalbitzer, S. and W. Melzer 1967, Nucl. Instr. and Meth. 56, 301.

Kalbitzer, S. and W. Stumpfi 1970, Nucl. Inst. and Meth. 77, 300.

Kelson, I. and G. T. Barvey 1966, Phys. Letters 23, 689.

Kingston, F. G., R. J. Griffiths, A. R. Johnston, W. R. Gibson and E. A. McClatchie 1966, Phys. Letters 22, 458.

Kuan, H. M. D. W. Heikkinen, K. A. Snover, F. Riess and S. S. Hanna
1967, Phys. Letters 25B, 217.

Lee, L. L., J. P. Schiffer, B. Zeidman, G. R. Satchler, R. M. Drisko
and R. H. Bassel 1964, Phys. Rev. 136, B971.

Lynch. B., G. M. Griffiths and T. Lauritsen 1965, Nuc. Phys. 65, 641.

Matous, G. M., G. H. Herling and E. A. Wolicki 1966, Phys, Rev. 152,
908.

Mattauch, J. H. E., W. Thiels and A. P. Wapstra 1965, Nuc. Phys. 67, 1.

McGrath, R. L., J. C. Hardy and J. Cerny 1968, Phys. Letters 27B, 443.

McGrath, R. L. 1969, in Nuclear Isospin, edited by J. D. Anderson,
S. D. B oom, J. Cerny and W. W. True, Academic Press
(New York and London), page 29.

Moss, C. E. 1968, Ph. D. Thesis, Caltech (unpublished).

McDonald, A. B. 1969, Ph. D. Thesis, Caltech (unpublished).

McNally, J. H. 1966, Ph. D. Thesis, Caltech (unpublished).

Nettles, P. H., D. C. Hensley and T. Tombrello 1969, in Nuclear
Isospin, edited by J. D. Anderson, S. D. Bloom, J. Cerny
and W. W. True, Academic Press (New York and London),
page 819.

Newns, H. C. 1960, Proc. Phys. Soc. 76, 489.

Olsen, D. K., W. D. Harrison, R. E. Brown and C. A. Barnes 1968,
Annual Report COO-1265-67, John H. Williams Laboratory
of Nuclear Physics, University of Minnesota, Minneapolis
(unpublished), page 83.

Poskanzer, A. M., P. L. Reeder and I Dostrovsky 1965, Phys. Rev. 138,
B18.

Richards, H. T. 1960, in Nuclear Spectroscopy (Part A), edited by
    F. Ajzenberg-Selove, Academic Press (New York), page 99F.

Riess, F., W. J. O'Connell, D. W. Heikkinen, H. M. Kuan and S. S. Hanna
    1967, Phys. Rev. Letters 19, 367.

Satchler, G. R. 1964, Nuc. Phys. 55, 1.

Snover, K. A., D. W. Heikkinen, F. Riess, H. M. Kuan and S. S. Hanna
    1969, Phys. Rev. Letters 22, 239.

Tobocman, W. 1961, Theory of Direct Nuclear Reactions, Oxford University
    Press (London).

Weinberg, S. and S. B. Treiman 1958, Phys. Rev. 116, 465.

Wilkinson, D. H. 1964a, Phys. Letters 11, 243.

Wilkinson, D. H. 1964b, Phys. Letters 12, 348.

Wilkinson, D. H. 1964c, Phys. Rev. Letters 13, 571.

Wigner, E. P. 1957, in Proc. Robert A. Welch Found. Conf. on Chemical
    Research, Houston, Texas, edited by W. O. Milligan (the
    Robert A. Welch Foundation, Houston, Texas), Vol. I,
    page 88.

TABLE 1

Fractional Changes in Spectrometer Calibration
Factor with Magnetic Field

f(MHz)	$\Delta(\times 10^{-3})$
14	.24
16	.05
18	-.30
20	-.52
22	-.60
24	-.52
26	-.37
28	0.0
30	.57
32	1.22
34	1.96
36	2.80
38	3.73
40	4.77
42	5.80
44	6.90

TABLE 2

Excitation Energies Predicted for the Lowest
T = 2 States in ^{12}C and ^{12}B

(entries in MeV)

^{12}C	^{12}B	Based On	Reference
27.58	12.47	T = 3/2 levels in A = 11, 13	Jänecke 1969, Adelberger 1970
< 31.3	< 16.2	Upper limit for $m(^{12}Be)$	Cerny 1968
27.98	12.87	G.K. prediction for $m(^{12}Be)$	Garvey 1966
27.5 ± .1	12.67 ± .07	Experiment	Cerny 1968

TABLE 3

^{14}C Target Thickness/Composition Measurements
from 12-MeV ^{3}He Scattering at 90°

Material	Method[a]	Y_1/Y_2 [b]	ΔE(keV)	ϵ_{eff} [c]	$\lambda(\mu g/cm^2)$
Au(thick)	Width	-	99.2	10.45	275
Au(thin)	Yield	0.204	-	-	56
$(^{12}C + ^{14}C)$	Shift	-	389	1.73	375[d]
^{12}C	Yield[e]	1.41	-	-	62
^{14}C [f]	-	-	-	-	284

a. See Section II-C.

b. Yield Ratio, for yield method only.

c. Average stopping power (units 10^{-15} ev-cm^2) for incident and
    exiting energy.

d. Equivalent ^{12}C thickness, $\lambda = (\frac{12}{14})(\lambda_{14} + \lambda_{12})(\frac{\epsilon_C + \epsilon_H}{\epsilon_C})$ for
    use in energy loss calculation. The polymer was assumed to be
    of the form $(CH)_n$, from which the factor $\frac{\epsilon_C + \epsilon_H}{\epsilon_C}$ was obtained.

e. Thickness compared to previously measured ^{12}C target, $\lambda = 44$ $\mu g/cm^2$

f. Final ^{14}C thickness, corrected for ^{12}C and H content.

TABLE 4

Measurement of the Excitation Energy of the Lowest

$T = 2$ State in ^{12}C

Angle[a] (Θ_m/Θ_t)	Aperture	Field (kG)	D_1/D_2[b] (inches)	Channel[c] (f.s. = 100)	Excitation (MeV)	Identification
30°/20°	4°	8.2307	4.951 / 5.351	57.7	27.5973	$^{12}C(T = 2)$
25°/20°	4°	8.3101		58.7	27.6019	
20°/20°	4°	8.3902		52.0	27.5911	
20°/20°	1°	8.4512	4.529 / 4.802	45.5	27.5911	
20/20	1°	7.7500		59.1	-.0014	$^{11}B(0.0)$
20/20	1°	7.7821		36.0	+.0011	
20/20	1°	7.7251		81.7	+.0007	
20/20	1°	7.4201		56.9	4.4377	$^{11}B(4.444)$[d]
30°/20°	4°	8.6723	4.951 / 5.357	44.0	15.226	$^{13}C(15.112)$[e]
				Average	27.595	$^{12}C(T = 2)$

a. Target angle (Θ_t) is the angle between the target normal and the incident-beam momentum.

b. Focal-plane orientation (D_1 and D_2) defined in Appendix A.

(continued)

TABLE 4 (continued)

c. See Figure 18 for channel-to-position conversion.

d. Ajzenberg-Selove 1968.

e. Hensley 1969. See discussion on page 26 of the use of this group for calibration.

TABLE 5

Width Analysis for $^{14}C(p,t)^{12}C$ and $^{14}C(p,\alpha)^{11}B$ Measurements[a]

State	Angle	Aperture	Target (keV)	Focal Plane[b] (keV)	Quadrupole[c] (keV)	Total[d] (keV)	Observed (keV)	Revised Total[e] (keV)
^{11}B(g.s.)	20°	1°	51	42	81	104	76.5±5.0	76.5
^{12}C(27.59)	20°	1°	18	.5	47	50	32.4±5.0	29
^{12}C(27.59)	20°	4°	18	72[f]	47	88	82.4±8.0	78

a. The entries in this table are expressed in laboratory particle energy. After the observed width was corrected for the experimental resolution, the result was re-expressed in 12C excitation energy.

b. This contribution to the resolution arises from the improper orientation of the focal plane for the particular group being observed, resulting in a residual kinematic broadening.

c. The focusing of the beam by the last quadrupole before the target chamber gives rise to a spread in the incident angles of bombardment and a resulting kinematic shift.

d. The total resolution is calculated as the quadratic sum of the contributions listed.

e. See page 30 for a discussion of the entries in this column.

f. The measurements at 20° with the 4° aperture were made with a different focal plane orientation from that of the measurements made with the 1° aperture.

TABLE 6

Measurements of Excitation Energies of ^{12}B States

Angle[a] (θ_m/θ_t)	Aperture	Field (kG)	D_1/D_2[b] (inches)	Channel[c] (f.s.= 100)	Excitation (MeV)	Identification
20°/0°	4°	5.6600	4.171 4.412	61.5	12.7080	^{12}B(T = 2)
20°/0°	4°	5.6601		61.2	12.7107	
10°/10°	4°	5.7519	3.757 3.877	58.8	12.6925	
6°/6°	2°	5.7817	3.551 3.623	57.4	12.7134	
25°/15°	4°	5.6000	4.498 4.799	59.5	12.6958	
30°/15°	4°	5.5331	4.726 5.096	60.3	12.7133	
8°/8°	2°	5.7689	3.653 3.748	56.6	12.7160	
8°/8°		5.7689		56.6	12.7160	
8°/8°		6.7685		51.6	-0.0001	^{12}B(g.s.)
8°/8°		6.7671		52.5	-0.0008	

(continued)

TABLE 6 (continued)

Measurements of Excitation Energies of ^{12}B States

Angle[a] (Θ_m/Θ_t)	Aperture	Field (kG)	D_1/D_2[b] (inches)	Channel[c] (f.s. = 100)	Excitation (MeV)	Identification
3°/8°		6.7126		43.8	.948	^{12}B(0.950)[d]
8°/8°		6.7671		85.0	2.3056	^{14}N(2.313)[e]
10°/10°	4°	5.5619	3.757 3.877	60.0	14.860	^{12}B(14.86)

Average of the 12.7-MeV-State Measurements   12.710 ^{12}B(T = 2)

a. Target angle (Θ_t) is the angle between target normal and incident-beam momentum.

b. Focal plane orientation (D_1 and D_2) defined in Appendix A.

c. See Figure 24 for channel-to-position conversion.

d. Ajzenberg-Selove 1968.

e. Ajzenberg-Selove 1970.

91

TABLE 7

Width Analysis for the $^{14}C(p, ^3He)^{12}B$ Measurements[a]

State (MeV)	Angle	Aperture	Target (keV)	Focal Plane[a] (keV)	Quadrupole[c] (keV)	Total[d] (keV)	Observed (keV)	Revised Total[e] (keV)
0.0	8°	2°	40	14	32	53	81±5	81
12.71	8	2	54	0	28	60	79±10	74.5
12.71	10	4	54	0	30	62	81±10	76
14.86	10	4	57	0	20	60	228±30	68

a. All entries in this table for widths are expressed in particle energy in the laboratory.

b. This contribution to the resolution arises from improper orientation of the focal plane for the particular group being observed, resulting in a residual kinematic broadening.

c. The focusing of the beam by the last quadrupole before the target chamber gives rise to a spread in the incident angle of bombardment and a resulting kinematic shift.

d. The total resolution is calculated as the quadratic sum of the contributions listed.

e. See page 36 for a discussion of this term.

TABLE 8

Predictions of the Mass of ^{12}Be

T[a]	$-\dfrac{\Delta(T)}{T}$ [a] (MeV)	$m(^{12}\text{Be})$ (MeV)	Source[b]
1	3.968	25.503	$T=1$, $A=12$ mass difference[c]
2	4.042	25.577	$T=1$, $A=10$, 14 mass differences[d]
2	4.014	25.549	$T=\frac{1}{2}$, $A=9$, 11, 13, 15 mass differences
		25.0	Garvey-Kelson prediction[e]
		25.1	Estimated beta-decay endpoint energy, from the measured lifetime and calculated ft value [f]
		<28.3	Upper limit from beta-decay endpoint[g]

a. The quantities $\Delta(T)$ and T were defined on page 39 of the text.

b. All masses not otherwise referenced were taken from Mattauch (1965).

c. The ^{12}N mass was obtained from Adams (1968).

d. The ^{10}C mass was obtained from Freeman (1966).

e. Garvey 1966.

f. Poskanzer 1965.

g. Cerny 1968.

TABLE 9

Predictions and Previous Measurements of the Excitation
Energy of the Lowest $T = 2$ State of ^{20}F

Excitation (MeV)	Source or Input	References
6.59	^{20}O, $^{20}Na - ^{20}F$	a,b
6.48	$^{20}Ne(T = 2)$; $(^{20}Na - ^{20}F)$	a,b,c
6.43 ± 0.1	(Experiment)	d
6.523 ± 0.035	Experiment	e

a. Mattauch 1965.

b. The ^{20}Na mass was taken from Endt 1967.

c. Adelberger 1967a, b; Bloch 1967, Kuan 1967.

d. Cerny 1964.

e. Hardy 1969.

TABLE 10

Measurements of the Excitation Energy
of T = 2 States in $^{20}F^{(a)}$

Angle Magnet/target	Frequency[b] (kHz)	Excitation[c] (keV)	Uncertainty[d] (keV)	Nucleus
10°/10°	34775	-0.163	2.4	^{18}F
20°/20°	34626	+0.267	3.2	^{18}F
10°/10°	32547	6514.0	2.2	^{20}F
20°/20°	32415	6512.5	2.2	^{20}F
10°/10°	30053	8211.9	3.4	^{20}F
20°/20°	29923	8208.7	3.4	^{20}F

a. The results of these measurements are summarized on page 46.

b. The tabluated frequency is the effective NMR frequency, defined in Appendix A, at the centroid of the peak.

c. All nuclear masses used in this analysis were taken from the current tabulations (Mattauch 1965).

d. This column gives the contribution to the probable error from the estimated uncertainty in the frequency. The complete error analysis is discussed on page 45.

TABLE 11

Predictions and Previous Measurements of the Excitation
Energy of the Lowest T = 2 State in ^{28}Al

Excitation (MeV)	Source	Reference
6.06	^{28}Mg, ^{28}P - ^{28}Al	a,b
5.983 ± 0.025	Experiment	c
[5.989 ± ?]	Experiment	d

a. Mattauch 1965.

b. The ^{28}P mass taken from Endt 1967.

c. Hardy 1970.

d. Clark 1970.

TABLE 12

Measurements of the Excitation Energies of States in ^{28}Al [a]

Angle (magnet/target)	Frequency (kHz)	Excitation (keV)	Uncertainty[b] (keV)	Identification
5°/5°	35310	5995.4	3.0	Lowest T=2
10°/10°	35283	5997.9	3.0	State of ^{28}Al
15°/15°	35245	5996.6	3.0	(protons)
15°/15°	33279	7490.7	10	1st-Excited T=2
20°/10°	33223	7491.8	10	State of ^{28}Al
30°/15	33071	7490.6	10	(protons)
15°/15°	33335	7449.5	10	Second member of
20°/10°	33284	7446.5	10	doublet near 7.5 MeV excitation
5°/5°	37030	6813	1.5	Deuterons
10°/10°	36979	6813	1.5	^{27}Al(T=3/2)
15°/15°	36899	6812	1.5	E_x=6815±2 keV[c]
20°/20°	36780	6814	1.5	
10°/10°	42739	2.0	3	(Alphas) ^{25}Mg ground-state
10°/10°	42215	1065	3	(tritons) ^{26}Al, 1059 keV[c]

a. The results of these measurements are summarized on page 53.

b. The tabulated uncertainty is the contribution to the total uncertainty resulting from the determination of the central frequency only. The complete analysis of probable errors for the ^{28}Al states is discussed on page 53.

c. Endt 1967.

TABLE 13

Optical Potentials[a],[b] Used for Analysis of Angular Distributions

Channel	V (MeV)	W (MeV)	r_0 (f)	a (f)	r_0' (f)	a' (f)	V_{so} (MeV)	W' (MeV)	Reference
$^{14}C + p$, 50.5 MeV	59.74	-	1.25	0.40	1.25	0.40	-	29.11	c
$^{12}C + t$	171.29	-	1.25	0.60	1.25	0.60	-	28.83	c
$^{14}C + p$, 63.4 MeV	53.3	21.7	1.25	0.40	1.25	0.40	-	-	c
$^{12}B + {}^3He$	155.0	35.9	1.25	0.60	1.25	0.60	-	-	c
$^{18}O + {}^3He$	183.3	23.2	1.05	0.829	1.81	0.592	-	-	d,e
$^{20}F + p$	64.3	0	1.2	0.65	1.25	0.45	8	44	d,f
$^{26}Mg + {}^3He$	153.0	12.0	1.08	0.30	1.77	0.60	-	-	g
$^{28}Al + p$	63.7	12.0	1.25	0.45	1.25	0.47	-	-	g

a. These parameters are defined in Appendix C.

b. The Coulomb radius parameters r_C = 1.25 f for all channels. In all cases W_{so} = 0.

c. Cosper 1967. (See also the discussion in Appendix C.)

d. Hensley 1969.

e. Matous 1966.

f. Lee 1964.

g. Clark 1970.

TABLE 14

Summary of Masses for the Lowest $T = 2$ Multiplets
in $A = 4n$ Nuclei[a]

A	$T_z = 0$	$T_z = 1$	$T_z = 2$
8	32427 ± 10[b]	?	31600 ± 115[c]
	27483 ± 10		
12	27595 ± 20[d]	26080 ± 20[d]	$(< 28300$[e]$)$
	27595 ± 20	12710	
16	17981 ± 8[f]	15613 ± 8[g]	13693 ± 16[h]
	22717 ± 8	9928 ± 7	
20	9690.5 ± 2.8[i]	6501 ± 3[j]	3799 ± 8[h]
	16732 ± 2.8	6513 ± 5	
24	1503 ± 5[k]	-2450 ± 10[l]	-5949 ± 10[h]
	15436 ± 5	5968 ± 10	
28	-6269 ± 5[m]	-10859 ± 4.4[n]	-15020 ± 6[h]
	15221 ± 5	5997 ± 5.5	

a. Each entry gives the ($T=2$) atomic mass excess/excitation energy,
    in keV.
b. Black 1969.
c. Cerny 1966, Batusov 1967.
d. Present work; Cerny 1968.
e. Poskanzer 1965.
f. Adelberger 1970.
g. Hensley 1968.
h. Mattauch 1965.
i. Adelberger 1967a,b; Bloch 1967; Kuan 1967; Hardy 1969.
j. Present work; Hardy 1969.
k. Adelberger 1967b, Riess 1967, Hardy 1969.
l. Hardy 1969, Hensley 1970.
m. Hardy 1970, Snover 1969.
n. Present work; Hardy 1970.

TABLE 15

Mass Equation Coefficients and Coulomb Energies for A = 4n, T = 2 Multiplets

A	a (keV)	b (keV)	c (keV)	$E_c^{(1)}$ (keV)	$E_c^{(2)}$ (keV)
8[a]	32427 ± 10	[-988.5 ± 50]	288 ± 96	[1771 ± 50]	97 ± 32
12[a]	27595 ± 20	[-2004 ± 60]	489 ± 34	[2787 ± 60]	163 ± 11
16	17981 ± 8	-2592 ± 20	224 ± 11	3375 ± 20	75 ± 4
20	9690 ± 3	-3433 ± 8	244 ± 5	4216 ± 8	81 ± 2
24	1503 ± 5	-4180 ± 22	227 ± 11	4962 ± 22	76 ± 4
28	-6269 ± 5	-4805 ± 12	215 ± 6	5587 ± 12	72 ± 2

a. The b coefficient for A = 8 was taken from the T = 1 multiplet, and used to extract the c for T = 2. For A = 12, b was calculated from the average predicted mass of ^{12}Be from Table 8. The prediction schemes are discussed on pages 38-39.

TABLE 16

Mass and Stability Predictions for $T_z = -2$ Nuclei

Nuclide	Mass Excess[a] (keV)	Proton Threshold (keV)	(2p) Threshold (keV)	Stability[c]
^{12}O	33559 ± 250	–	30280 ± 2	unbound
^{16}Ne	24061 ± 88	–	22586 ± .5	unbound
^{20}Mg	17532 ± 38	20263 ± 70	19897 ± 5	bound
^{24}Si	10771 ± 90	14055 ± 80	14199 ± 25	bound
^{28}S	4198 ± 50	(7136)[b]	7410 ± 15	bound

a. The quoted uncertainty is from experimental uncertainties in masses for T_z = 0, 1, and 2 members of the multiplet, only.

b. The mass of ^{27}P was predicted from ^{27}Mg and the lowest $T = 3/2$ states in ^{27}Al and the ground-state mass difference for ^{27}Si and ^{27}Al, according to a procedure analogous to that outlined in Chapter III for $T = 2$ states.

c. The stability indicated refers to decay by prompt heavy-particle emission. The bound nuclides indicated are expected to be β^+-delayed proton emitters.

TABLE 17

Mass, Excitation and Stability Predictions for the Lowest T = 2 States

in A = 4n, T_z = -1 Nuclei

Nuclide	T = 2 Mass Excess[a] (keV)	Excitation[b] (keV)	p Threshold[c] (keV)	2p Threshold[c] (keV)	Stability
^{12}N	30088 ± 100	12750 ± 100[d]	-	28370	unbound
^{16}F	20797 ± 36	10104 ± 39[d]	-	19755	unbound
^{20}Na	13368 ± 15	6505 ± 42[e]	16567 ± 25	16492	bound
^{24}Al	5910 ± 35	5810 ± 97	9605 ± 25	10162	bound
^{28}P	-1250 ± 21	5902 ± 23	[1718]	2405	bound

a. The uncertainties indicated are contributions from experimental uncertainties for the masses of T_z = 0, 1, and 2 members of the multiplet, only.

b. Unless otherwise indicated, these are based on the ground-state masses given in recent tabulations (Mattauch 1965).

c. The thresholds indicated are the lowest isospin allowed channels, i.e., p + (A-1, T = 3/2) and 2p + (A-2, T = 1). The stability indicated is thus that relative to isospin-allowed heavy-particle decay channels.

d. Ground-state masses from Adams 1968.

e. Ground-state mass from Armini 1968.

FIGURE 1

A schematic diagram indicating the configuration of the target, spectrograph and particle detector. Reaction products were analyzed in a magnetic spectrograph positioned at a known angle θ_m relative to the incident-beam momentum. The target orientation was specified by the angle θ_t. For the Oak Ridge spectrograph, the particle trajectory in the spectrograph is in the reaction plane, as shown. In the Caltech spectrograph, the trajectory is perpendicular to the reaction plane. The detector was either one of an array of 16 detectors (Caltech measurements only) or a 5-cm-long, position-sensitive detector. See page 3 for further discussion.

Figure 1

Spectrograph

Detector

Slits

θ_t

θ_m

Beam Catcher

Target

Incident Beam
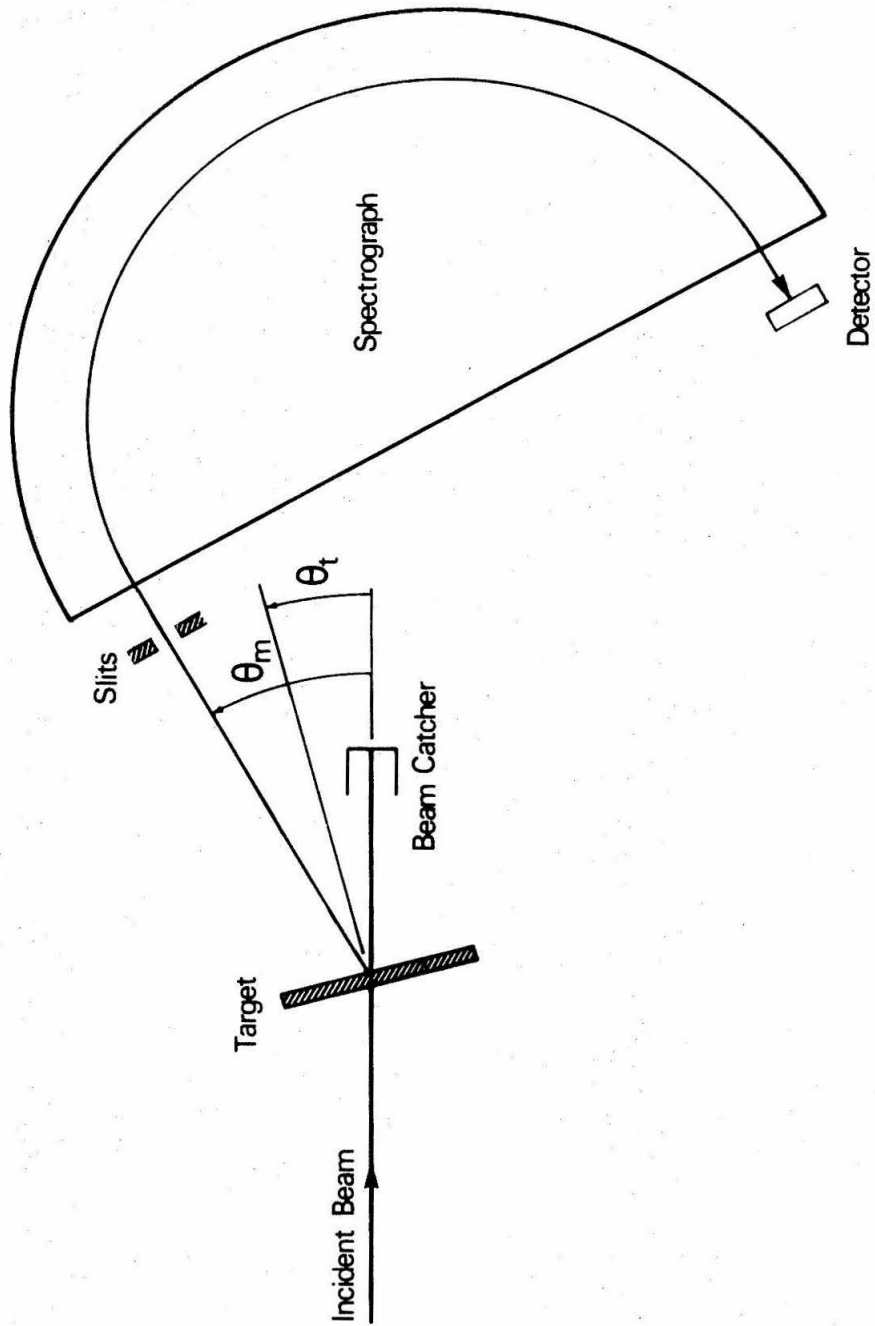
FIGURE 2

Spectra of 12-MeV ^{3}He elastically scattered at 90° from the gold backing of a ^{26}Mg target for two target orientations. The shift in the high-energy edge of the group provides a measure of the Mg-layer thickness. The width of the group in the upper orientation measures the gold-layer thickness. See page 8 for further discussion.
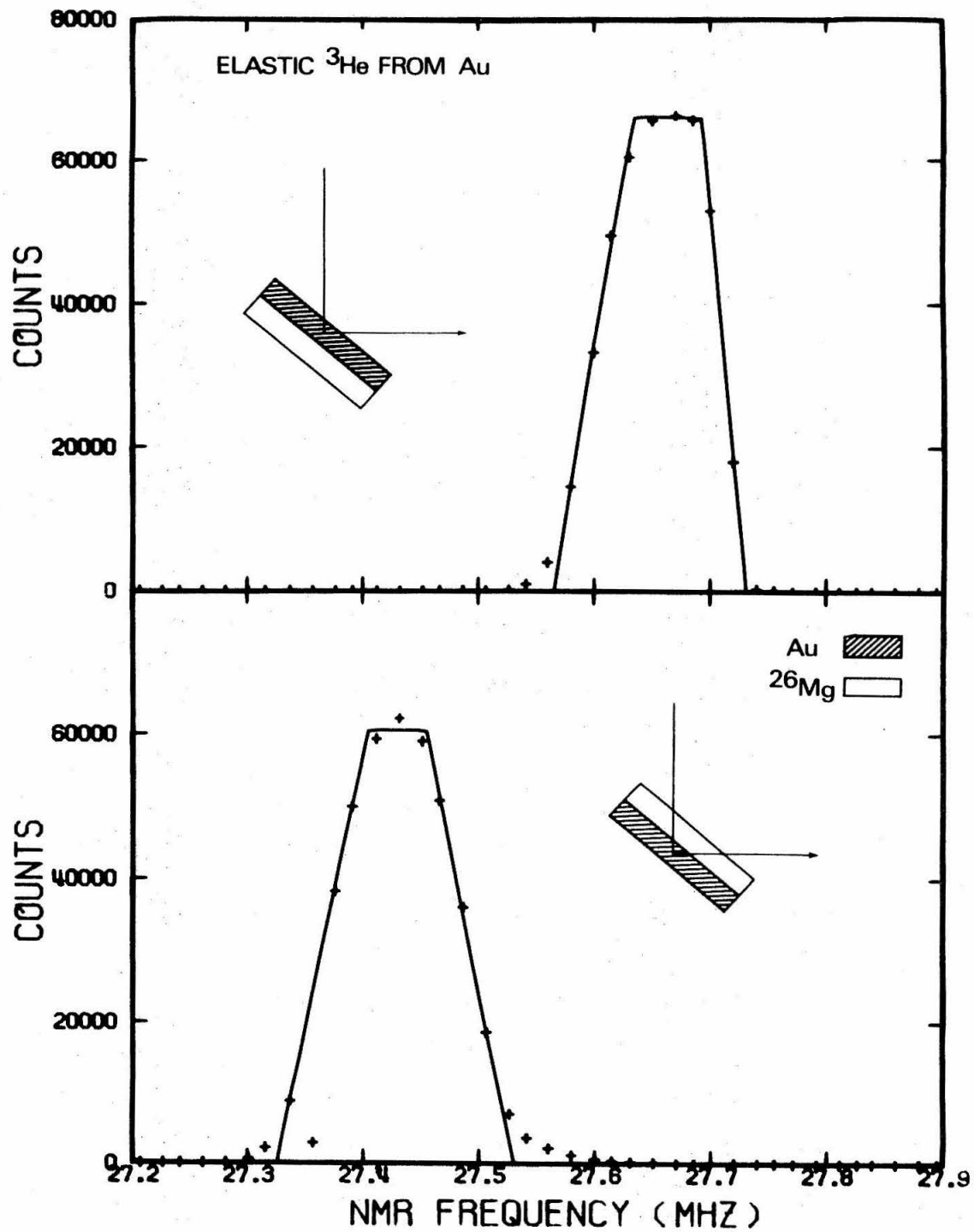
Figure 2

FIGURE 3

Spectra of 12-MeV ^{3}He elastically scattered at 90° from the ^{26}Mg layer of gold-backed ^{26}Mg target for two target orientations. The shift in the high-energy edge of the group measures the thickness of the gold layer. The width of the group in the upper orientation measures the ^{26}Mg-layer thickness. See page 8 for further discussion.

Figure 3

ELASTIC ^{3}He FROM ^{26}Mg

^{26}Mg □
Au ▨

COUNTS

NMR FREQUENCY (MHZ)
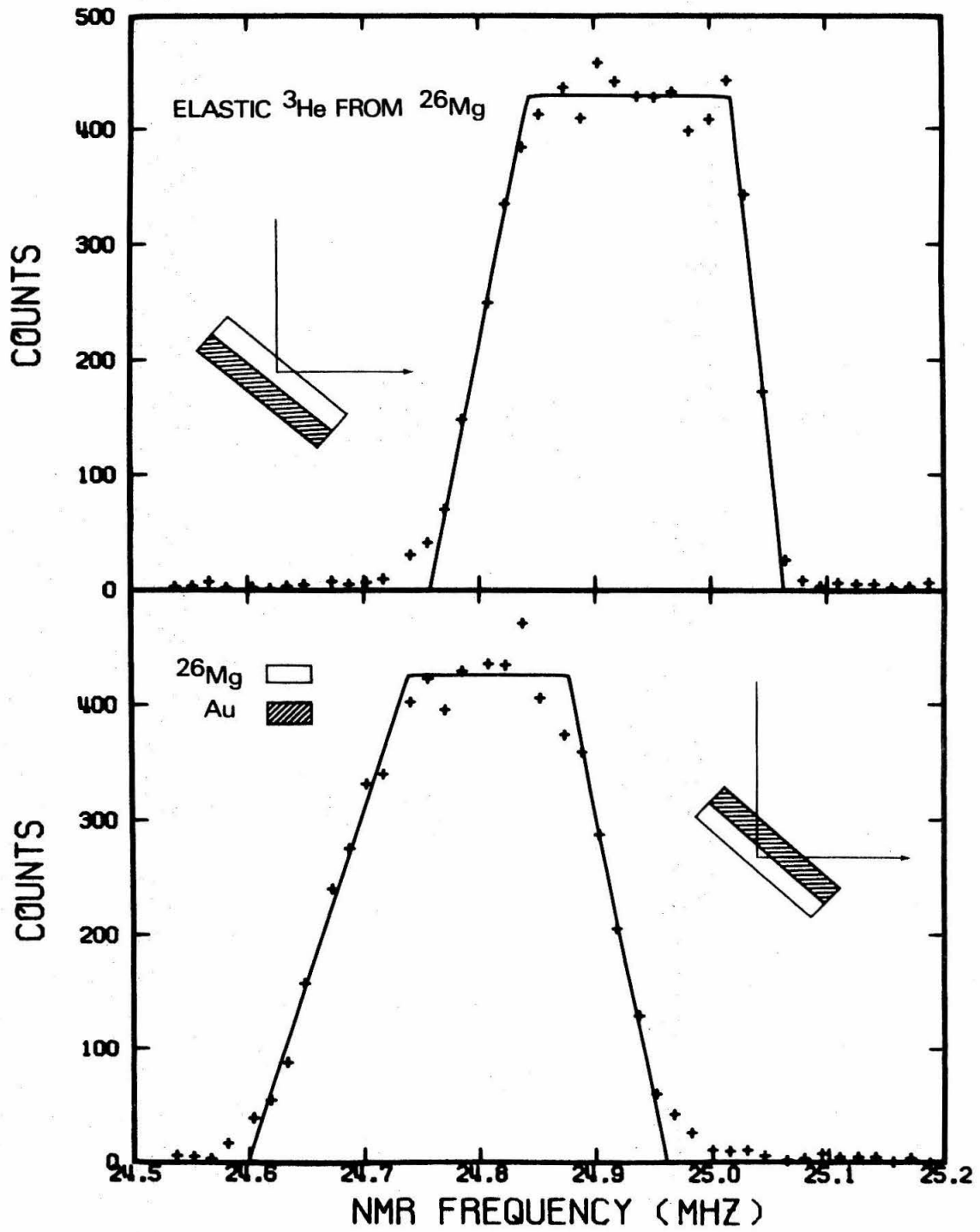
FIGURE 4

Spectra of 12-MeV ^{3}He elastically scattered at 90° from gold layers in a ^{14}C target for two target orientations. The width of the higher-energy group in the upper orientation measures the thickness of the thicker gold layer. A comparison of the yields of the higher-energy groups for the two configurations, gives the relative thicknesses of the two gold layers. The separation in energy between the two groups is a measure of the ^{14}C-enriched-polymer thickness. See page 8 for further discussion.
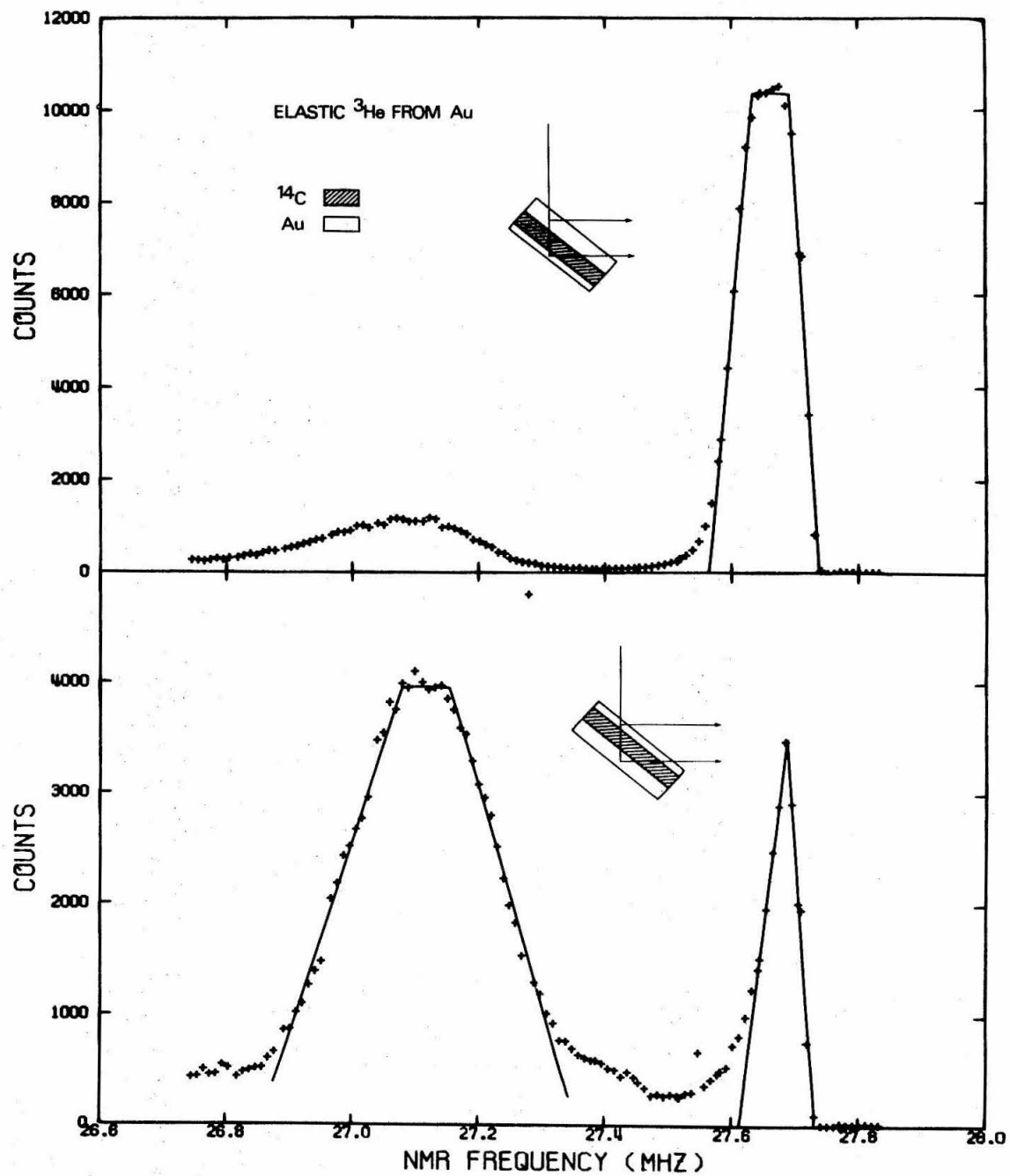
Figure 4

FIGURE 5

Geometric details at the focal plane of the Oak Ridge spectrograph (not drawn to scale).

The position X_d at which a particle is detected is projected along a straight-line extension of the particle trajectory to nominal focal-plane position X_e, from which the orbit radius and particle kinetic energy are calculated. See pages 65-66 for further discussion.

Figure 5

$$x_e = x_d \cos\theta + \Delta_1 + \Delta_2$$

112
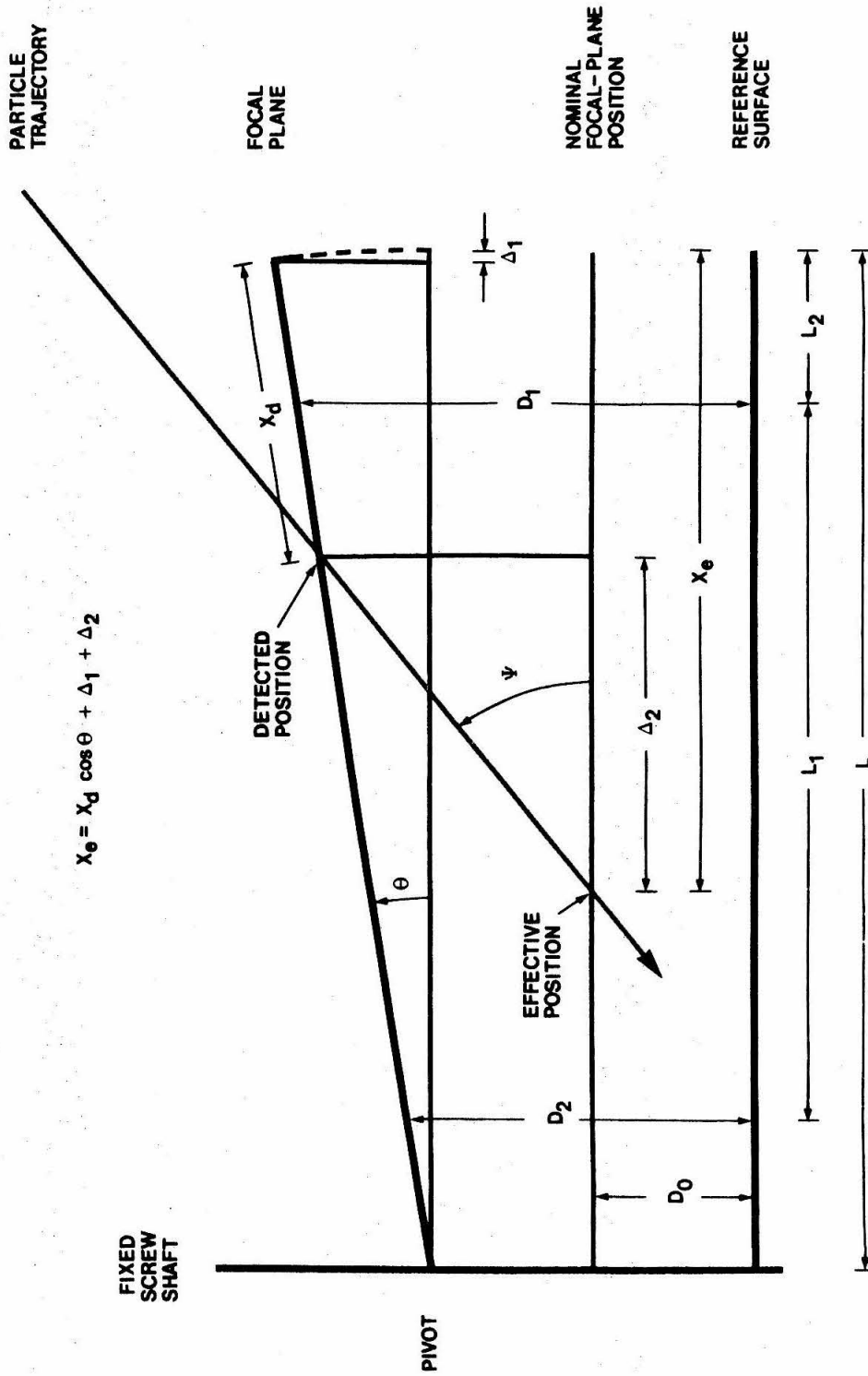
FIGURE 6

Schematic diagram showing the simple gating network used with the position-sensitive detector at Caltech. See page 69 for a discussion of this data-acquisition method.
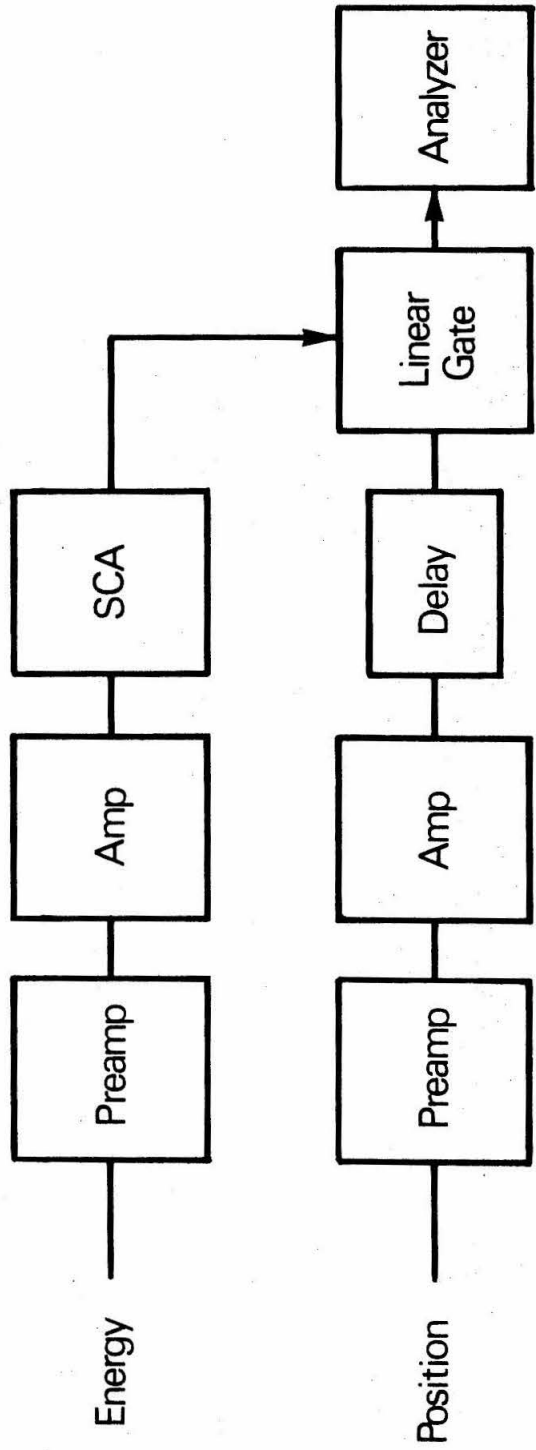
Figure 6

FIGURE 7

Schematic diagram of the electronic network used with the position-sensitive

detectors at Oak Ridge. In this arrangement, the two energy signals are mixed and fed to

a common ADC. The coincident position signal selects the appropriate half of the memory

for storage and the two pulse heights are recorded in a 50 x 200 (energy x position) array,

for each detector. See page 70 for further discussion.
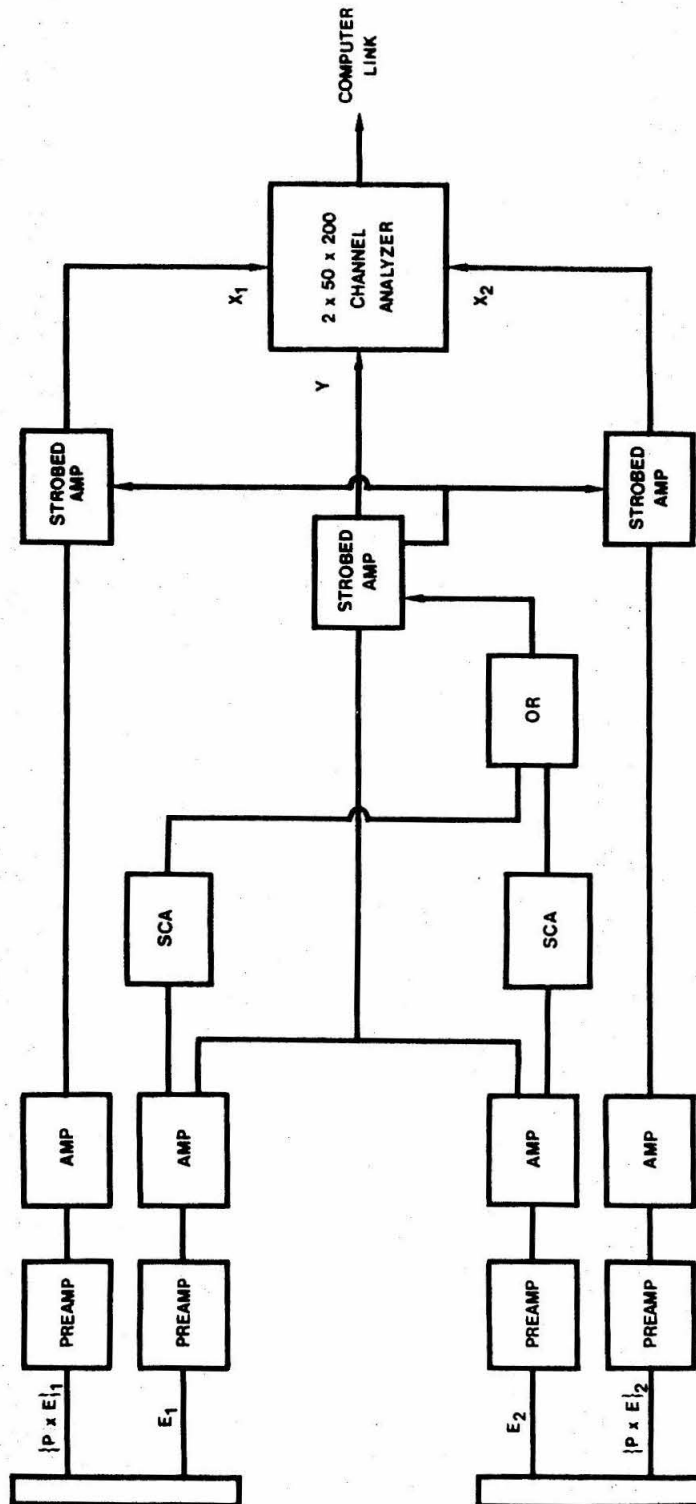
Figure 7

FIGURE 8

Energy spectrum from the position-sensitive detector, for the $^{14}C(p,t)^{12}C$ experiment. The groups identified as tritons and deuterons are indicated. The smoothly varying background is associated with the elastic proton group, which was on the detector. See page 23 for further discussion.

Figure 8

$^{14}C(p,t)^{12}C$
PSC Energy Spectrum

Deuteron

Triton

COUNTS

ENERGY (CHANNELS)

118
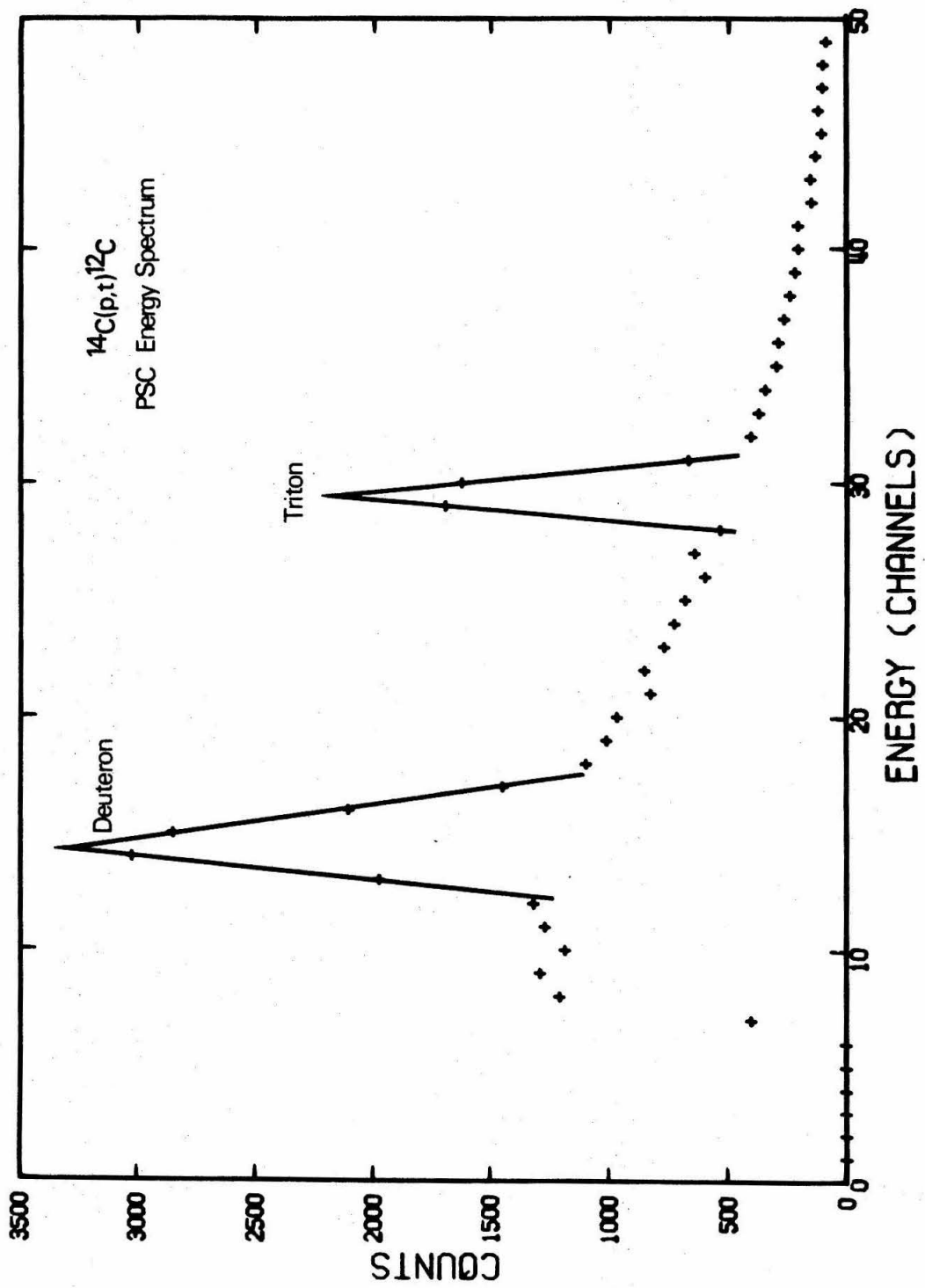
FIGURE 9

A typical array of raw data from the $^{14}C(p,t)^{12}$ experiment. For compactness, the data are displayed logarithmically ($0 \rightarrow$ blank, $1 \rightarrow 1$, $2-3 \rightarrow 2$, $4-7 \rightarrow 3$, $8-15 \rightarrow 4$, etc.). The diagonal cutoff on the right is produced by the edge of the detector. The tritons are seen as a horizontal line at about channel 29. The broad feature on the left of the array is the high-energy tail associated with the elastic protons. The deuteron line is suppressed by the logarithmic scale. See page 23 for further discussion.

Figure 9

$^{14}C(p,t)^{12}C$

POSITION X ENERGY

ENERGY

FIGURE 10

A composite triton spectrum at 30° from the $^{14}C(p,t)^{12}C$ reaction. The two spectra shown correspond to the two sets of data collected simultaneously from the two position-sensitive detectors at the focal plane of the spectrograph. No attempt has been made to subtract the background contribution from under the triton line. The trapezoidal peak in each spectrum is the result of the elastic protons, and can be subtracted out with some care. The triton group identified as the lowest $T = 2$ state in ^{12}C is indicated. The insert at the top shows a triton spectrum, also uncorrected for background contribution under the triton line, from a ^{12}C target of similar construction. See page 23 for further discussion.
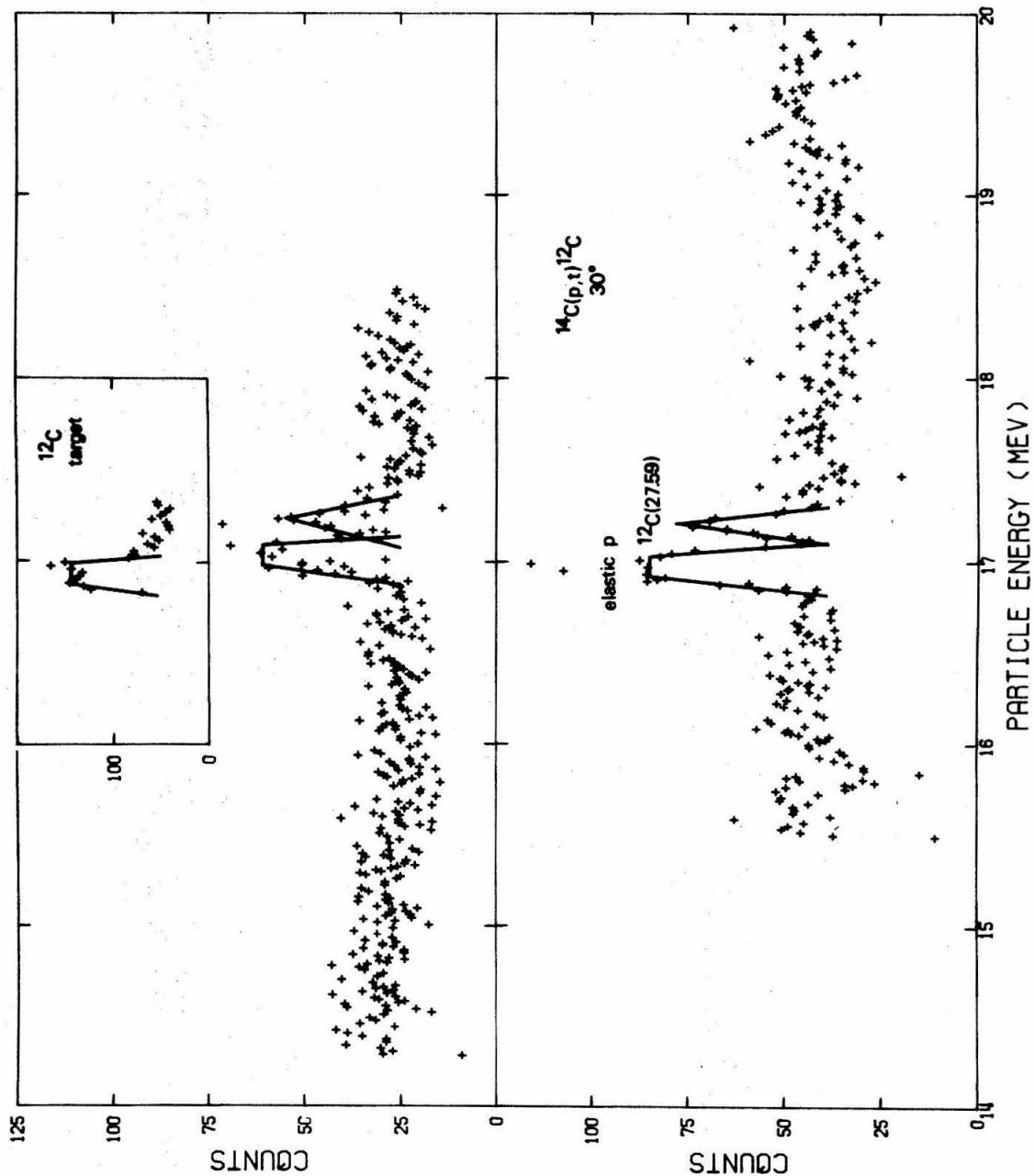
Figure 10

Figure 10

FIGURE 11

A typical triton spectrum accumulated in a single run for the $^{14}C(p,t)^{12}C$ measurements, at 25° in the laboratory. The elastic proton group previously noted adjacent to the triton group of interest was suppressed in the spectrum by removing the contribution of the smoothly varying background (in particle energy) under the triton line from the final extracted triton spectrum (see Figures 8 and 9). See page 24 for additional discussion.

$^{14}C(p,t)^{12}C$
$25°$

POSITION (CHANNELS)

COUNTS

124
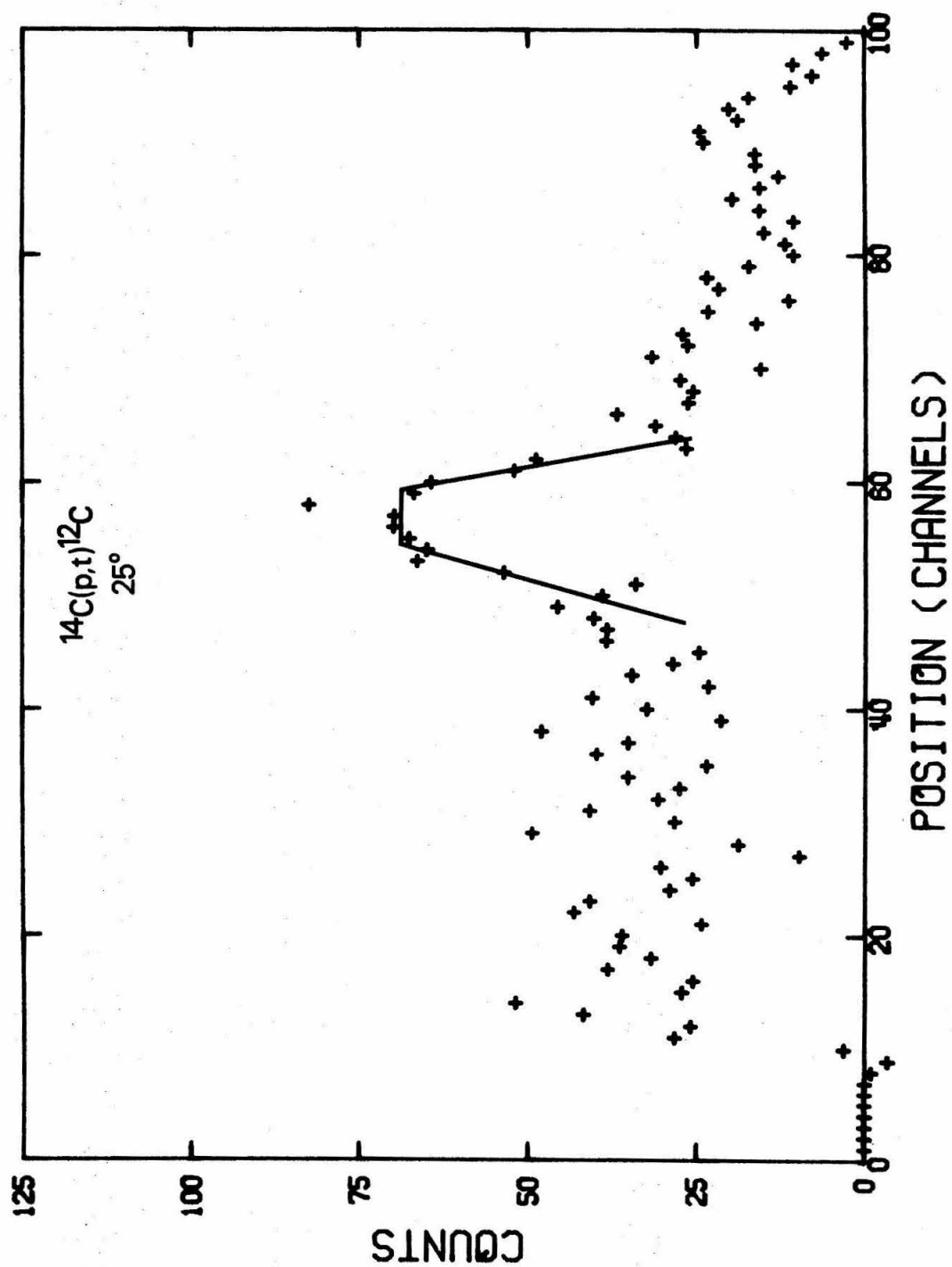
FIGURE 12

A composite triton spectrum showing the scan over triton energy measured at

10° in the lab, for the $^{14}C(p,t)^{12}C$ experiment. The two spectra shown correspond to

the two sets of data collected simultaneously from the two position-sensitive detectors

at the focal plane of the spectrograph. The bracket indicates the expected location of

the $T = 2$ state. See page 24 for further discussion.

Figure 12

^{14}C(p,t)^{12}C
10°
E_i = 50.5 MeV

T=2?

COUNTS

COUNTS

PARTICLE ENERGY (MEV)

126
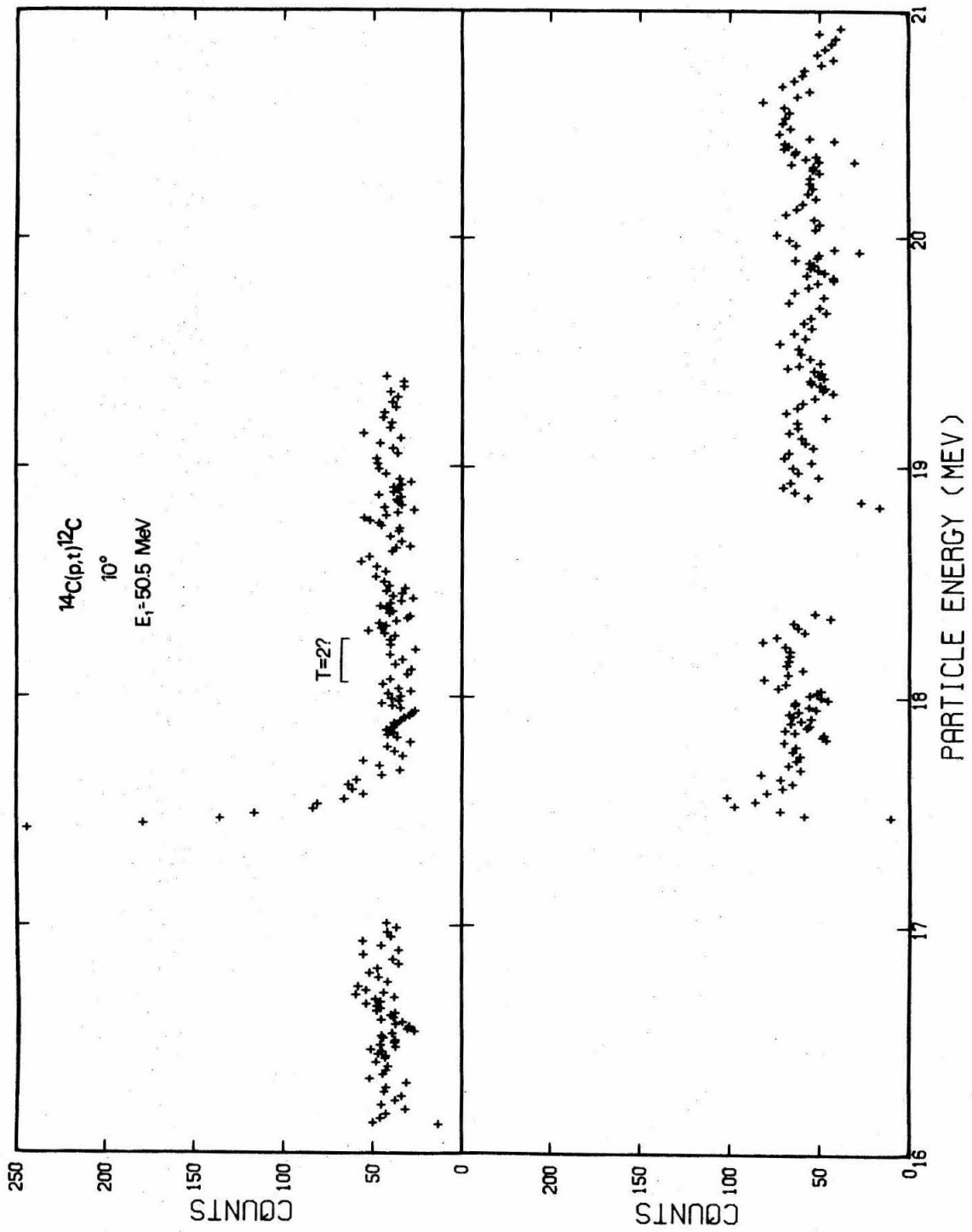
FIGURE 13

Typical alpha-particle spectra for calibration of the $^{14}C(p,t)^{12}C$ measurements. Three observations of the ground-state alpha-particle group from $^{14}C(p,\alpha)^{11}B$ are shown, along with a spectrum from $^{27}Al(p,\alpha)^{24}Mg$ which was used for determining the endpoint of the detector. See pages 24-25 for additional discussion.

Figure 13

128
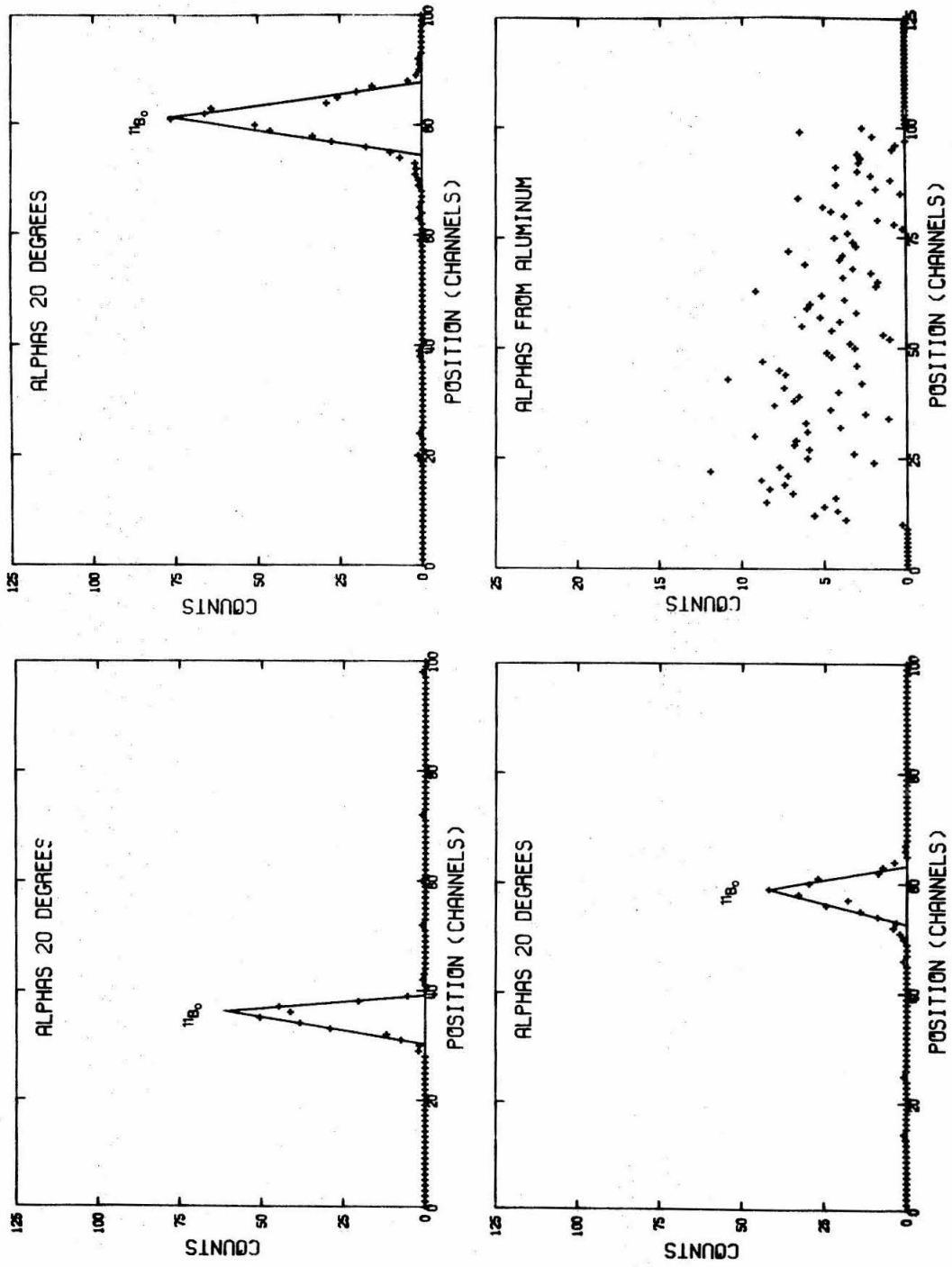
FIGURE 14

Calibration curve to determine focal-plane position from measured pulse height (100 channels = detector length) for the $^{14}C(p,t)^{12}C$ experiment. The calibration data obtained from $^{14}C(p,\alpha)^{11}B$ measurements are shown. The smooth curve was constructed by least-squares analysis of these data. See page 25 for additional discussion.
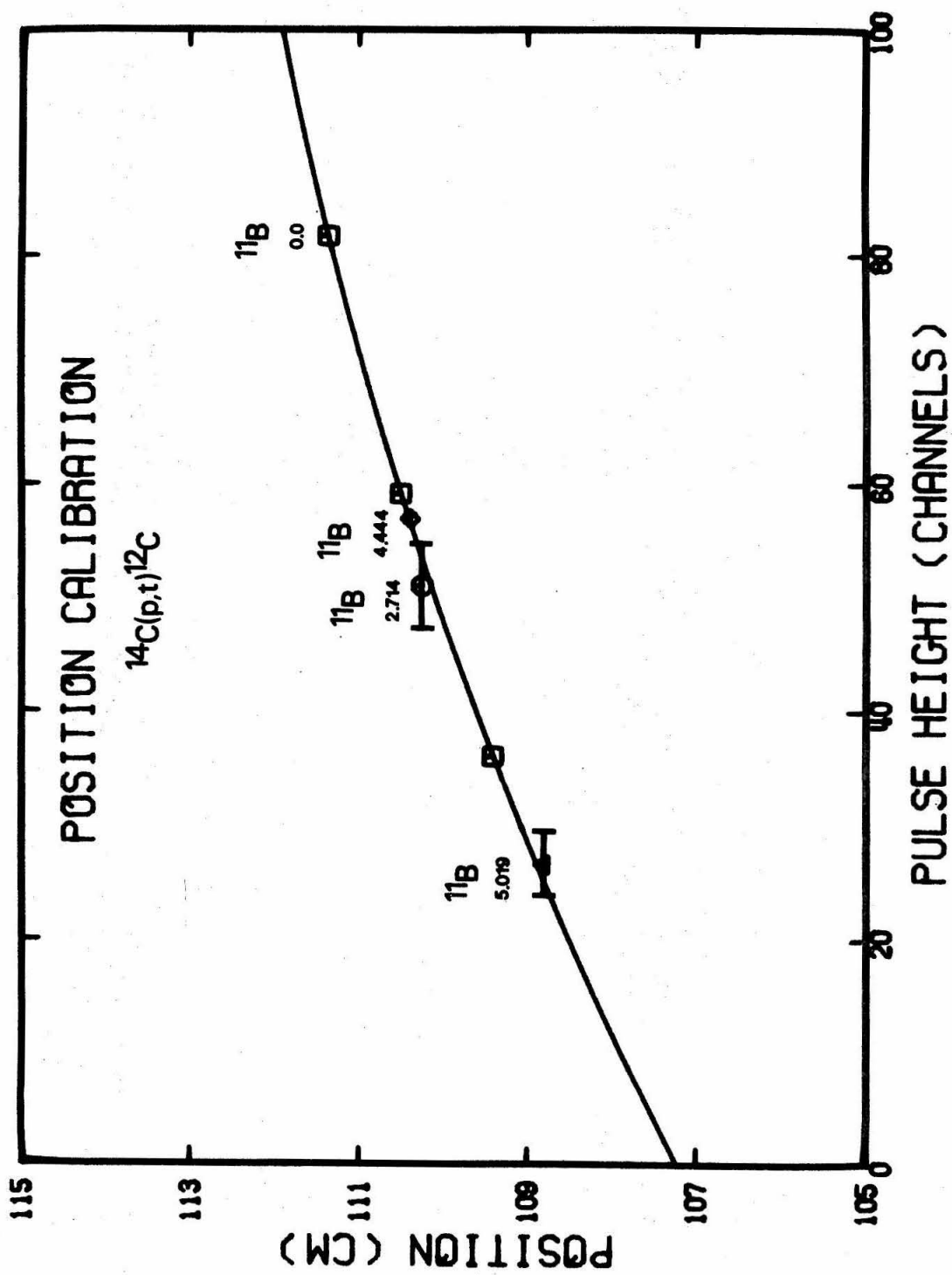
Figure 14

FIGURE 15

Angular distribution measurements for the $^{14}C(p,t)^{12}C$ reaction. The vertical bars indicate estimated uncertainties for the data points. The horizontal bars indicated the spectrograph aperture in the center-of-mass. The data points at $12°$ and $17°$ are estimated upper limits; the group of interest was not distinguished above background and continuum yield at these angles. See page 28 for additional discussion.

Figure 15

132
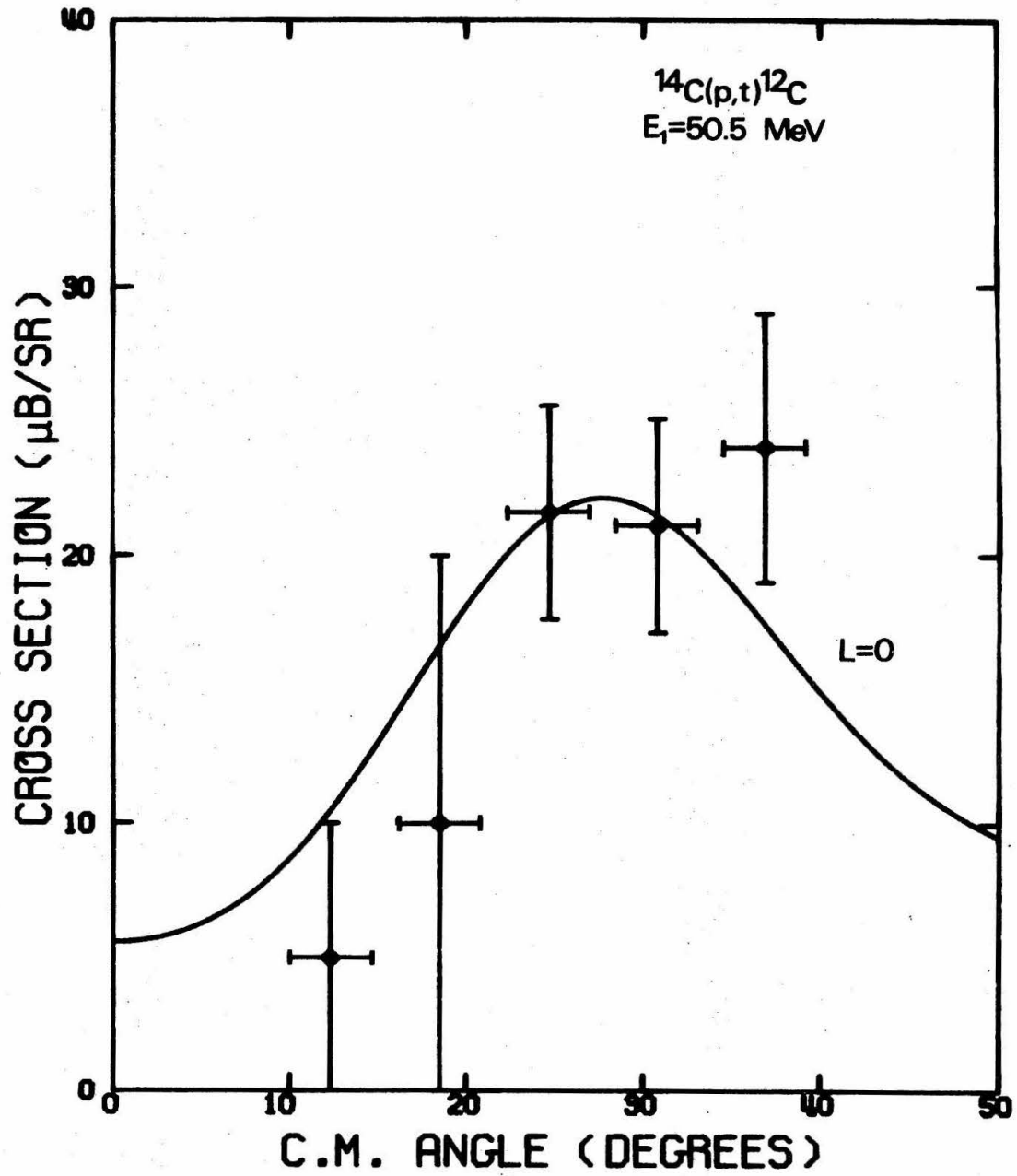
FIGURE 16

Energy spectrum from the position-sensitive detector, for the $^{14}C(p, ^{3}He)^{12}B$ experiment. The $^{3}He^{++}$ and alpha-particle groups are indicated. Deuterons at this field setting were penetrating through the active region of the detector, and these events are lost among the other low-energy events. See page 32 for further discussion.

Figure 16

PSC ENERGY SPECTRUM
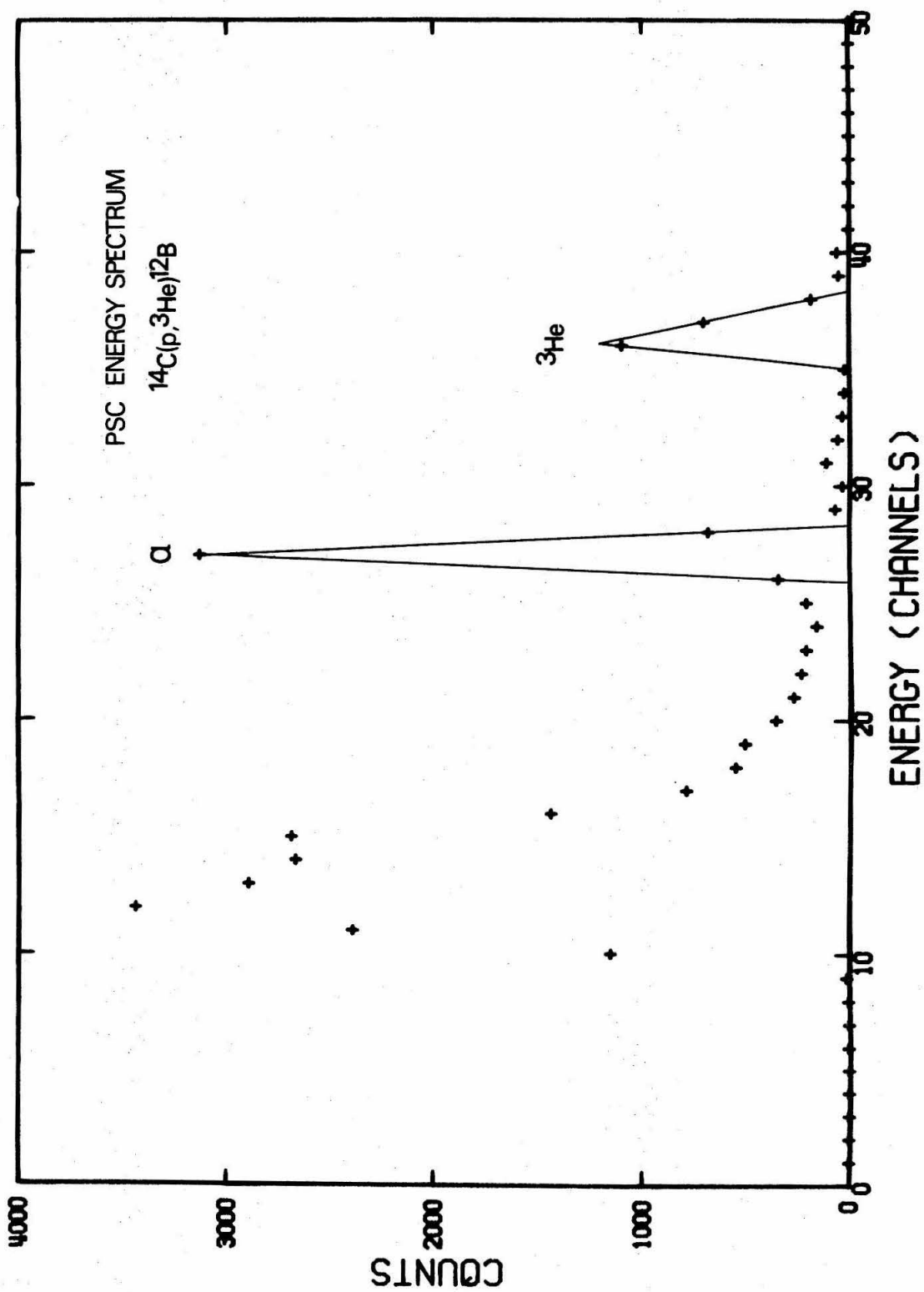
$^{14}C(p,^3He)^{12}B$

FIGURE 17

Composite ^{3}He spectra at 20° from the ^{14}C(p, ^{3}He)^{12}B reaction. The two spectra shown correspond to the two sets of data collected simultaneously from the two position-sensitive detectors at the focal plane of the spectrograph. A comparison spectrum from ^{12}C(p, ^{3}He)^{10}B is shown in the insert, near these two levels. The ^{12}B ground-state group, used for primary Q-value calibration, is slightly off scale at the high-energy end.

Figure 17

$^{14}C(p,^3He)^{12}B$
$20°$

$^{12}B(12.7)$

$^{12}B(14.86)$

^{12}C target

×5

PARTICLE ENERGY (MEV)

COUNTS

COUNTS

FIGURE 18

A typical ^{3}He spectrum accumulated in a single run, for the ^{14}C(p, ^{3}He)^{12}B measurements, at 8° in the laboratory. See page 33 for discussion.
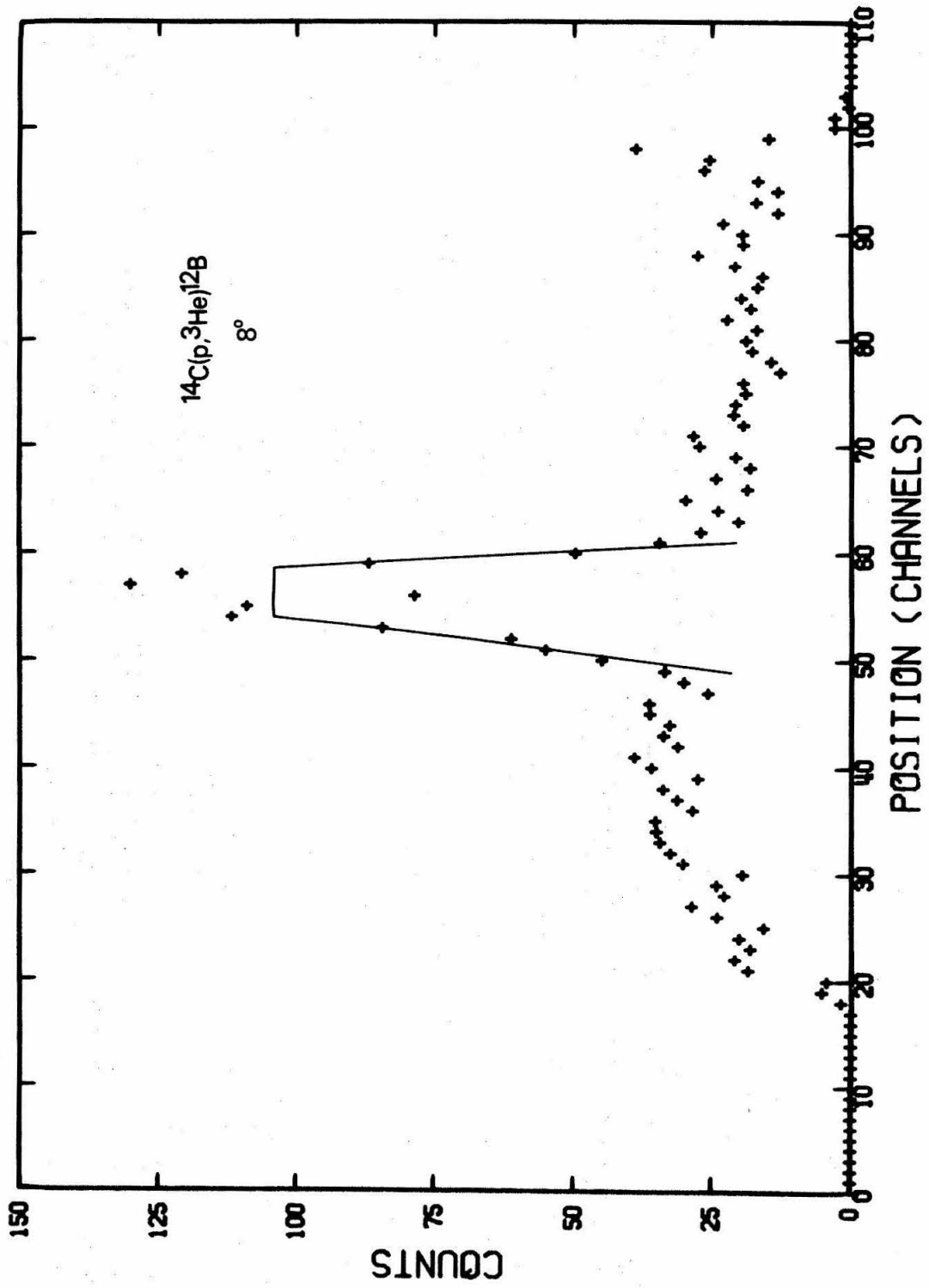
Figure 18

FIGURE 19

Calibration curve to determine focal-plane position from measured pulse height (100 channels = detector length) for the $^{14}C(p, ^{3}He)^{12}B$ measurements. The calibration points obtained from observations through a ladder mask are shown. The uncertainties are smaller than the indicated points. The smooth curve was constructed by a least-squares analysis of these data. See page 34 for further discussion.

Figure 19

POSITION CALIBRATION

$^{14}C(p,^{3}He)^{12}B$

POSITION (CM)

PULSE HEIGHT (CHANNELS)
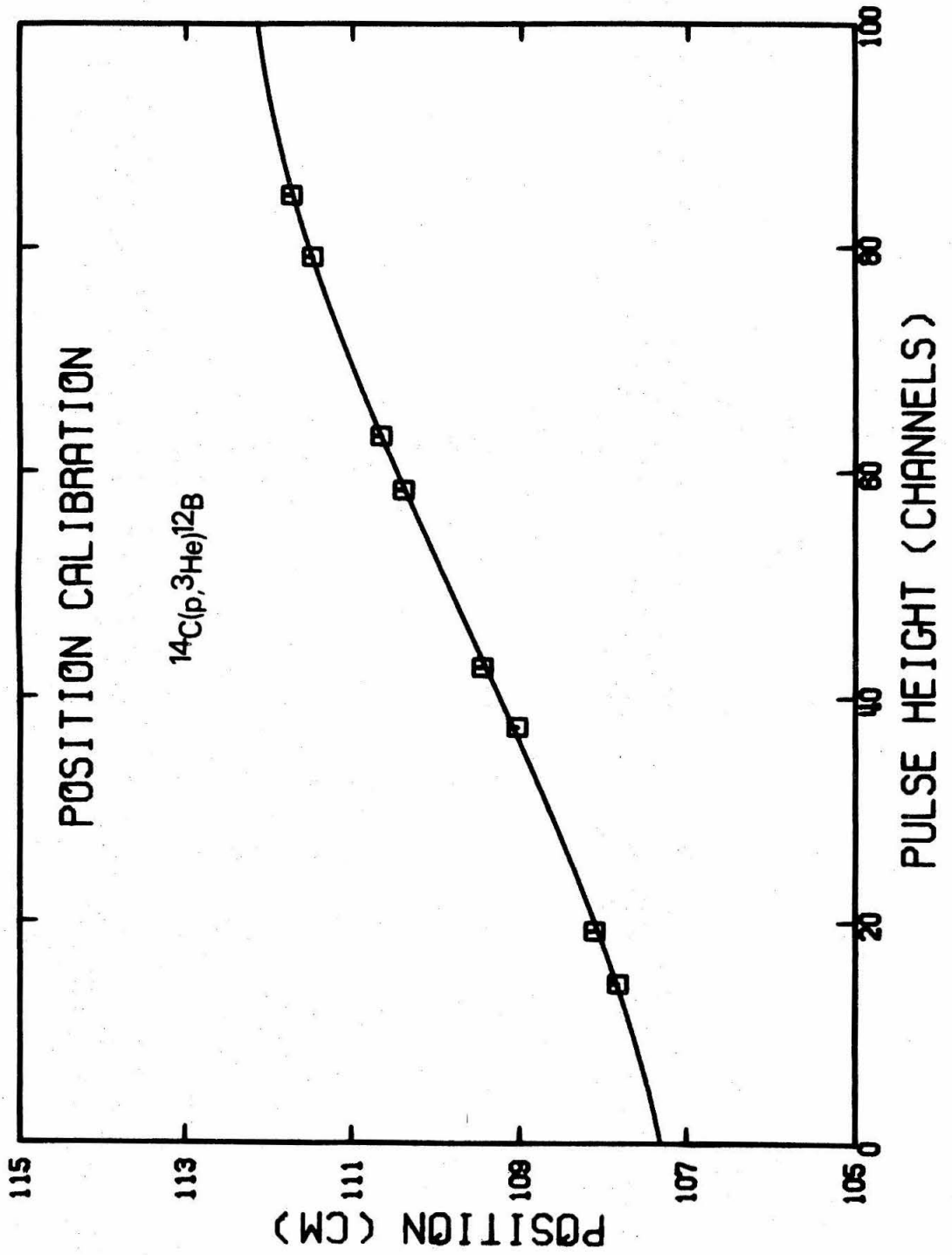
FIGURE 20

Angular distribution measurements from the $^{14}C(p, ^{3}He)^{12}B$ experiment. The upper half of the figure shows the distribution for the lowest T = 2 state. The lower portion shows the partial distribution measured for the broader group at 14.9-MeV excitation energy. The vertical bars indicate the probable error for the measured cross sections. The horizontal bars show the spectrograph aperture in the center-of-mass system.
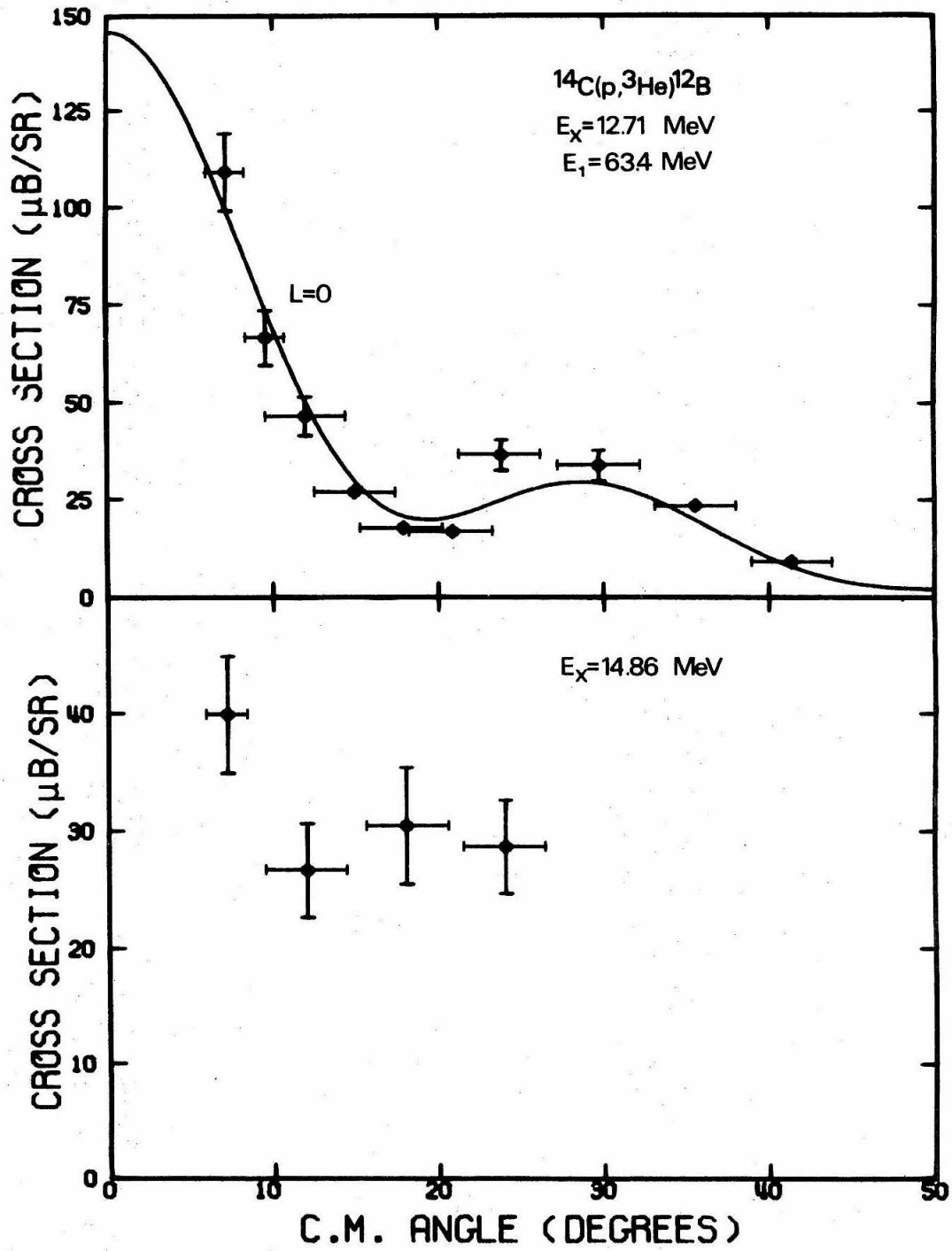
FIGURE 21

A comparison of proton spectra at 10° from (^{3}He,p) reactions on ^{12}C, ^{16}O and ^{18}O. See page 43 for discussion.

Figure 21

$(^3\text{He},p)$ reactions
$10°$
$E_1 = 12$ MeV
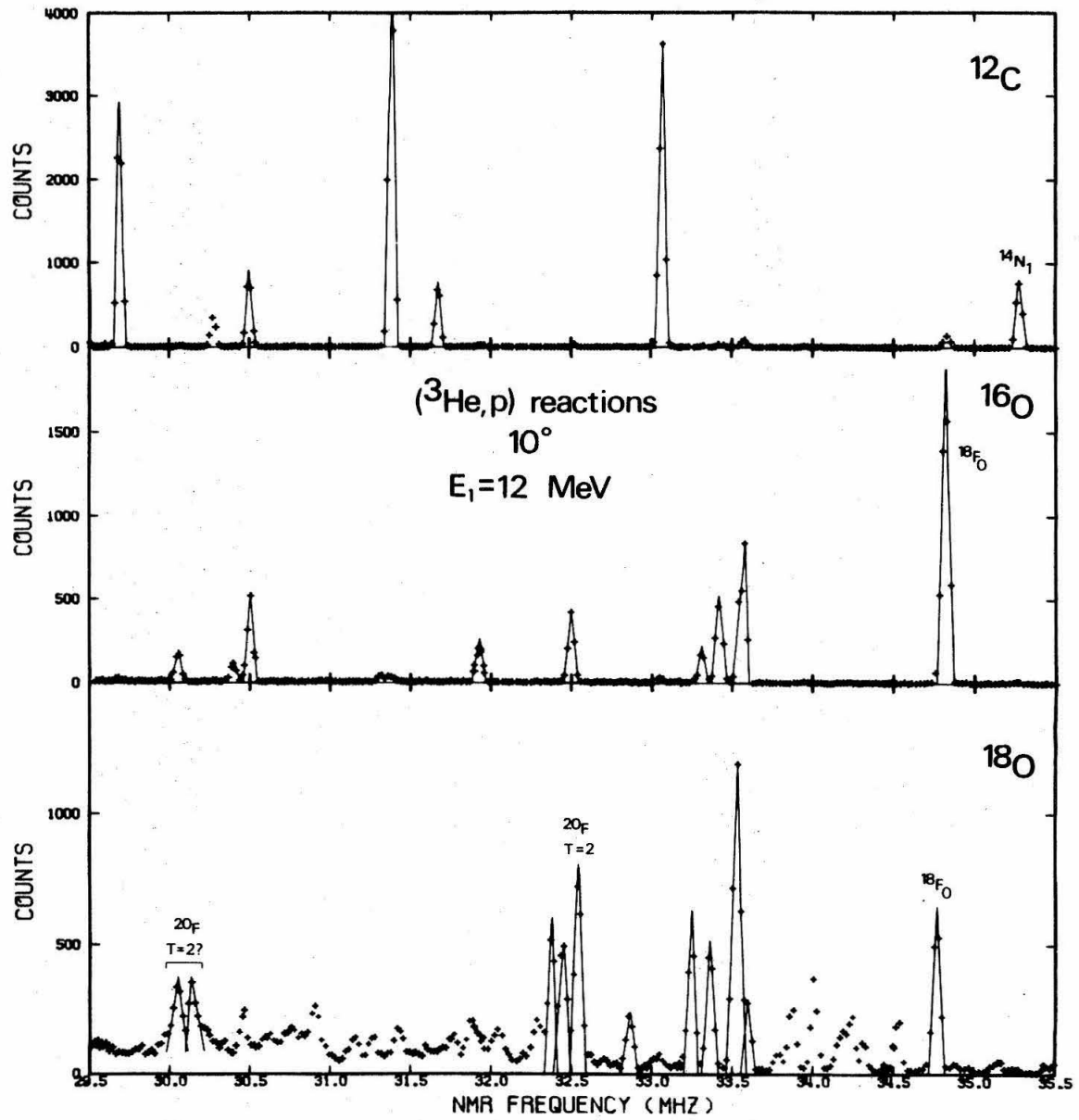
FIGURE 22

A comparison of proton spectra at 20° from (^{3}He,p)
reactions on ^{12}C, ^{16}O and ^{18}O. This shows the spectrum near
the predicted location of the first-excited T = 2 state of
^{20}F; the level identified as T = 2 is indicated. See page 43
for additional discussion.
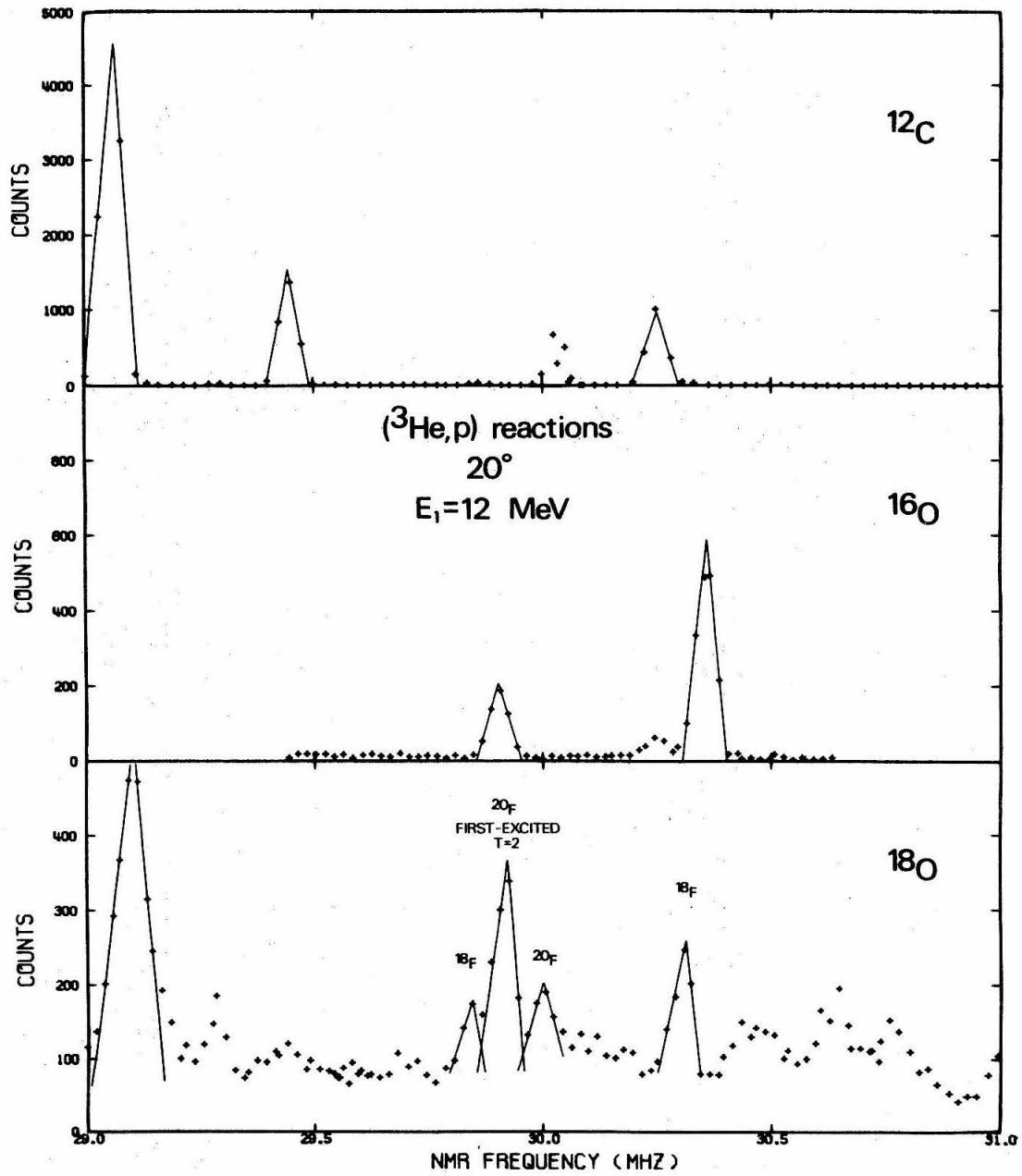
Figure 22

FIGURE 23

A typical spectrum of protons from $^{18}O(^{3}He,p)^{20}F$ measured by a position-sensitive detector, at 5° in the laboratory. This spectrum shows the region near the lowest T = 2 state. See page 43 for additional discussion.

Figure 23

$^{18}O(^3He,p)^{20}F$
$5°$

^{20}F
$T=2$

POSITION (CHANNELS)

COUNTS

148
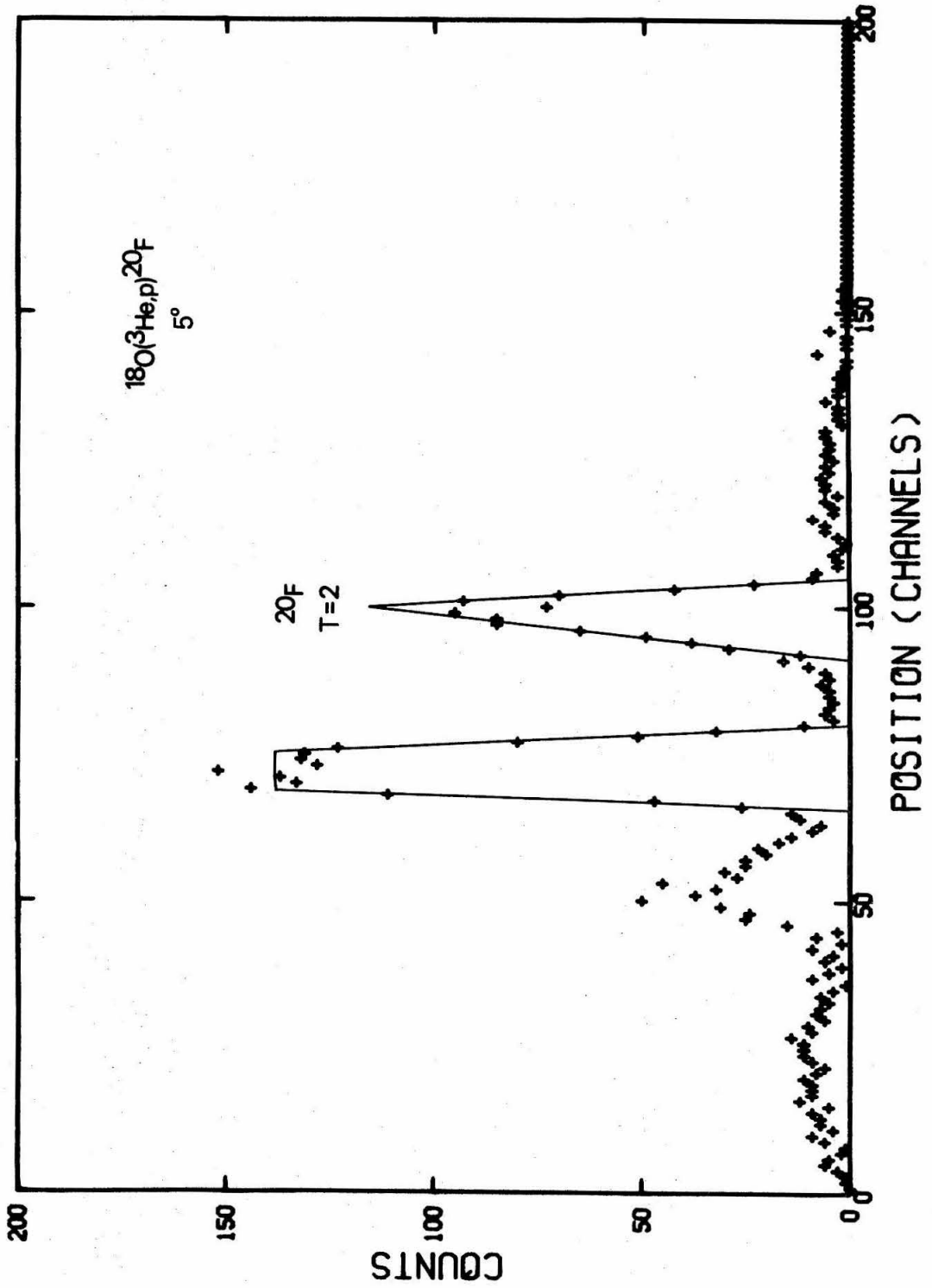
FIGURE 24

Angular distribution of the lowest T = 2 state of ^{20}F, at 6.51-MeV excitation, for 12-MeV incident ^{3}He energy. See page 46 for discussion.

Figure 24

$^{18}O(^3He,p)^{20}F$
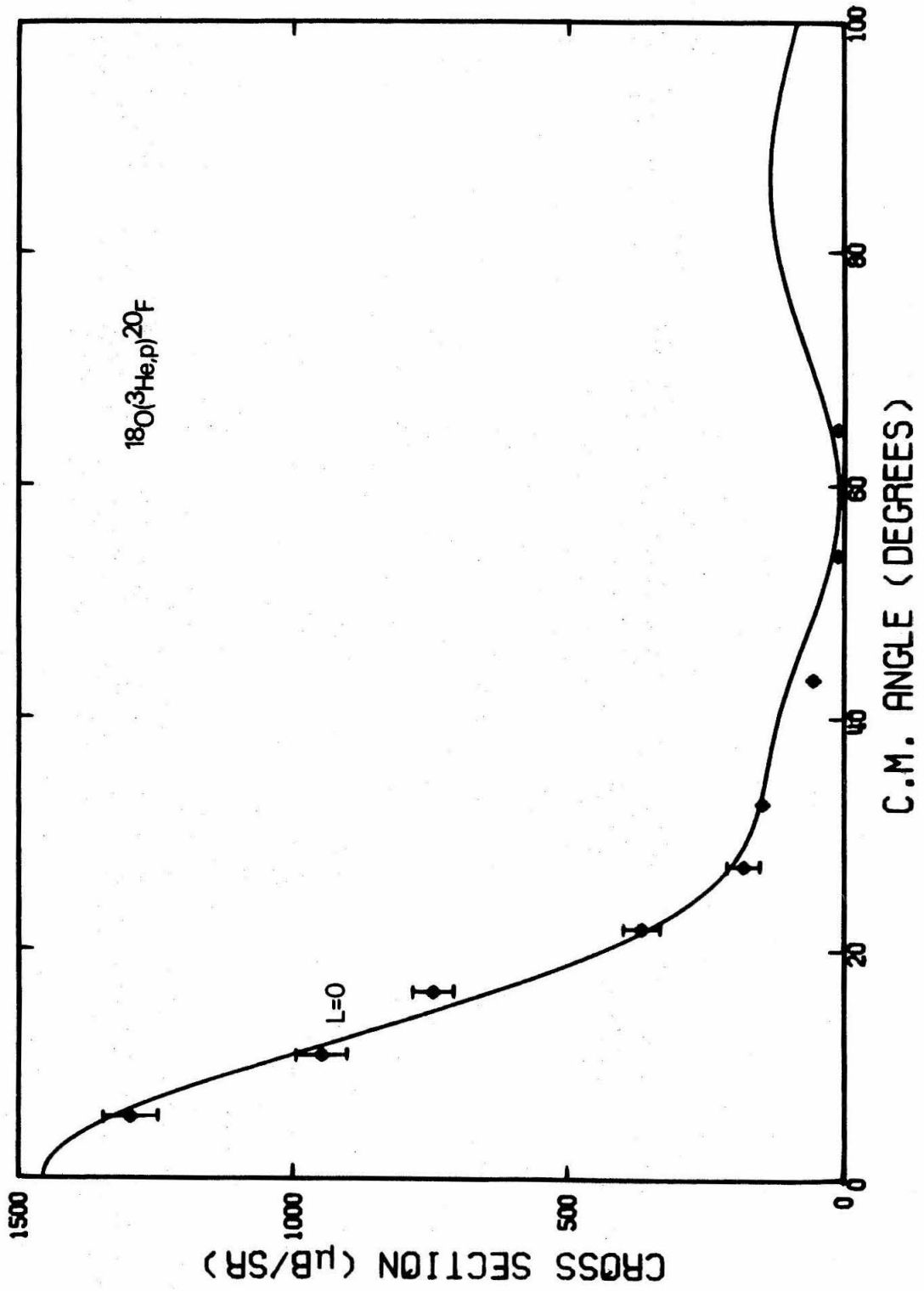
FIGURE 25

A comparison of proton spectra at 10° from (^{3}He,p) reactions on ^{24}Mg, ^{26}Mg, ^{12}C and ^{16}O. See page 50 for discussion.

Figure 25

152
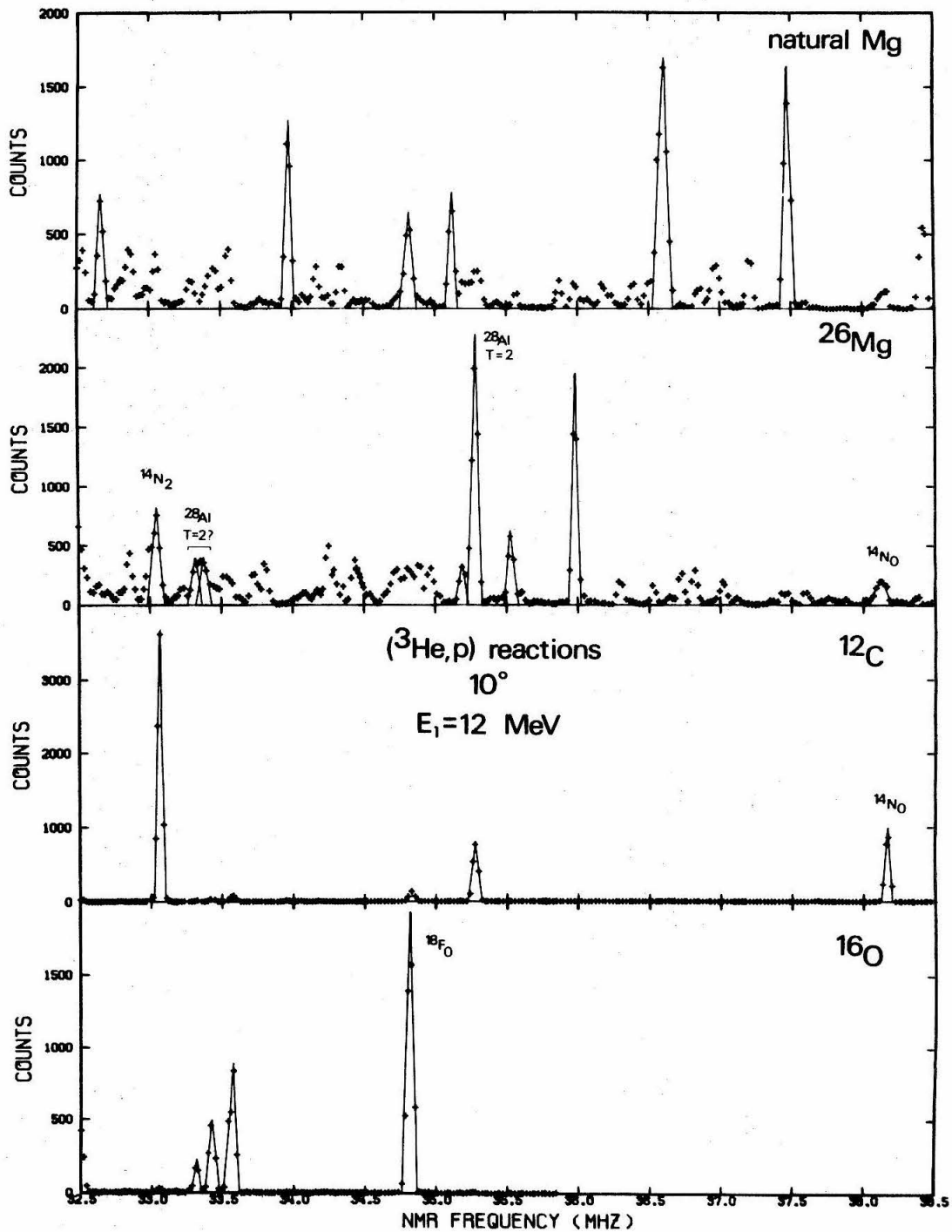
FIGURE 26

A typical proton spectrum from $^{26}Mg(^3He,p)^{28}Al$ measured by a position-sensitive detector, in the vicinity of the lowest $T = 2$ state, at $10°$ in the laboratory. See page 51 for discussion.

Figure 26

$^{26}Mg(^{3}He,p)^{28}Al$
$10°$

^{28}Al
$T=2$

POSITION (CHANNELS)

COUNTS

154
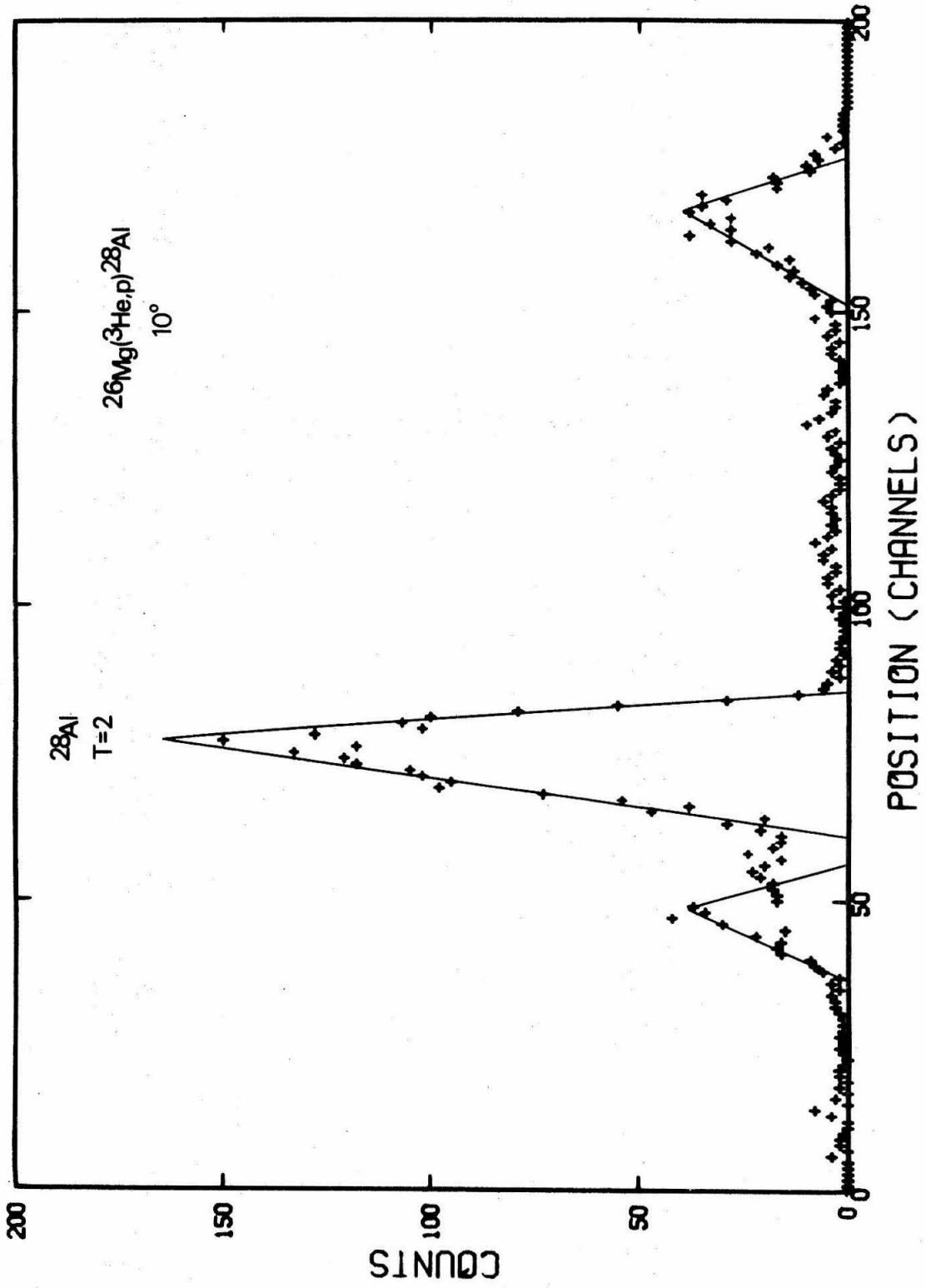
FIGURE 27

Protons from $^{26}Mg(^{3}He,p)^{28}Al$ at 20° in the lab, near the predicted location of

the first-excited T = 2 state. See page 51 for discussion.
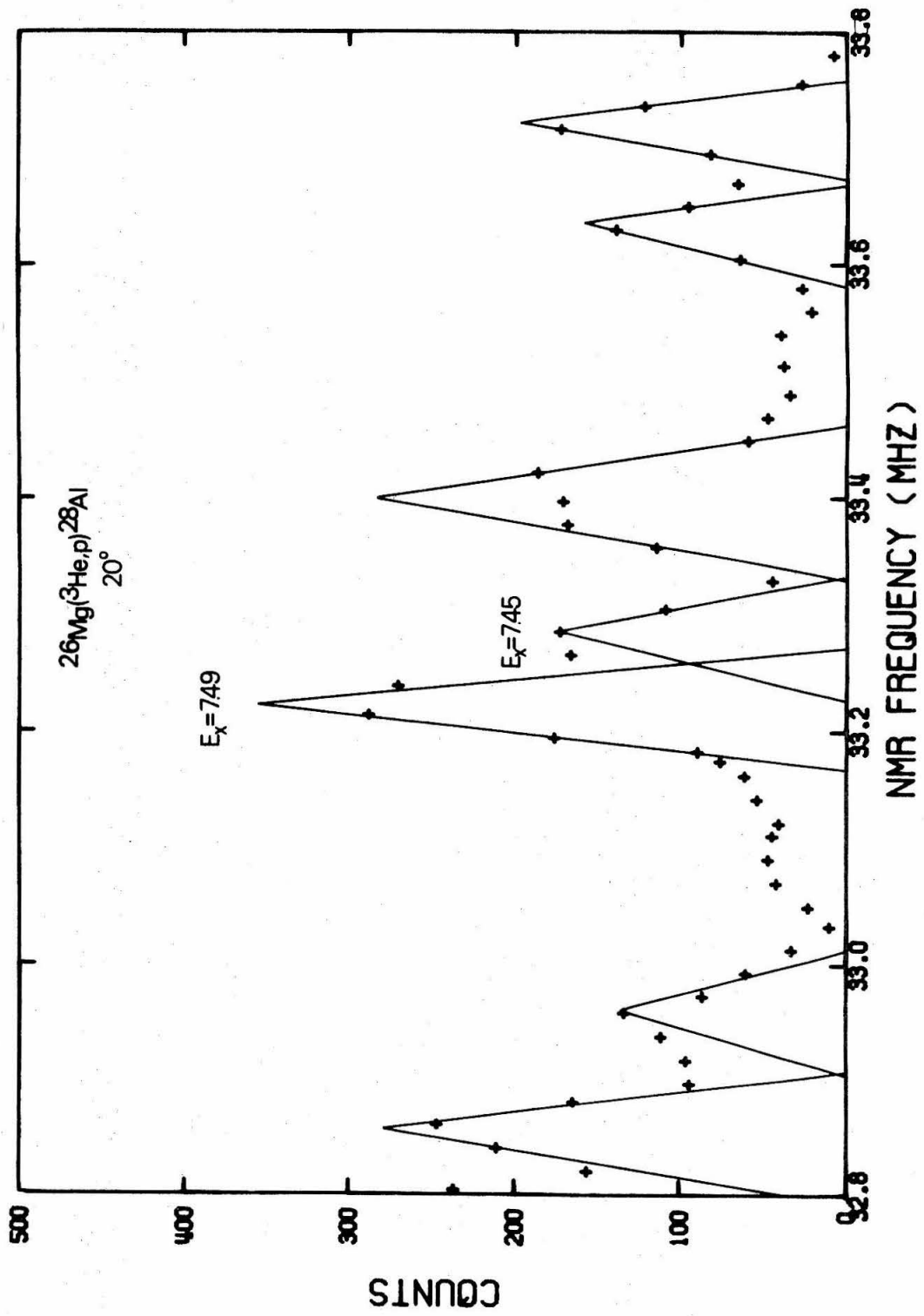
Figure 27

FIGURE 28

Angular distribution of the lowest T = 2 state of ^{28}Al, at 6.00-MeV excitation.

See pages 53-54 for discussion.
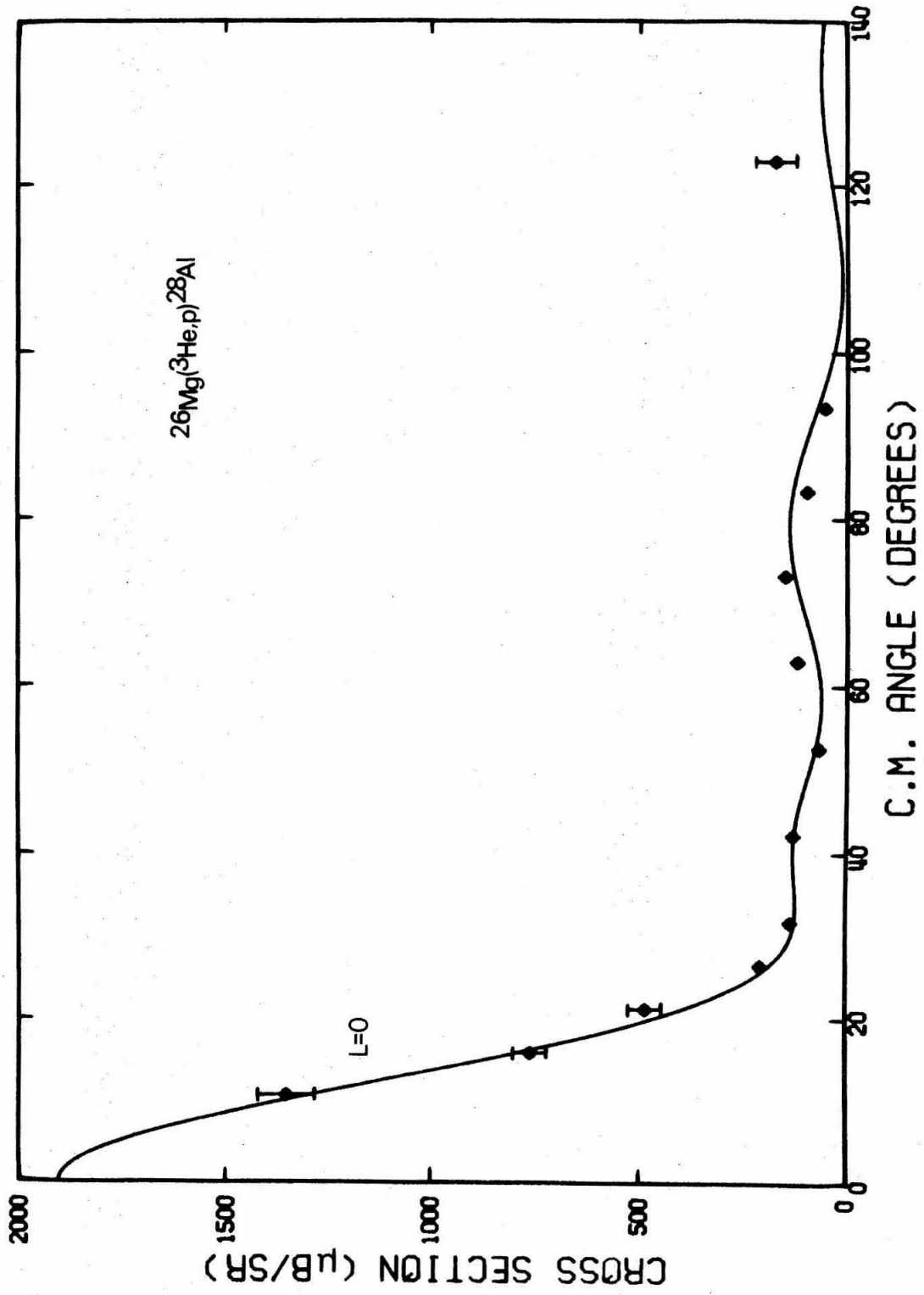
Figure 28

FIGURE 29

Angular distribution of the two members of the ^{28}Al doublet near 7.5-MeV excitation, from ^{26}Mg(^{3}He,p)^{28}Al. See for discussion.

$^{26}Mg(^3He,p)^{28}Al$
$E_x=7.49$ MeV

$E_x=7.45$ MeV
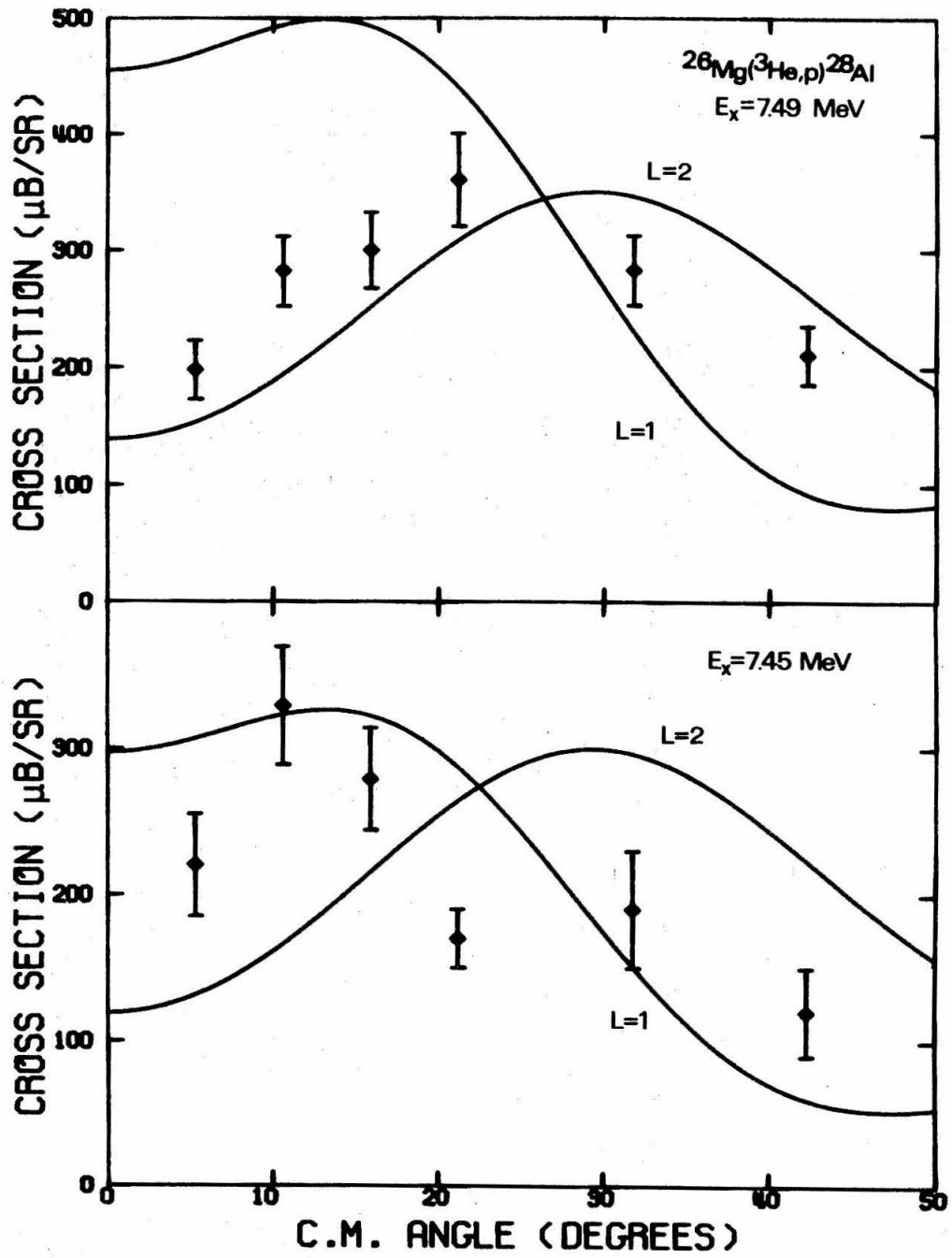
FIGURE 30

The vector Coulomb energies $E_c^{(1)}$ as a function of mass number for $T = 1$ and $T = 2$ multiplets. This term is essentially the coefficient of T_z in the quadratic mass equation. See page 57 for additional discussion.
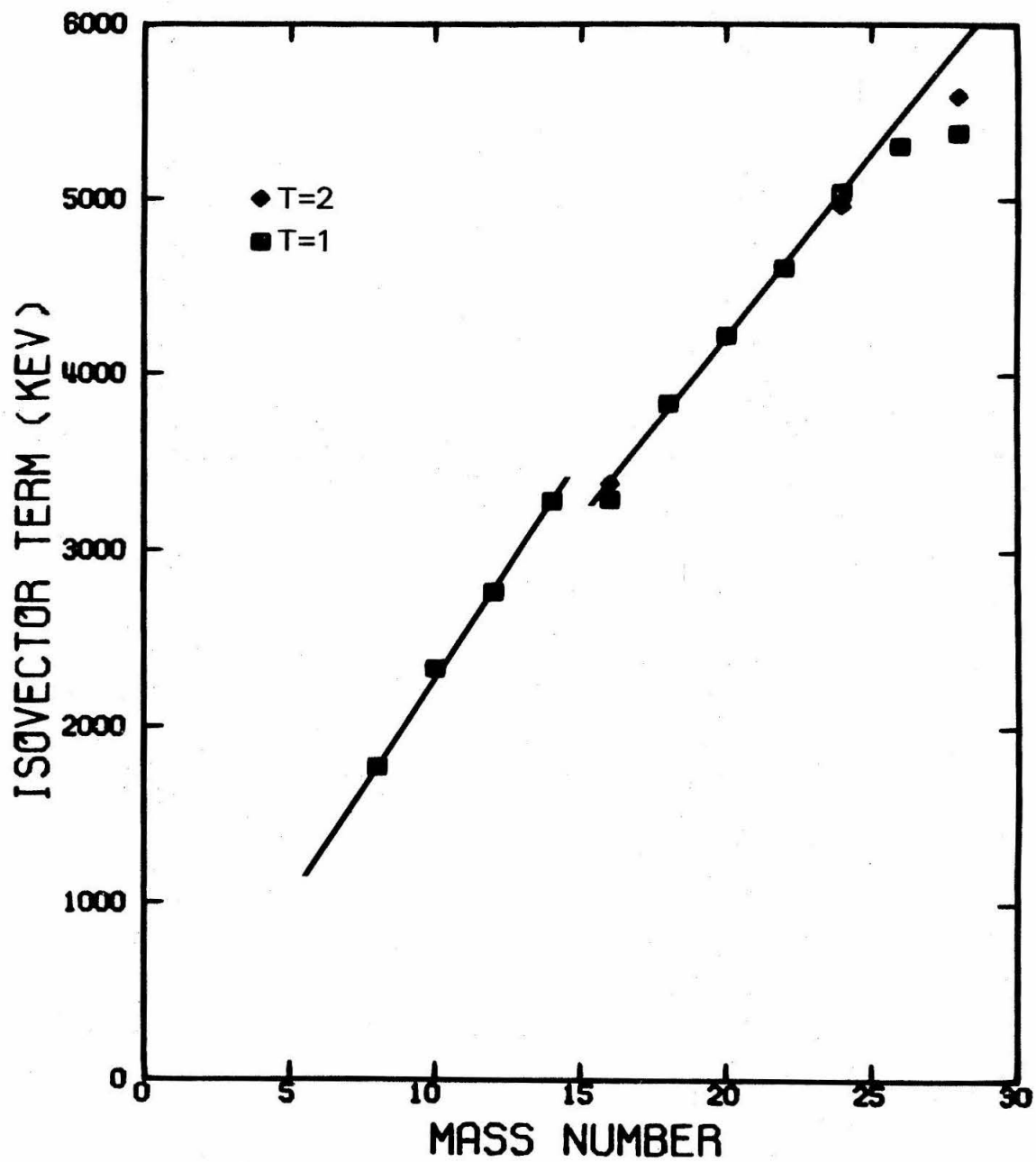
Figure 30

FIGURE 31

The tensor Coulomb energies $E_c^{(2)}$ as a function of mass number for $T = 1$ and $T = 2$ multiplets. This term is $\frac{c}{3}$, where c is the coefficient of T_z^2 in the quadratic mass equation. See page 58 for additional discussion.
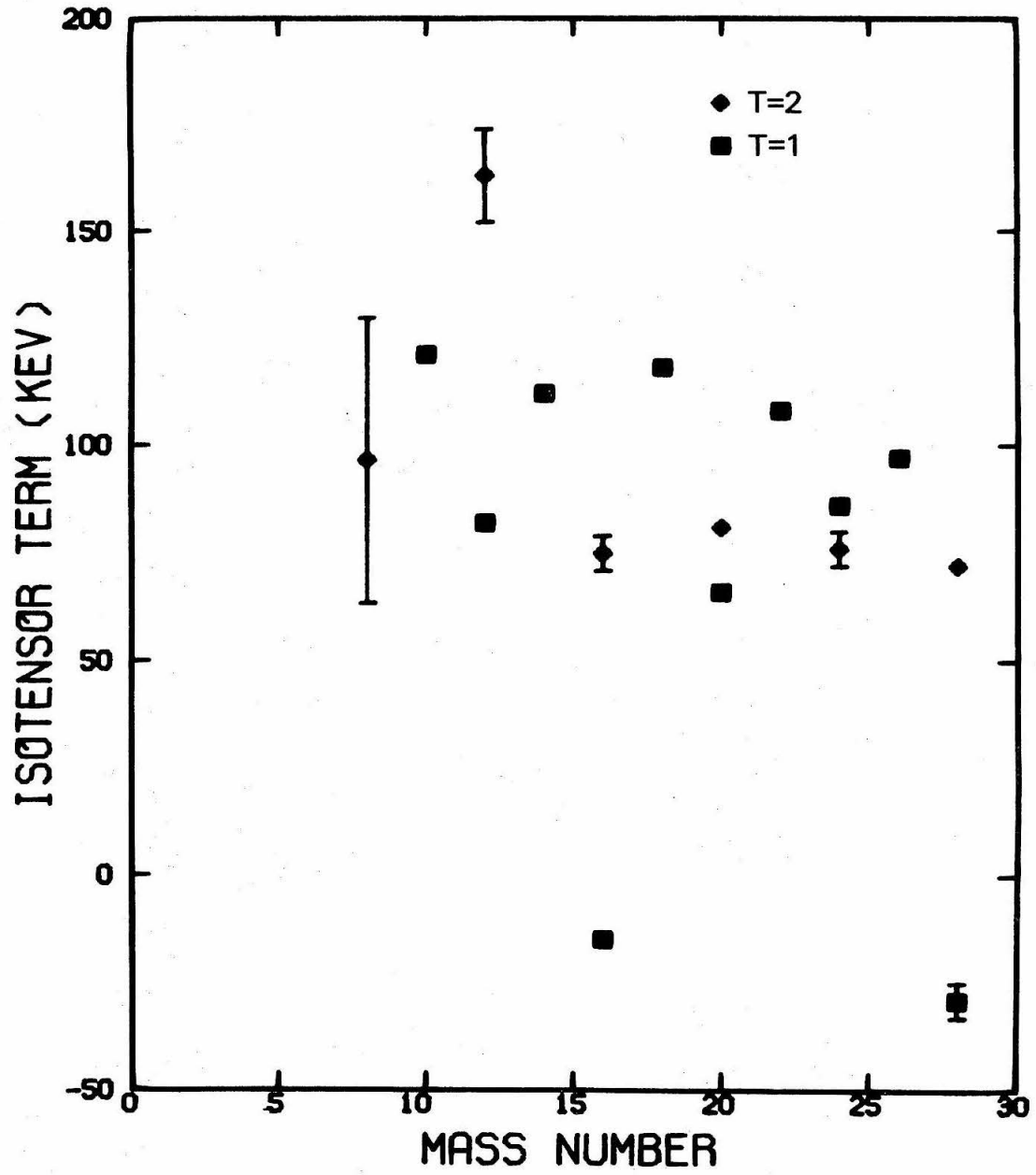
Figure 31

FIGURE 32

The isoscalar coefficient from the quadratic mass formula as a function of mass number, for T = 0, T = 1, and T = 2. See page 59 for discussion.

Figure 32